A study of the time-dependent modulation of cosmic rays in the inner heliosphere

E Magidimisha, B.Sc (Hons)

A study of the time-dependent modulation of cosmic rays in the inner heliosphere

E Magidimisha, B.Sc. (Hons)

Dissertation submitted in partial fulfilment of the requirements for the degree Master of Science in Physics at the Potchefstroom Campus of the North-West University

Supervisor: Prof. S. E. S. Ferreira

Co-supervisor: Prof. M. S. Potgieter

2010

North-West University, Potchefstroom Campus, South Africa

Abstract

A two-dimensional (2-D) time-dependent cosmic ray modulation model is used to calculate the modulation of cosmic-ray protons and electrons for 11-and 22-year modulation cycles using a compound approach to describe solar cycle related changes in the transport parameters. The compound approach was developed by Ferreira and Potgieter (2004) and incorporates the concept of propagation diffusion barriers, global changes in the magnetic field, time-dependent gradient, curvature and current-sheet drifts, and other basic modulation mechanisms. By comparing model results with ∼2.5 GV Ulysses observations, for both protons and electrons, it is shown that the compound approach results in computed intensities on a global scale compatible to observations. The model also computes the expected latitudinal dependence, as measured by the Ulysses spacecraft, for both protons and electrons. This is especially highlighted when computed intensities are compared to observations for the different fast latitude scan (FLS) periods. For cosmic ray protons a significant latitude dependence was observed for the first FLS period which corresponded to solar minimum conditions. For the second, which corresponded to solar maximum, no latitude dependence was observed as was the case for the third FLS period, which again corresponded to moderate to minimum solar activity. For the electrons the opposite occurred with only an observable latitude dependence in intensities for the third FLS period. It is shown that the model results in compatible intensities when compared to observations for these periods. Due to the success of the compound approach, it is also possible to compute charge-sign dependent modulation for 2.5 GV protons and electrons. The electron to proton ratio is presented at Earth and along the Ulysses trajectory. Lastly, it is also shown how the modulation amplitude between solar minimum and maximum depends on rigidity. This is investigated by computing cosmic ray intensities for both protons and electrons, not only at ~ 2.5 GV, but also up to ~ 7.5 GV. A refinement for the compound approach at higher rigidities is proposed.

Key words: cosmic rays, modulation, solar activity, Ulysses, heliosphere.

Acronyms and Abbreviations

ACR	Anomalous cosmic ray
AU	Astronomical unit = 1.49×10^8 km
CIR	Co-rotating interaction region
CME	Coronal mass ejection
COSPIN	Cosmic and Solar Particle Investigation
CR	Cosmic ray
FLS	Fast latitude scan
GCR	Galactic cosmic ray
GMIR	Global merged interaction region
HCS	Heliospheric current sheet
HMF	Heliospheric magnetic field
KET	Kiel Electron Telescope
LISM	Local interstellar medium
LIS	Local interstellar spectrum
MHD	Magnetohydrodynamic
PAMELA	Payload for Antimatter/Matter Exploration and Light-nuclei Astrophysics
PDB	Propagating diffusion barriers
QLT	Quasilinear theory
SCR	Solar cosmic rays
TPE	Transport equation
TS	Termination shock
2-D	Two-dimensional
3-D	Three-dimensional

Contents

Abstract **i**

Acronyms and Abbreviations **ii**

1 Introduction **1**

2 Cosmic rays in the heliosphere **3**

2.1 Introduction 3

2.2 Cosmic rays 3

2.3 The Sun 5

2.4 Sunspots and solar activity 6

2.5 The solar wind 7

2.6 The heliosphere 10

2.7 The heliospheric magnetic field 13

2.8 The heliospheric current sheet 16

2.9 Solar cycle related changes in the heliospheric magnetic field 18

2.10 Spacecraft missions 19

2.10.1 The Ulysses mission 20

2.10.2 The Kiel Electron Telescope (KET) 22

2.10.3 Payload for Antimatter/Matter Exploration and Light-nuclei Astrophysics (PAMELA) Spacecraft 22

2.10.4 Summary 24

3 Cosmic ray transport and modulation models 25

3.1 Introduction . . . 25

3.2 The transport equation and the diffusion tensor . . . 25

3.3 Modulation models . . . 26

3.4 The diffusion tensor . . . 27

3.5 Parallel diffusion . . . 27

3.6 Perpendicular diffusion . . . 29

3.7 Particle drifts . . . 33

3.8 Summary . . . 36

4 Time-dependent cosmic ray modulation 37

4.1 Introduction . . . 37

4.2 Propagating diffusion barriers: The effect on cosmic ray intensities . . . 37

4.3 The GMIR-drift approach . . . 39

4.4 The compound approach . . . 41

4.5 Application of the compound approach . . . 45

4.6 Constructing a time dependence in $(K_A)_0$ . . . 47

4.7 Summary and conclusions . . . 49

5 Modeling of cosmic ray proton and electron intensities along the Ulysses trajectory 50

5.1 Introduction . . . 50

5.2 Comparison between model results and the Ulysses spacecraft observations . . . 50

5.3 The fast latitude scan periods . . . 53

5.4 Global distributions . . . 56

5.5 Summary and conclusions . . . 62

6 Charge-sign dependent modulation and refinement of the compound approach 63

6.1 Introduction . . . 63

6.2 Model results at higher rigidities and charge-sign dependent modulation. . . . 63

6.3 Refinement of the compound approach . . . 67

6.4 Summary and conclusions . . . 71

7 Summary and conclusions **72**

References **75**

Acknowledgements **93**

Chapter 1

Introduction

Cosmic ray modulation is studied with emphasis on describing the Ulysses cosmic ray observations as a function of time. The concept of modulation refers to the propagation of particles in the inner heliosphere, and in this process their intensities are reduced as a function of position, energy and time. Because cosmic rays are charged particles, they get scattered by irregularities in the heliospheric magnetic field (HMF) which is convected out with the solar wind and also undergo adiabatic deceleration in the expanding solar wind and experience gradient curvature and current sheet drifts. Changes in solar activity also result in cosmic ray intensities changing over a solar cycle. Parker (1965) derived a time-dependent transport equation which describes all the modulation processes experienced by cosmic rays as they make their way into the inner heliosphere. This equation has been solved numerically with an increasingly sophistication and complexity over the years (e.g. Fisk 1971; Kota and Jokipii 1983; Potgieter and Moraal 1985; le Roux and Potgieter 1990; Jokipii and Kota 1995; Steenberg 1998; le Roux and Fichtner 1999; Zhang 1999; Burger et al. 2000; Ferreira and Potgieter 2004; Scherer and Ferreira 2005).

This equation is solved numerically in this study to calculate cosmic ray intensities over a solar cycle, with focus on the different fast latitude scan periods of the Ulysses spacecraft which corresponds to different levels of solar activity and magnetic polarity. During the two different magnetic epochs positively and negatively charged particles behave differently. During the $A > 0$ magnetic epochs and for solar minimum periods, a more flattered time profile for positively charged particles is expected. For the $A > 0$ magnetic epoch positively charged particles drift in mainly from the poles to the inner heliosphere and outward along the heliospheric current sheet (HCS). They are insensitive to any changes in the HCS. During the $A < 0$ polarity cycle positively charged particles drift in along the current sheet and out via the poles so that a more peaked profile is expected due to changes in the current sheet (e.g. Heber et al. 2009).

It will be shown in this work that it is possible to use an existing 2-D time-dependent modulation model, with the implementation of the compound approach introduced by Ferreira (2002) and Ferreira and Potgieter (2004), to realistically compute cosmic ray intensities

for different polarity and solar cycles. The compound approach, and its refinement from Ndiitwani et al. (2005), makes it not only possible to compute cosmic ray modulation over multiple solar cycles, but also to compute charge sign dependent modulation. The compound approach incorporates changes in the global magnetic field and the tilt angle to calculate a time-dependence in the transport and drifts coefficients. Apart from this, results from Ndiitwani et al. (2005) and Minnie et al. (2007) suggest an additional scaling of drifts over time, especially to zero drifts for solar maximum, in order to compute realistic charge-sign dependent modulation. This aspect will be revisited.

In this work the aim is

1. To refine the compound approach by investigating the additional scaling down of drifts toward solar maximum. See also Ndiitwani et al. (2005) and Minnie et al. (2007).

2. To compute intensities of 2.5 GV cosmic rays in the inner heliosphere, for both protons and electrons and to compare them with recent observations by the Ulysses spacecraft. It will be shown that such a comparison results in a better understanding of the observations.

3. Modeling the fast latitude scan periods of the Ulysses spacecraft. Of particular interest is the third fast latitude scan period which was not modelled before. This recent fast latitude scan shows no measurable latitudinal gradient for protons but for the electrons a latitudinal gradient is observed (Heber et al. 2009).

4. Once compatibility between the model and the Ulysses observations has been established, contour graphs are presented to show the distribution of cosmic rays for the different fast latitude scan periods and for the whole computed heliosphere.

5. To compute charge-sign dependent modulation at different rigidities by calculating the electron to proton ratio, not only at 2.5 GV, but also for higher rigidities.

6. To propose a refinement, by studying the modulation amplitude between solar minimum and maximum, of the compound approach as a function of increasing rigidity.

Chapter 2

Cosmic rays in the heliosphere

2.1 Introduction

In this chapter the necessary background regarding cosmic ray modulation and the heliosphere (influence sphere of the Sun) is given. Important concepts like cosmic rays, the solar wind, the heliosphere, the HMF, the HCS and tilt angle are discussed. The Ulysses mission is also briefly discussed. Data from this spacecraft are frequently used later for comparison of model results with observations. The next chapter focuses on the different transport processes and the numerical models used to compute cosmic ray modulation.

2.2 Cosmic rays

Cosmic rays are highly energetic charged particles originating in outer space. They travel at nearly the speed of light and arrive at Earth from all directions. Most cosmic rays are nuclei of atoms ranging from the lightest to the heaviest elements (e.g. Mewaldt 1994). Cosmic rays mostly include electrons ($\sim$1%), protons ($\sim$89%) and other subatomic particles ($\sim$10%).

Cosmic rays are produced by a number of different sources such as supernova explosions and their remnants, neutron stars and black holes, as well as active galactic nuclei and radio galaxies (see e.g. Forbush 1946; Garcia-Munoz et al. 1973; Axford et al. 1977; Bell 1978; Blandford and Ostriker 1978; Scherer et al. 2008).

Cosmic rays were discovered by Victor Hess (Hess 1911) during his historic balloon flights. Figure 2.1 *(from http://www.ast.leeds.ac.uk/haverah/cosrays)* shows the balloon in which Hess did the first measurements. Hess found that an electroscope discharged more rapidly as he was ascending in the balloon, proving that this source of radiation is entering the atmosphere from above. In 1936 Hess was awarded the Nobel Prize for his discovery. For some time it was believed that the radiation was electromagnetic in nature, hence the name cosmic rays.

Figure 2.1: Hess's balloon in which he observed that the amount of radiation increased with increasing altitude. From *(http://www.ast.leeds.ac.uk/haverah/cosrays.shtml.)*

Cosmic rays can be classified into different groups, namely:

Galactic cosmic rays (GCRs): Galactic cosmic rays originate far outside our solar system and penetrate the heliosphere up to Earth's orbit. These particles are composed mainly of protons, helium and electrons. When entering the heliosphere they encounter an outward-flowing solar wind which carries a turbulent magnetic field (Parker 1965). This turbulent field influences the propagation of these particles, a process called the modulation of cosmic rays. Galactic cosmic rays can serve as messengers from outer space (e.g. Lee and Fichtner 2001), providing valuable information about this region which cannot yet be measured directly. It is generally believed that these particles are accelerated to high energies via diffusive shock acceleration (Axford et al. 1977; Bell 1978; Blandford and Ostriker 1978) at supernova remnants.

Solar cosmic rays (SCRs): These particles are also called solar energetic particles which originate mostly from solar flares (e.g. Forbush 1946). Coronal mass ejections and shocks in the interplanetary medium can also produce these energetic particles. SCRs have energies typically up to several hundred MeV/nucleon, sometimes even up to a few GeV/nucleon. For more details regarding solar energetic particles see e.g. Cliver (2000).

Anomalous cosmic rays (ACRs): These particles are freshly-ionized interstellar neutrals which get ionized in the solar wind and then accelerated at the solarwind termination shock (TS)(see section 2.6) by the mechanism of diffusive shock acceleration. Apart from this they may also be continuously accelerated and heated in the inner heliosheeth via Fermi-2 (stochastic) acceleration and also adiabatically heated (see e.g. Kallenbach et al. 2005; Langner et al. 2006a, 2006b; Zhang et al. 2006; Moraal et al. 2006; Ferreira et al. 2007; Strauss et al. 2010). These particles were discovered in the 1970's when Garcia-Munoz et al. (1973) found an unexpected shape of the Helium spectra below $\sim$100 MeV/nucleon. Fisk et al. (1974) postulated that neutral particles entering the heliosphere get ionized and picked up by the solar wind and then accelerated at the solar wind TS. These particles where named anomalous because of their

unusually high intensities at lower energies.

As an alternative to continuous acceleration in the heliosheath McComas and Schwadron (2006) postulated that these particles may also be accelerated at the flanks of the heliosphere. Langner and Potgieter (2006) and also Ngobeni and Potgieter (2008) showed that when preferred acceleration regions, like the equatorial nose of the heliosphere, are assumed, a modulation model can produce compatible intensities when compared to observations (see also Strauss 2009).

The Jovian electrons: In 1973 the Pioneer 10 spacecraft confirmed that the Jovian magnetosphere at ∼5 AU is a relatively strong source of electrons of a few MeV (Simpson et al. 1974; Teegarden et al. 1974; Chenette et al. 1974; Mewaldt et al. 1974). These electrons have also been observed at Earth (e.g. Teegarden et al. 1974). Using Pioneer 10 data up to 1980, Eraker (1982) calculated that the dominant component of interplanetary electrons below ∼25 MeV inside the first ∼11 AU has a Jovian origin. This was confirmed by model results by Ferreira et al. (2001a,b) who showed that at 7 MeV Jovian electrons dominate their galactic electron counter parts in intensity up to ∼10 AU in the equatorial regions. For recent model calculations of the transport of these particles in the inner heliosphere see work done by Sternal (2010). For a review, see Heber and Potgieter (2006).

2.3 The Sun

The Sun is by far the largest object in the solar system. It contains more than ∼99% of the total mass of the solar system with Jupiter most of the rest. The Sun is a massive ball of plasmatic gas, held together by and compressed under its own gravitational attraction. It consists principally of hydrogen (∼90%) and helium (∼10%) with a small fraction of elements such as C, N, and O (e.g. Parks 1991). The Sun has a north and south magnetic pole and rotates on its axis. However, unlike the Earth which rotates at all latitudes every ∼24 hours, the Sun rotates every ∼25 days at the equator and takes progressively longer to rotate at higher latitudes, up to ∼35 days at the poles.

Figure 2.2 shows a picture of the Sun with the solar atmosphere consisting of different layers (From *www.oulu.fi/spaceweb/textbook/sun.html*). Starting with the photosphere which is the zone from which sunlight is emitted. Then follows the chromosphere (visible surface of the Sun) and after that one find a transition region which is a thin and very irregular layer of the Sun's atmosphere that separates the hot corona from the much cooler chromosphere. The fourth layer is the corona which is the outer atmosphere of the Sun. The corona extends up to $\sim 2 \times 10^6$ km from the Sun's surface. This region extends into the interplanetary space where it becomes the solar wind.

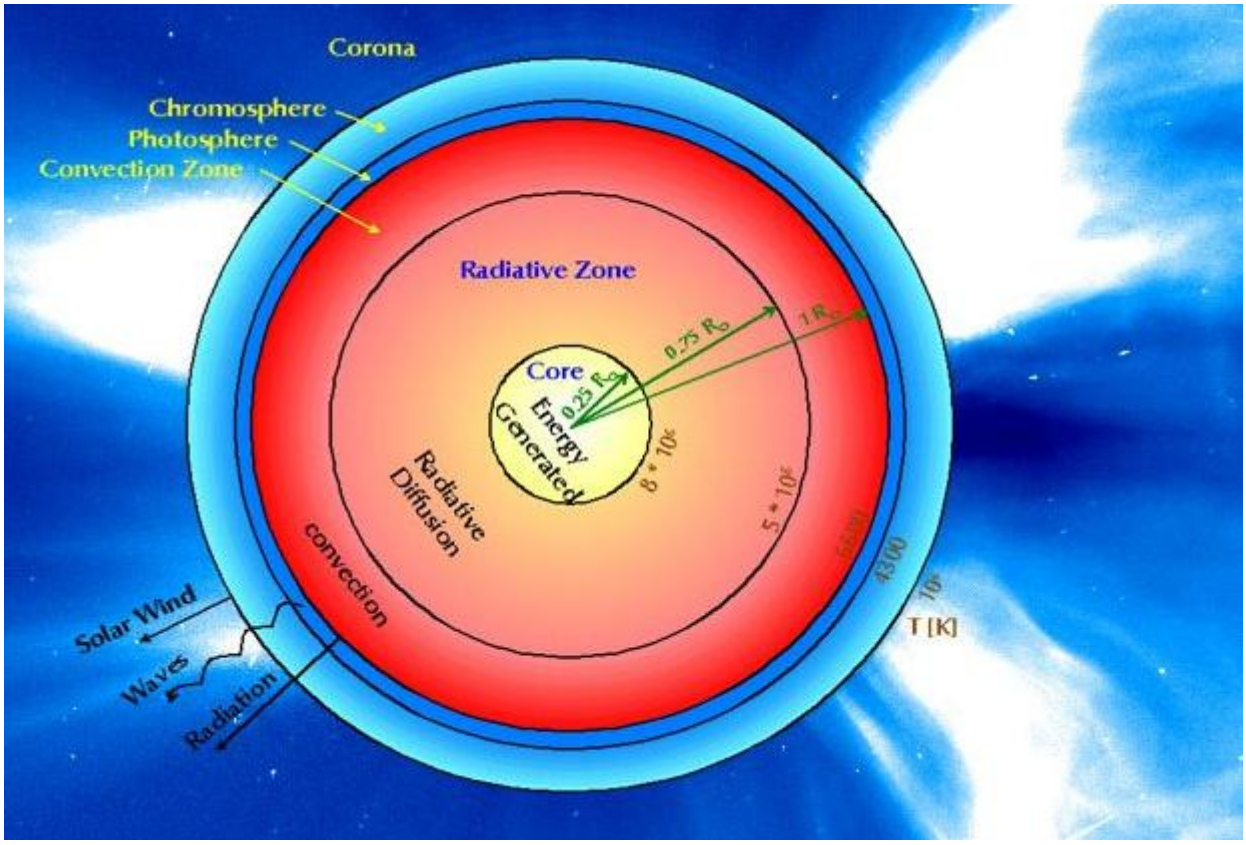

Figure 2.2: The different layers of the Sun as discussed in the text. From *(www.oulu.fi/spaceweb/textbook/sun.html).*

2.4 Sunspots and solar activity

Visible on the photosphere of the Sun are dark, cooler areas of irregular shape appearing on the solar surface, which can have a diameter up to $\sim 10^5$ km and are called sunspots. They first appear as small dark pores which, over $\sim$24 hours or so, gradually grow bigger and develop into sunspots (e.g. Gombosi 1994). The sunspot pores (meaning a small sunspot without a penumbra) tend to be associated with weaker magnetic fields than the larger sunspots. According to Thomas and Weiss (1992), sunspots can be regarded as the advanced stage of pores that have acquired a penumbra (literally meaning "almost shadow"). They have a cold central umbra (T $\approx$ 4100 K) with very strong local magnetic field of $\sim$0.3 T or $\sim 3\times 10^4$ G which then is surrounded by penumbra of light and dark radial filaments. The lower effective temperature of a sunspot means that it emits much less photons than the surrounding areas and therefore appears much darker. Its lower effective temperature is linked with the strong local magnetic field.

It was discovered in the middle of the nineteenth century that the number of sunspots exhibits a $\sim$11 year periodicity. Detailed records of the sunspot numbers, which are direct indications of the level of solar activity, have been kept since 1750 and are shown in Figure 2.3 up to 2009. (Data from *ftp://ftp.ngdc.noaa.gov/stp/solar_data/sunspot_numbers*).

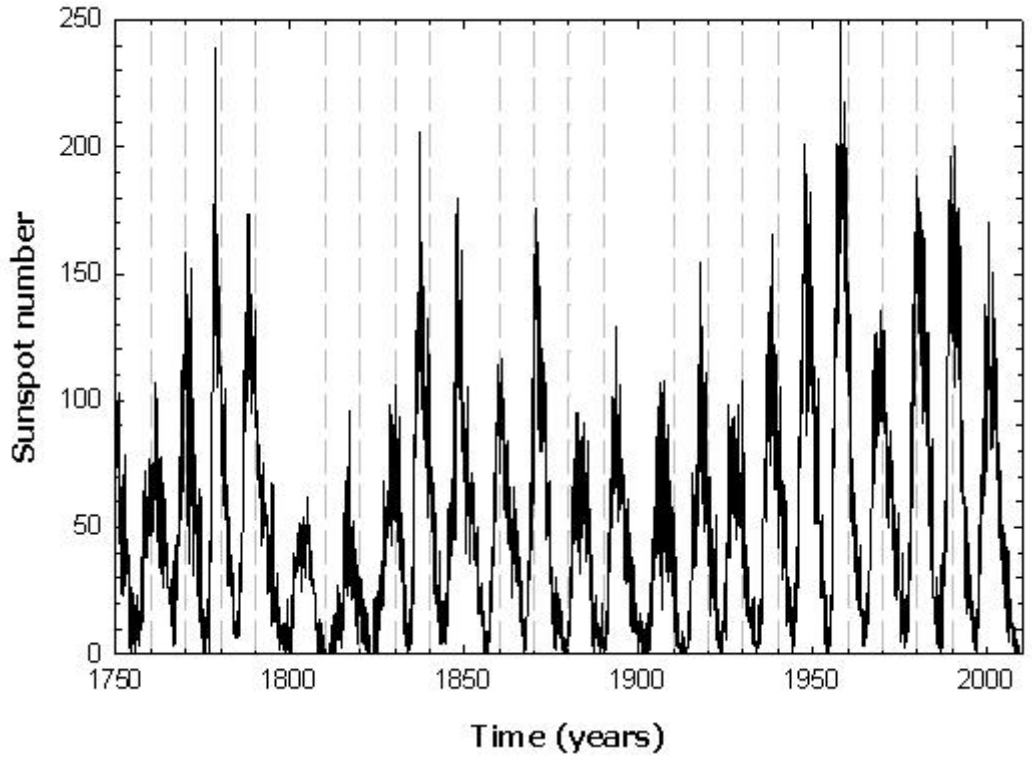

Figure 2.3: Monthly averaged sunspot numbers from ∼1750 to ∼2009 as a function of time. Data from *ftp://ftp.ngdc.noaa.gov/stp/solar_data/sunspot_numbers/monthly.*

From observations of the monthly sunspot average it is evident that the Sun goes through a period of fewer and smaller sunspots called solar minimum and then a period of more and larger sunspots called solar maximum (e.g. Smith and Marsden 2003). This rise and fall in sunspot counts is referred to as a solar cycle with the length approximately ∼11 years on average. The period from 1755 to 1766 has been chosen as solar cycle 1. Solar cycle 22 began in ∼1986, reached its maximum in ∼1991 and ended in ∼1996. Solar cycle 23 began in ∼1996, reached its maximum in ∼2001 and ended in ∼2005. Solar cycle 24 began in ∼2005 and will reach its maximum soon.

2.5 The solar wind

The solar wind is the supersonic flow of fully ionized plasma from the solar corona outward. This plasmatic atmosphere of the Sun is constantly blowing away to maintain equilibrium (Parker 1958). The wind comprises ∼95% protons and electrons, ∼4.5% helium and other minor ions. Biermann (1951, 1961) proposed the solar wind to account for the behavior of comet tails which point directly away from the Sun. He suggested that the solar wind always exists and effects the formation of comet tails and also estimated the solar wind speed to be in the range of $\sim$ 400 - 700 km.s^{-1} at Earth.

There are two distinct types of solar wind speeds, the fast solar wind originating from

open magnetic fields in coronal holes (Krieger et al. 1973; Zirker 1977) with speeds up to ∼800 km.s^{-1} and the streamer belts that are regarded as the most plausible sources of the slow solar wind with typical velocities of up to ∼400 km.s^{-1} (Schwenn 1983; Marsch 1991; Withroe et al. 1992; McComas et al. 2000). Other indications are that the slow solar wind might arise from the edges of large coronal holes or from smaller coronal holes (e.g. Hundhausen 1977). In regions where the solar magnetic field is directed outward, such as the polar regions, the magnetic field will assist rather than oppose the coronal outflow and here a fast solar wind is expected. Figure 2.4 (from McComas et al. 2000) shows the latitudinal dependence of the solar

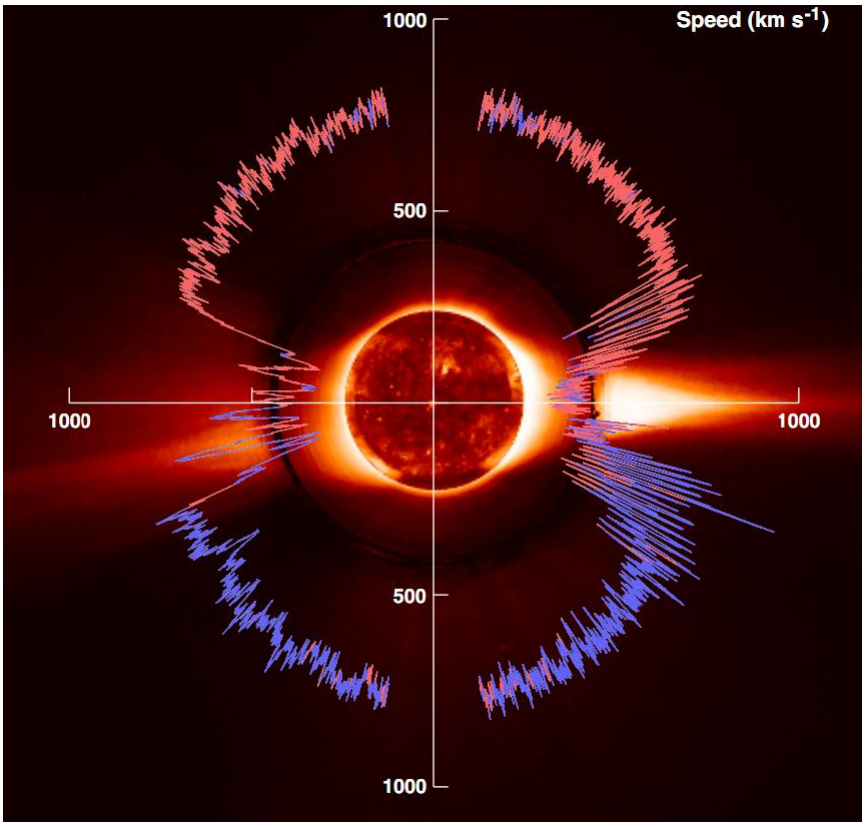

Figure 2.4: Ulysses observations of the solar wind. For reference the polar plot is overlaid with the SOHO LASCO/C2 and Mauna Loa MK3 Coronagraph images and with the SOHO EIT image of the solar disk (from McComas et al. 2000).

wind speed near solar minimum. The red and blue lines in the colour version of this figure show the solar wind speed for outward and inward magnetic field direction respectively.

Shown in Figure 2.5 are the solar wind speed variations with latitude for the three fast latitude scan (FLS) periods of the Ulysses spacecraft (data from *http://cohoweb.gsfc.nasa.gov/*). It is shown how the latitude dependence of the solar wind speed changes as a function of solar activity. Ulysses observed a fast speed wind, ∼800 km.s^{-1}, in both polar regions during the first (FLS1) and third (FLS3) fast latitude scan periods, both which occurred during moderate to minimum solar conditions. For the second fast latitude scan period (FLS2), which occurred during solar maximum, there is no well defined high speed solar wind (see also Richardson et al. 2001).

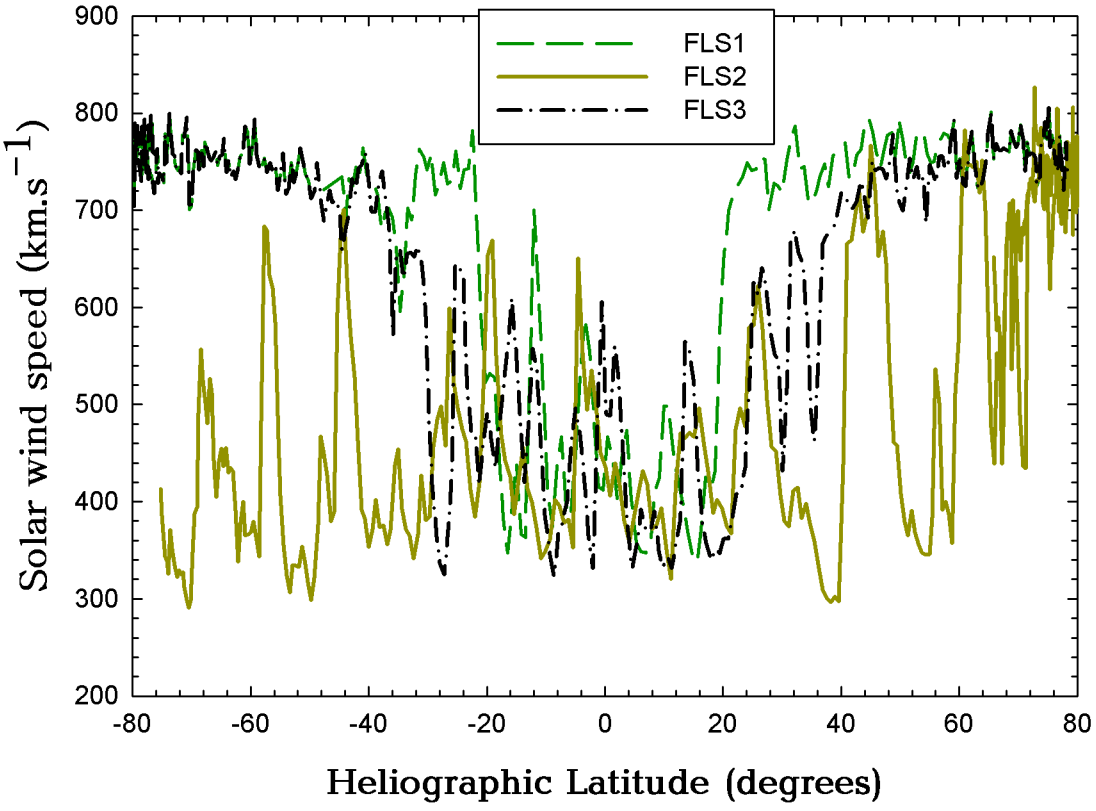

Figure 2.5: The solar wind speed as a function of heliographic latitude for the three fast latitude scan periods of the Ulysses spacecraft. The dashed dark green line indicates the FLS1 period while the solid dark yellow line indicate the FLS2 period and the black dashed dotted line indicate the FLS3 period. These scans took place in ∼1995, ∼2001 and ∼2007 respectively. Data from: *http://cohoweb.gsfc.nasa.gov/.*

In the cosmic ray modulation model, used in this work, the solar wind velocity $\vec{V}_{sw}$ is taken to be radial and it is assumed to have the form:

$$\vec{V}_{sw}(r,\theta) = V_r\,(r,\theta)\,V_\theta\,(\theta)\,\vec{e_r} \tag{2.1}$$

where r is the radial distance, θ the polar angle with $\vec{e_r}$ the unit vector in the radial direction, $V_r\,(r,\theta)$ is in units of km.s^{-1} while V_θ is a dimensionless function only resulting in a variation with polar angle. Recent observations from the Voyager spacecraft (Richardson et al. 2009) show that $\vec{V}_{sw}$ is already developing a latitudinal component at the Voyager 2 position. However, as argued by Strauss et al. (2010), Equation (2.1) is still a good approximation in the inner heliosheath, especially in the nose direction of the heliosphere. Since this study focuses on the inner heliosphere and is limited to high energy cosmic rays, Equation (2.1) is applicable.

The radial dependence of $V_r\,(r)$ follows from Hattingh (1998) and has the form

$$V_r(r) = 400\left\{1 - \exp\left[\frac{40}{3}\left(\frac{r_\odot - r}{r_0}\right)\right]\right\}\,\text{km.s}^{-1} \tag{2.2}$$

with $r_0 = 1$ AU and $r_\odot$ the radius of the Sun. The latitudinal dependence $V_\theta(\theta)$ of the solar wind speed during solar minimum conditions is also given by Hattingh (1998) and is

$$V_\theta(\theta) = 1.5 \mp \tanh\left[\frac{2\pi}{45}(\theta - 90^\circ \pm \psi)\right], \tag{2.3}$$

in the northern and southern hemispheres respectively with ψ taken as 35°.

2.6 The heliosphere

The heliosphere can be defined as the region of space influenced by the Sun and its expanding corona called the solar wind. The shape as well as the structure of the heliosphere is mainly determined by three components, which are: the local interstellar medium (LISM), the solar wind and the relative motion of the Sun with respect to the LISM (see e.g. Marsden 1986; Holzer 1989; Baranov 1990; Schwenn and Marsch 1991; Fahr and Fichtner 1991; Fichtner 1996).

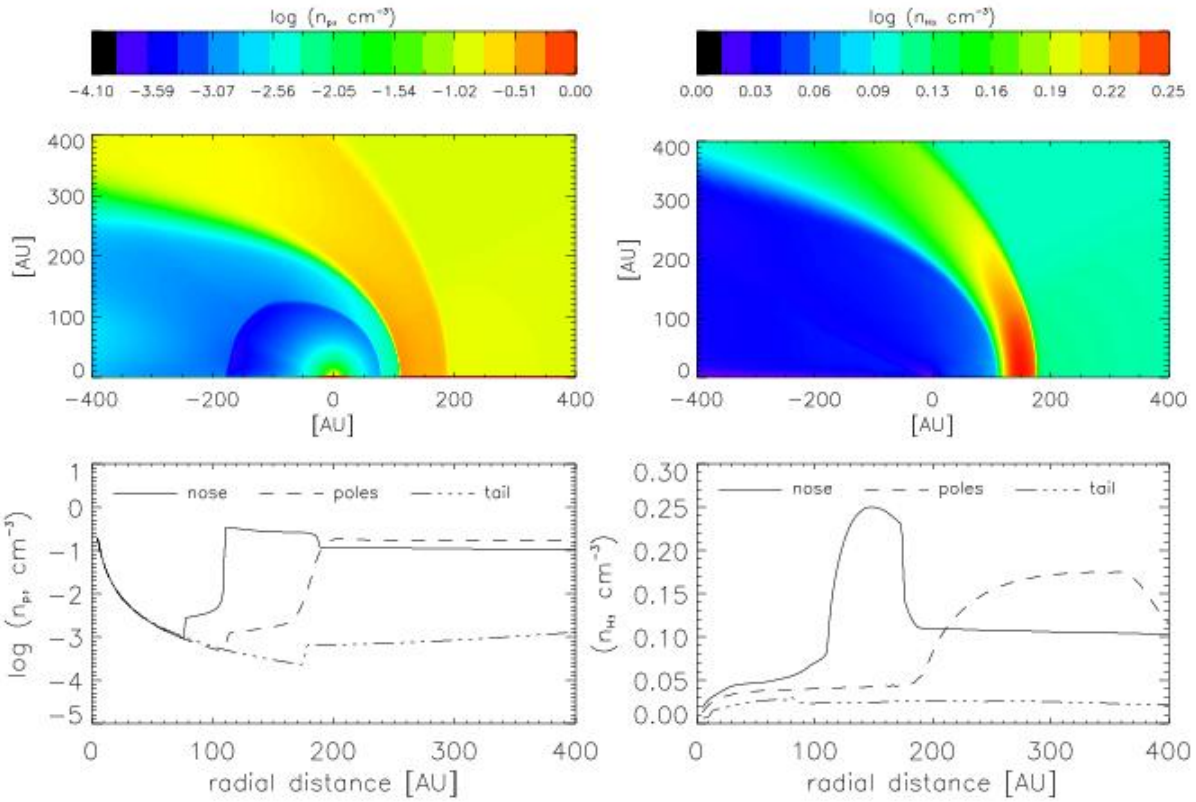

Figure 2.6: The computed heliosphere. Shown on the left is the solar wind-LISM density, n_p, and on the right the neutral H density, n_H, as particles per cubic centimetre. The top panels show the density as contours in the meridional plane, and the bottom panels show the radial profiles in the nose, poles and tail direction respectively (from Ferreira et al. 2007).

However, the LISM is partly ionized with an equal number of protons and hydrogen. This interstellar neutral hydrogen can charge exchange with the LISM protons. This usually occurs

in the nose of the heliosphere where the plasma has been decelerated and heated. Charge exchange with the interstellar protons leads to the formation of the high density region called the hydrogen wall (Baranov and Malama 1993, 1995; Zank and Pauls 1996). Neutral hydrogen atoms that pass through the heliopause into the heliosphere can also experience charge exchange with the subsonic solar wind and also with the supersonic solar wind (Baranov and Malama 1995; Zank and Pauls 1996; Fahr et al. 2000).

An illustration of the heliospheric structure in terms of number density is shown in Figure 2.6 (from Ferreira et al. 2007). The top panels of Figure 2.6 show the density as contours in the meridional plane and the bottom panels are the radial profiles in the nose, poles and tail direction respectively. Shown on the left is proton density, n_p, and on the right is the neutral hydrogen density, n_H, both as a function of radial distance. The solar wind speed, with temperature of 10^5 K, is $\sim$400 km.s^{-1} at all latitudes and the LISM speed is $\sim$26 km.s^{-1} with a temperature of 8000 K. Shown here is that due to the supersonic motion of the heliosphere in the interstellar plasma, a bow shock forms which decelerates and deflects the interstellar charged particles. Also the solar wind outflow is supersonic which leads to the formation of a termination shock discussed below.

The inclusion of neutral hydrogen in the model reduces the size of the heliosphere because of the removal of momentum from the supersonic solar wind by charge-exchange (Zank and Pauls 1996; Fahr and Lay 2000). Apart from the asymmetry due to the movement through the LISM, the heliosphere is also elongated toward the poles (e.g. Pauls and Zank 1996, 1997; Scherer and Ferreira 2005, Opher et al. 2009). For solar minimum conditions, the elongation of the heliosphere is expected to be more pronounced because of the latitudinal variation of the solar wind speed (Phillips et al. 1995; McComas et al. 2000).

An indirect influence on the structure of the heliosphere arises from neutral atoms getting ionized, and "picked up" by the solar wind (e.g. Rucinski et al. 1996; Fahr et al. 2000). These pick-up ions affect the heliospheric geometry, because they cause deceleration of the solar wind via mass and momentum loading. In other words, the presence of the pick-up ions (PUIs) lowers the effective Mach number upstream of the heliospheric shock and changes the compression ratio from $\sim$4 (as expected from standard hydrodynamics) to $\sim$3.4. Generally it can be said that the presence of neutral atoms and the associated PUIs tends to smooth the structure of the heliosphere and also reduces its size (e.g. Fichtner and Scherer 2000).

The $\sim$26 km.s^{-1} laminar LISM flow is commonly believed to be supersonic, although in principle it could be subsonic if the poorly known ISM magnetic field is strong enough (Zank and Pauls 1996). Nevertheless, most heliospheric models in the past assumed the existence of a bow shock where the LISM flow is shocked to subsonic speeds (see Figure 2.6). However, of importance is the effect of the interstellar magnetic field pressure on the heliospheric geometry. Opher et al. (2009) suggested a possible asymmetry in the heliosphere due to the pressure of the interstellar magnetic field (see also Pogorelov et al. 2008). If the angle between the interstellar magnetic field and the interstellar velocity is not zero, the external magnetic pressure

can break the axial symmetry of the heliosphere.

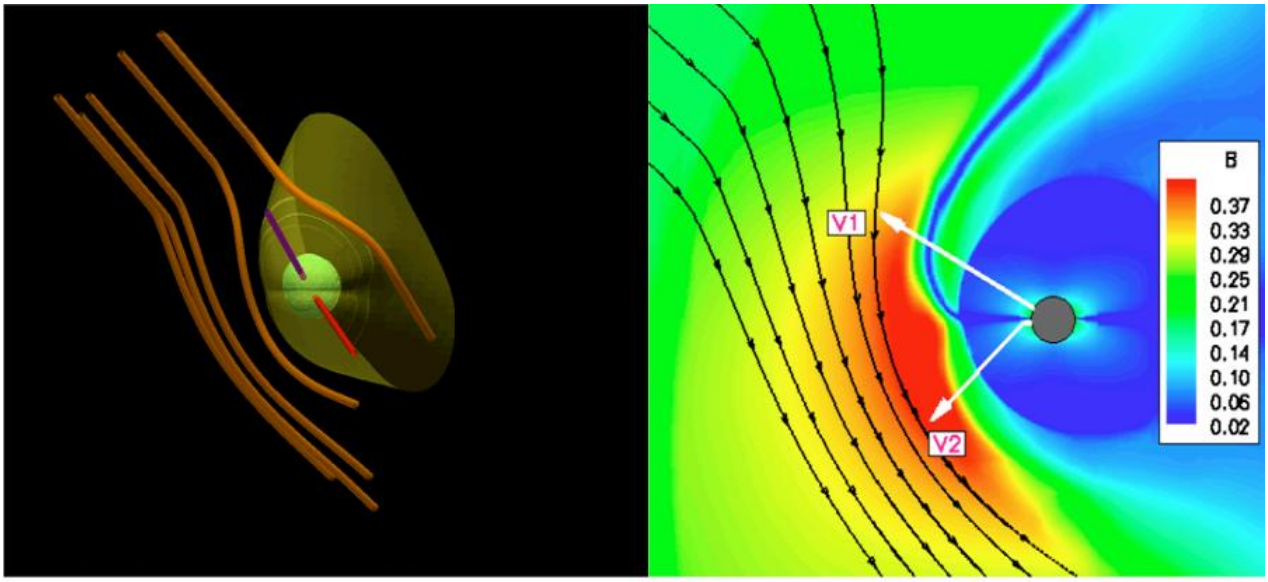

Figure 2.7: (a) An example of a computed heliosphere which is strongly influenced by the interstellar magnetic field direction (b) The effects of the piling up of the interstellar magnetic field, with the corresponding pressure larger at the southern rather than the northern hemisphere. The trajectories of the Voyager 1 and 2 spacecraft are indicated. From Opher et al. (2006).

In this case, the heliopause is distorted by the pressure of the local interstellar magnetic field, as shown in Figure 2.7 (from Opher et al. 2006). The orange field lines in Figure 2.7 (left hand) are the interstellar magnetic field lines.

The transition from supersonic to subsonic occurs at a shock called the termination shock (TS). This is of special importance to cosmic ray studies because of the acceleration of low energy particles. In 2004, Voyager 1 passed the TS at a distance of ∼94 AU from the Sun in the upwind direction of the LISM flow (Decker et al. 2005; Burlaga et al. 2005; Stone et al. 2005). Indications of this crossing were already seen years prior to the crossing (Krimigis et al. 2003 and Burlaga et al. 2003). Voyager 2 crossed the TS in August 2007 at a distance of ∼84 AU (Burlaga et al. 2008; Decker et al. 2008a; Richardson et al. 2008a; Stone et al. 2008) providing us for the first time with in-situ measurements of the subsonic flows in the heliosheath. The difference in position between these two crossings shows that there is a time-dependence in the position of the shock and a possible asymmetry (Burlaga et al. 2008).

For the heliopause and bow shock, recent models predict upwind distances of ∼140 AU to ∼240 AU. The heliopause is considered to be the outer boundary of the heliosphere. It is expected that neither of the Voyager spacecraft may survive long enough to get far beyond the heliopause. In this study the boundary of the heliosphere is assumed to be at 120 AU, and the effect of the TS is neglected because the focus is on modeling only the high energy galactic

cosmic rays which are generally not strongly influenced by the presence of a shock, especially at the energies considered here.

2.7 The heliospheric magnetic field

The plasmatic atmosphere of the Sun, which constantly blows radially outward, carries with it the Sun's magnetic field. This field is dragged into outer space forming the HMF. This field changes polarity during each solar maximum. Although the solar wind moves out almost radially from the Sun, the rotation of the Sun gives the magnetic field a spiral form as shown in Figure 2.8.

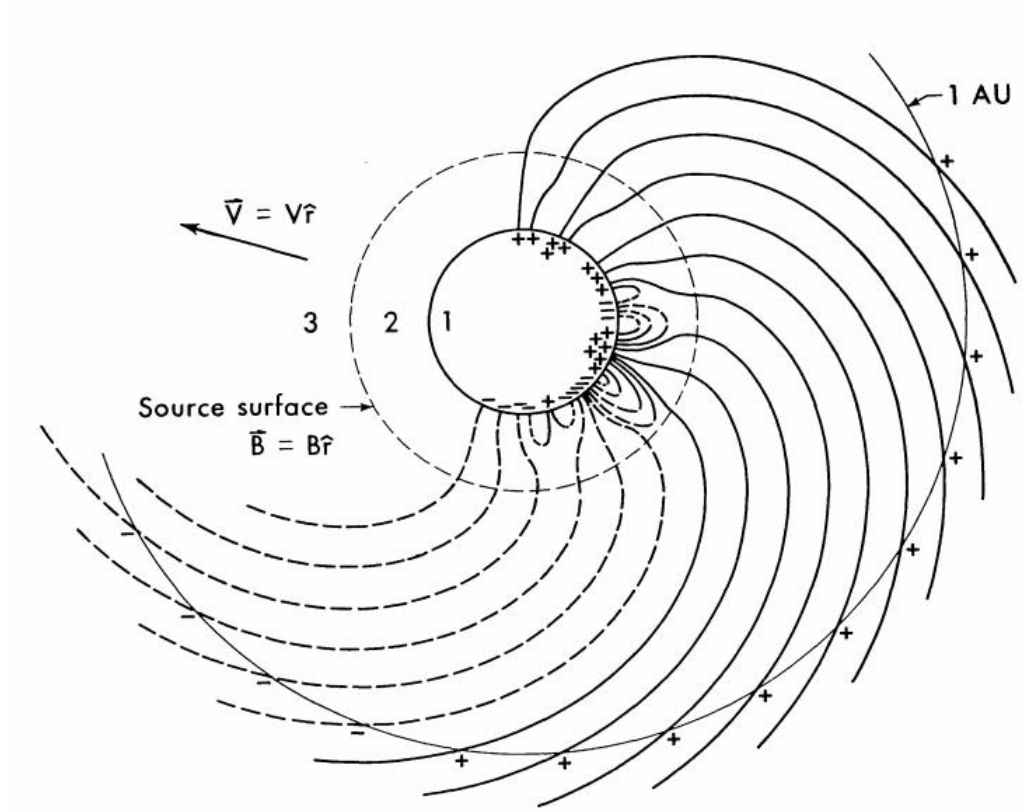

Figure 2.8: Schematic representation of the HMF. The photospheric magnetic field is shown in region 1. Closed field lines (loops) exist in region 2. The field in this region is calculated from potential theory. Currents flowing near the source surface eliminate the transverse components of the magnetic field, and the solar wind extends this field into interplanetary space (region 3). The magnetic field can then be observed by spacecraft near 1 AU. The + and - signs show regions of opposite HMF polarity (from Schatten 1972).

The distance where the field becomes a spiral is indicated by the dashed circle in Figure 2.8 and is called the source surface which lies at a distance of about 2.5 $r_\odot$ (e.g. Wang and Sheeley 1995). An analytical equation for the Parker spiral for $r \geq r_\odot$ was first derived by Parker (1958) as

$$\vec{B} = B_0 \left(\frac{r_0}{r}\right)^2 (\vec{e_r} - \tan\psi \vec{e_\phi}) \tag{2.4}$$

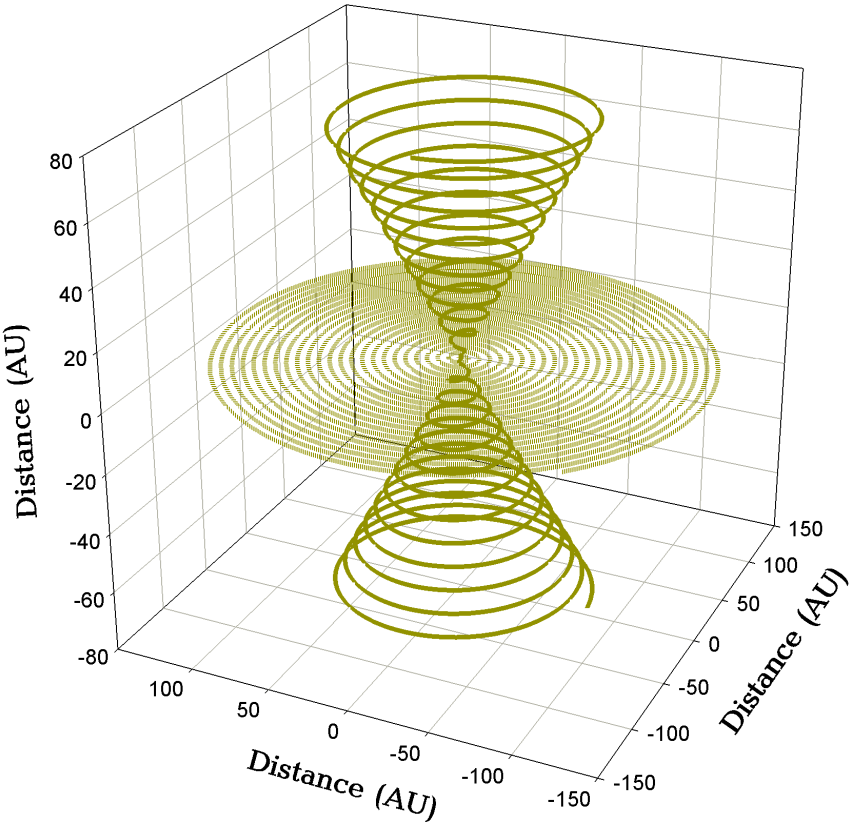

Figure 2.9: The Parker spiral which rotates around the polar axis at $\theta = 45°$, $\theta = 90°$ and $\theta = 135°$ respectively, with the Sun at the origin.

where $\vec{e_r}$ and $\vec{e_\phi}$ are unit vector components in the radial and azimuthal direction respectively, B_0 is the value of the HMF at Earth, r_0 =1 AU, and ψ is the spiral angle between the radial direction and the average HMF at certain position, giving an indication of how tightly wound the magnetic field is.

The spiral angle is given by

$$\tan\psi = \frac{\Omega\left(r - r_\odot\right)\sin\theta}{V}. \tag{2.5}$$

A three dimensional representation of the Parker HMF is shown in Figure 2.9. The spirals rotate around the polar axis with θ = 45°, θ = 90° and θ = 135° respectively. Here the angular speed of the Sun is Ω and $r_\odot$ is the solar radius. Substituting Equation (2.5) into (2.4) yields the magnitude of the HMF spiral structure throughout the heliosphere given by

$$B = B_0\left(\frac{r_0}{r}\right)^2\sqrt{1 + \left(\frac{\Omega\left(r - r_\odot\right)\sin\theta}{V}\right)^2}. \tag{2.6}$$

A modification to this equation was proposed by Jokipii and Kota (1989). They argued that the solar surface is not smooth but turbulent, and this may cause the foot points of the polar field lines to wander randomly, creating transverse components in the field. This causes deviations from the smooth Parker geometry with the effect of increasing the mean magnetic field strength. These authors suggested Equation (2.6) to be modified as

$$B_m = B_0 \left(\frac{r_0}{r}\right)^2 \sqrt{1 + \left(\frac{\Omega\left(r - r_\odot\right)\sin\theta}{V}\right)^2 + \left(\frac{r\delta_m}{r_\odot}\right)}. \tag{2.7}$$

The modification is applied by changing δ_m where δ_m = 0 for the standard Parker geometry. Although there are other proposed modifications, in this study Equation 2.7 is used, with $\delta_m = 0.002/sin\theta$, similar to the value used in Langner (2004) and Haasbroek (1993).

Fisk (1996) suggested an alternative to the Parker field. In a Fisk-type field, magnetic field lines exhibit extensive excursions in heliographic latitude, and this has been cited as a possible explanation for recurrent energetic particle events observed by the Ulysses spacecraft at high latitudes (see e.g. Simpson et al. 1995; Zhang 1997; Paizis et al. 1999), as well as the smaller than expected cosmic-ray intensities observed at high latitudes (Simpson et al. 1996).

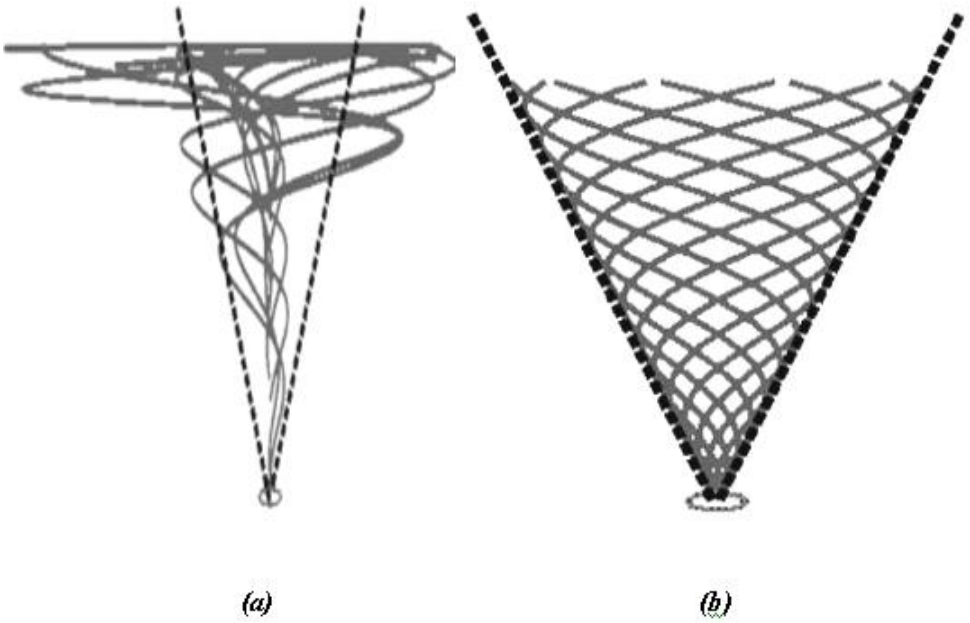

Figure 2.10: These diagrams compare (a) Fisk's new model of the Sun's magnetic field, which shows the heliospheric magnetic field assuming differential rotation. (b) Standard Parker field from Parker (1958). The small circle at the base of each diagram represents Earth's path around the sun. From Zurbuchen et al. (1997).

The Fisk field (see Figure 2.10) and the physics behind it have been discussed in various papers (e.g. Fisk and Schwadron 2001 and Burger et al. 2008). Over the last ten years various attempts have been made to incorporate the Fisk field into numerical modulation models (Kota

and Jokipii 1999; Burger and Hattingh 2001; Burger and Hitge 2004). A recent overview was given by Burger (2005). Recently Burger et al. (2008) presented a Fisk-Parker hybrid field where at high latitudes the field is a mixture of a Fisk field and a Parker field, but in the equatorial region it is a pure Parker field. They confirmed the result of Burger and Hitge (2004) that a Fisk-type heliospheric magnetic field provides a natural explanation for the observed linear relationship between the amplitude of the recurrent cosmic-ray variations and the global latitude gradient as first reported by Zhang (1997). See also Sternal (2010).

2.8 The heliospheric current sheet

The existence of the heliospheric current sheet (HCS), has been known since Wilcox and Ness first identified it three decades ago (Wilcox and Ness 1965). Many of its characteristics have been reported since then, e.g. its large-scale three-dimensional nature (Smith et al. 1978; Klein and Burlaga 1980; Thomas and Smith 1981), its evolution with solar cycle (Hoeksema et al. 1983), and its latitudinal extent (Smith et al. 1978).

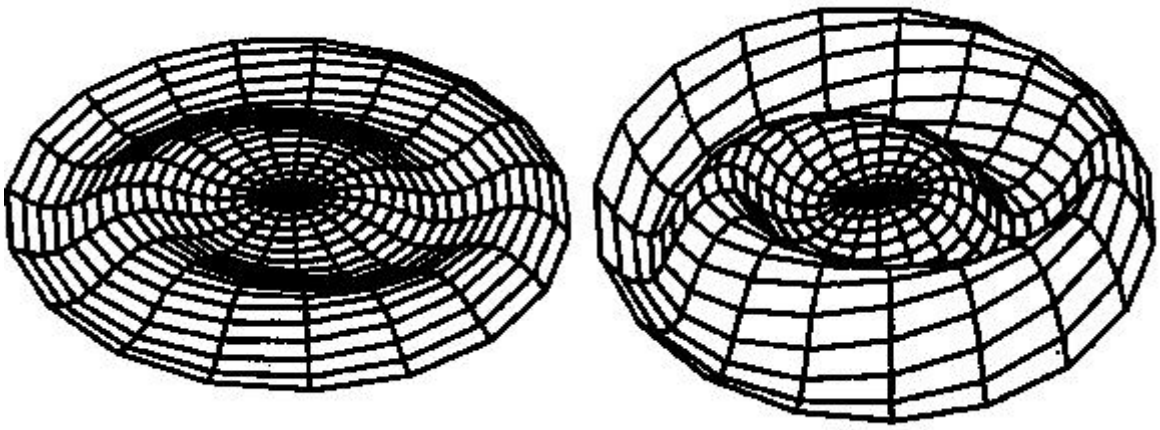

Figure 2.11: A three-dimensional visualization of the wavy HCS to a radial distance of 10 AU with tilt angle of $\alpha = 5°$ (solar minimum activity, left panel) and $\alpha = 20°$ (low to moderate activity, right panel). The Sun is at the centre (from Haasbroek 1997).

The HCS is a narrow plasma layer that divides the heliosphere into regions of different magnetic polarity (Czechowski 2010). Zhou et al. (2005) described the current sheet as a very thin layer of $\sim 10^3$ to 10^4 km. The shape of the HCS is determined by plasma convection (see e.g. Smith 2001, 2008) of the solar wind.

The tilt angle α of the HCS is defined as the mean of the maximum northern and southern extensions of the HCS. The tilt angle is an important parameter for the modulation of galactic cosmic rays in the inner heliosphere (Kota and Jokipii 1983; Ferreira and Potgieter 2004; Alanko-Huotari et al. 2007; Heber et al. 2009). The HCS oscillates about the heliographic

equator to form a series of peaks and troughs as shown in Figure 2.11 (from Haasbroek 1997).

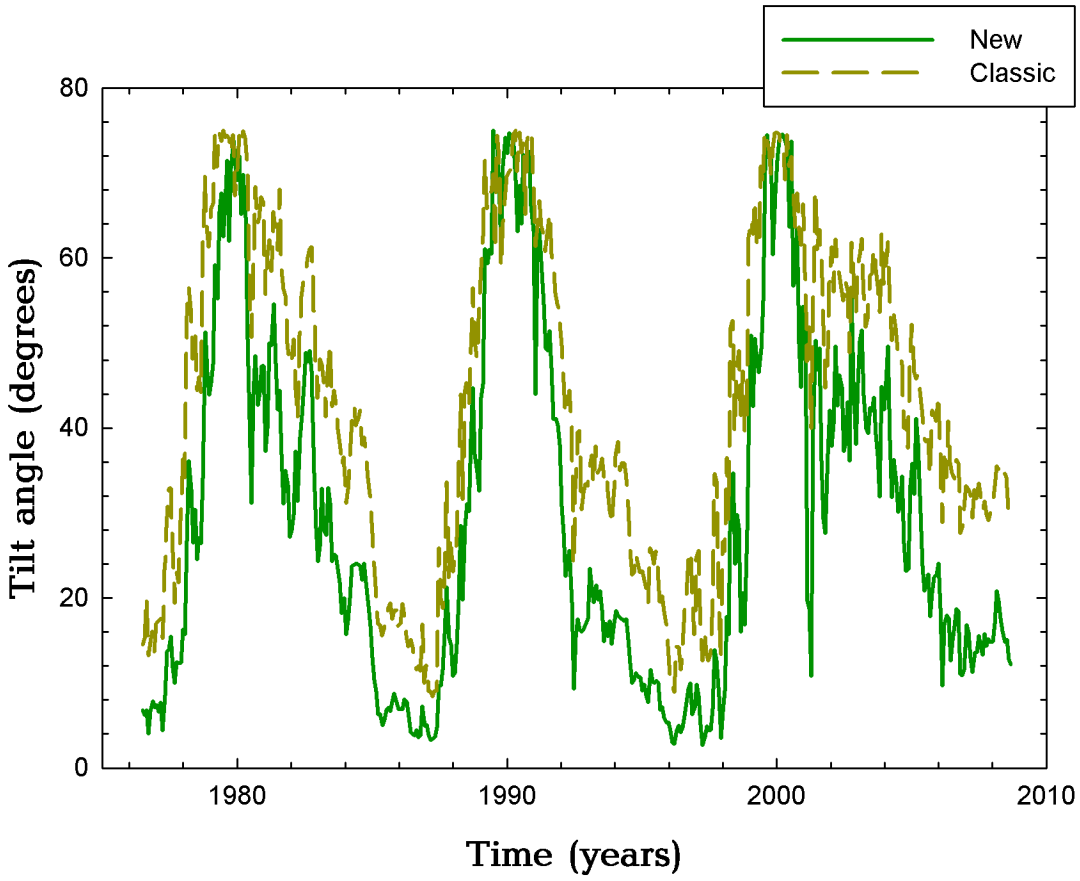

Figure 2.12: Variation of the tilt angle from 1976 up to 2008 (Hoeksema 1992). Two different models for the tilt angle are shown namely the "classic" and "new" model respectively. The classic model uses line-of-sight boundary conditions and the new model uses radial boundary conditions at the photosphere for calculations (data from *wilcox solar observatory, http://stanford.edu*).

$$\theta' = \frac{\pi}{2} + \sin^{-1}\left\{\sin\alpha \sin\left[\phi + \frac{\Omega\,(r - r_0)}{V}\right]\right\} \tag{2.8}$$

Due to the radially out-flowing solar wind the HCS is dragged into the heliosphere. In a constant and radial solar wind the HCS satisfies the Equation (2.8) by Jokipii and Thomas (1981), where r, θ and ϕ are spherical polar coordinates relative to the Sun's rotation axis, α is a tilt angle and Ω is the angular rotational velocity of the Sun. Because the model used is 2-D one has to simulate the effects of this current sheet. This was first done by Potgieter and Moraal (1985) and improved by Burger and Hattingh (1995) by replacing the 3-D drift velocity field by a 2-D drift field as will be shown in detail in Chapter 3. As shown by Ferreira et al. (1999) this approach used in a cosmic ray modulation model results in intensities comparable to a full 3-D model incorporating an actual HCS.

The tilt angle α changes with time, e.g. α = 5° - 10° for typical solar minimum conditions and increases its waviness to α >∼70° in maximum solar activity. Figure 2.12 shows

the tilt angle from 1976 until 2008 (Hoeksema 1992) (data from from Wilcox Solar Observatory, *http://stanford.edu*). Two different models are shown e.g. the "classic" and "new" model. The classic model uses line-of-sight boundary conditions while the new model uses radial boundary conditions at the photosphere to calculate values (Wilcox solar observatory: *http://sun.stanford.edu*). This figure shows that the tilt angle, from both models, varies from $\sim<$ 5° at solar minimum and increases to $\geq$ 70° with maximum solar activity. For some periods there is a large difference between the two models compared to other periods. The new model results in smaller angles than the classical model, especially between ∼1994 and ∼2000 and also more recently, from ∼2001 to ∼2008.

2.9 Solar cycle related changes in the heliospheric magnetic field

Already discussed above, the Sun moves through a period of fewer and smaller sunspots called solar minimum, and a period of larger and more sunspots called solar maximum. On top of this the magnitude of the measured magnetic field at Earth, $B\,(t)$, is also varying over a solar cycle. Figure 2.13 shows 26 day averages of the heliospheric magnetic field where it varies with time as measured at Earth (Data were obtained from *www.nssdc.gfc.nasa.gov/cohoweb*).

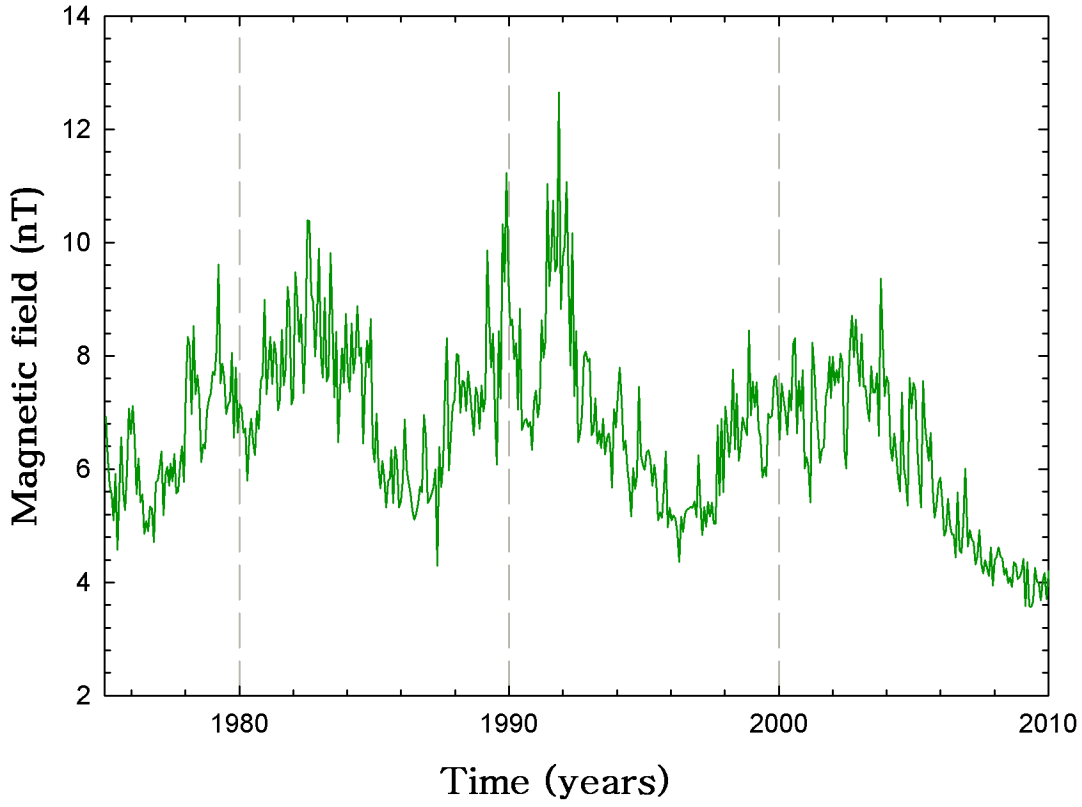

Figure 2.13: The 26 day omni data average of the HMF measured at Earth from 1975 to early 2010. (Data from *www.nssdc.gfc.nasa.gov/cohoweb*).

Shown here is that $B(t)$ is factor of $\sim$2 larger at solar maximum compared to solar minimum conditions. The polar magnetic field strength also varies with time as shown in Figure 2.14. This figure shows the polar field strength for both the southern and the northern poles of the Sun respectively. Data are from the year 1975 to 2010. Taken from *http://quake.stanford.edu/*. The field strengths show maximum value of $\sim$1-2 G ($\sim$1-2$\times 10^{-4}$ T) near solar minimum but decreases toward solar maximum and then reverses polarity. In the 1990's the field is positive over the northern and negative over the southern polar regions and vice versa in the 1980's and 2000's. The shaded regions in Figure 2.14 show the time periods where the solar polar field at both the southern and northern solar poles reverses e.g. when there is no well defined polarity in both hemispheres (e.g. Svalgaard and Wilcox 1974).

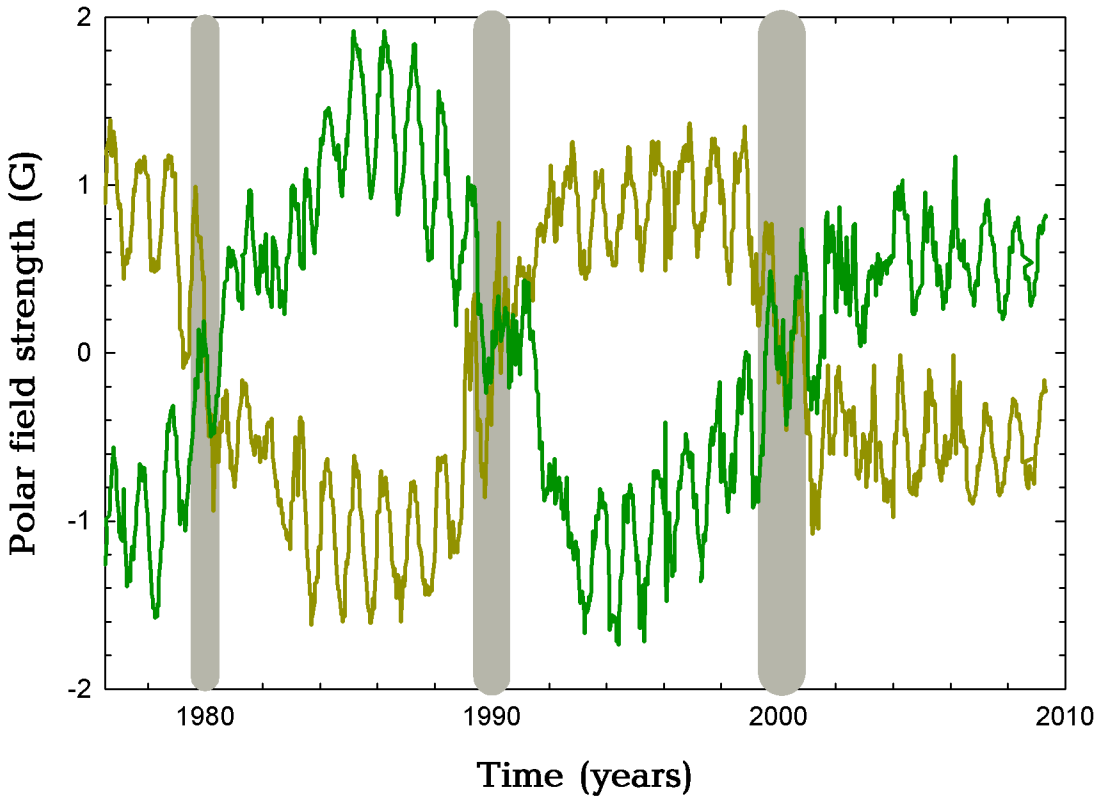

Figure 2.14: The solar polar magnetic field strength for both the northern and southern polar cap represented by the thick dark yellow and dark green lines respectively. The shaded regions are the time periods where the field has no well defined polarity. Data from the Wilcox Solar Observatory (http://quake.stanford.edu/).

2.10 Spacecraft missions

Different spacecraft missions are in operation and send information of the heliosphere and cosmic ray background to the Earth. This assists us in understanding the different regions

of the heliosphere. In this section, the Ulysses spacecraft, with the Kiel Electron Telescope (KET), and the PAMELA spacecraft missions, are briefly discussed. The observations used in this study are from the KET on board Ulysses. These observations are compared with model results in later chapters. The PAMELA mission is briefly discussed because results from this work may assist in understanding observations from this spacecraft in more detail in future.

2.10.1 The Ulysses mission

Previous spacecraft remained near the equatorial plane, while the Ulysses spacecraft had an orbit perpendicular or highly inclined to the heliospheric equatorial plane. The primary objective of this spacecraft was to gain definitive knowledge, by means of in-situ observations, of conditions and processes occuring in the inner heliosphere. In the process first-hand knowledge concerning the high latitudes of the inner heliosphere can be obtained (Heber et al. 1997). Objectives are listed and described by Wenzel et al. (1992).

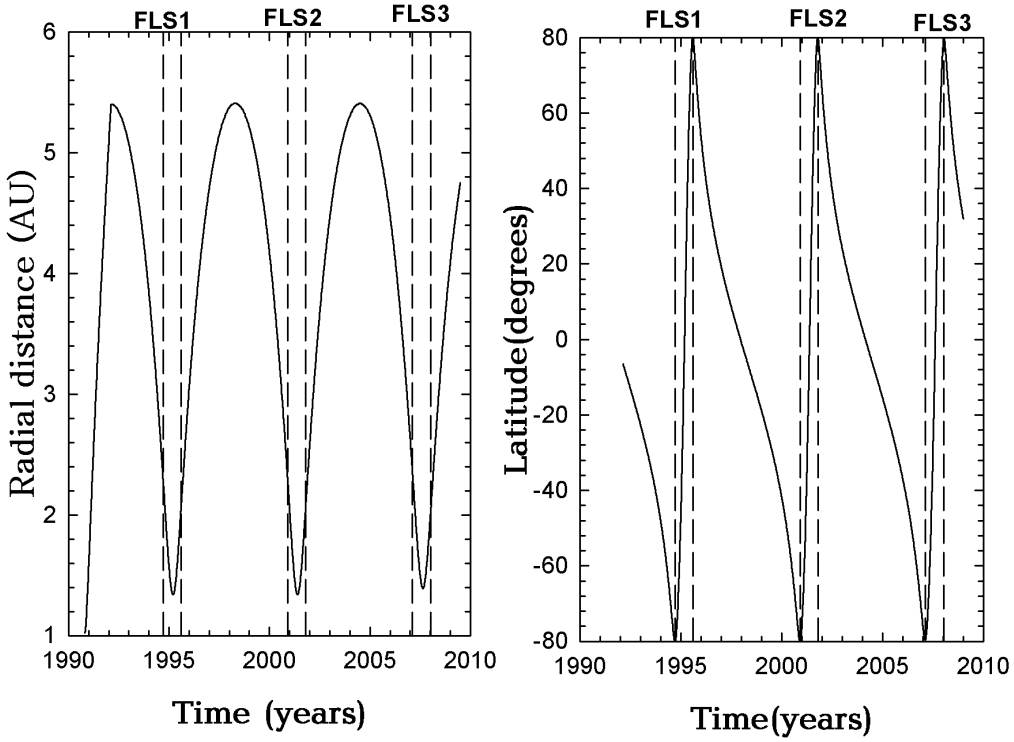

Figure 2.15: The radial (left panel) and the the latitudinal (right panel) components of the Ulysses spacecraft trajectory from early 1990s till recently. Shown by vertical lines are the three fast latitude scan periods of the spaceccraft (FLS1, FLS2 and FLS3) (Data from *http://cohoweb.gsfc.nasa.gov*).

Since its launch Ulysses had orbited the Sun's polar caps three times, first during solar minimum in 1995 and then during solar maximum in 2001 and recently during solar minimum to moderate solar conditions in 2007. These are referred to as the first (FLS1), second (FLS2) and third (FLS3) fast latitude scan periods.

The recent third fast latitude scan occurred under very different circumstances compared to the first, because of the reversal of the magnetic poles of the Sun. Recently, instruments on board this spacecraft reported the lowest solar wind densities ever measured (McComas et al. 2008; Issautier et al. 2008). In addition, the magnetic field magnitude was found to be lower than in the previous solar minimum (Smith and Balogh 2008). For an overview on this, see publications by Marsden (2001), Balogh et al. (2001), Smith and Marsden (2003) and Heber et al. (2009).

Shown in Figure 2.15 are the radial distance and heliographic latitude of the Ulysses spacecraft trajectory. Ulysses was launched on October 6, 1990 before the declining phase of the solar cycle 22 (Heber et al 2009). From launch it moved in the ecliptic plane to Jupiter and it then moved to higher latitudes south of the ecliptic plane. Ulysses reached its first southern heliographic latitude in September 1994 and within a year the spacecraft moved to the northern heliographic region. This is called the first fast latitude scan (FLS1) period of the spacecraft, indicated by the dashed lines in Figure 2.15. This occurred during solar minimum conditions. This rapid scanning in latitude was also repeated in ∼2001 (FLS2) and recently in ∼ 2007 (FLS3) which happened during the solar maximum and solar minimum respectively. Thus, Ulysses first and third fast latitude scans occurred at minimum to moderate solar conditions, but for different magnetic polarity cycles while the second occurred in solar maximum conditions.

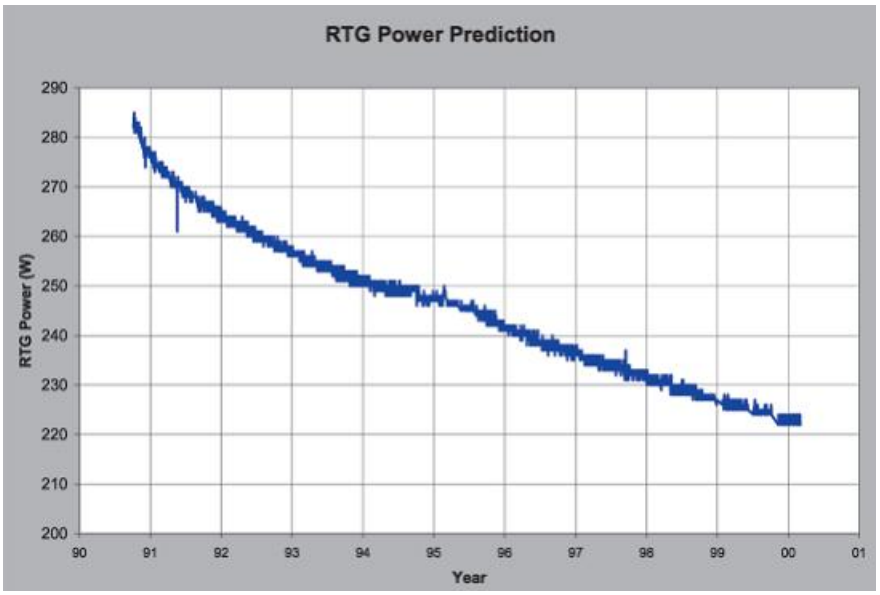

Figure 2.16: The power output of the Radioisotope Thermoelectric Generator (RTG) on board Ulysses (from Marsden 2000).

The Ulysses spacecraft proved to be highly reliable with remarkably few in-orbit anomalies during the past 10 years (Marsden 2000). The power source of the spacecraft was a Radioisotope Thermoelectric Generator (RTG) and its output decayed exponentially with time as shown in Figure 2.16. Delivering 285 W at launch, the RTG provided only 223 W in 2000. Because of this trend, maintaining an acceptable thermal balance while ensuring data return from all of the experiments has become a challenge. After 18 years of operations the Ulysses

spacecraft officially ceased operations on Tuesday, June 30, 2008 (*http://www.astronomy.com*).

2.10.2 The Kiel Electron Telescope (KET)

The Kiel Electron Telescope (KET), Figure 2.17 was part of the Ulysses cosmic ray and solar particle investigation (COSPIN) experiment, which was described in detail by Simpson et al. (1992). The KET measured protons and helium in the energy range from a few MeV/nucleon to above 2 GeV/nucleon and electrons in the energy range from of a few MeV to a few GeV to determine the energy spectra of cosmic rays using particle energy loss and particle velocity measurement techniques (Simpson 1992).

The telescope has three particles channels, measuring cosmic rays (e.g. Heber et al. 1996, Heber et al. 1997 and Heber et al. 2009). In Figure 2.17 we show a sketch of the KET telescope, which is said to have two parts which are the entrance telescope which has semiconductor detectors shown by D1 and D2, the cherenkov detector C1, and the anticoincidence A. The calorimeter consists of a lead fluoride cherenkov detector C2, in which an electromagnetic shower can develop, and a scientillation detector S2 which counts the number of charged particles leaving from C2 (Heber et al. 1999).

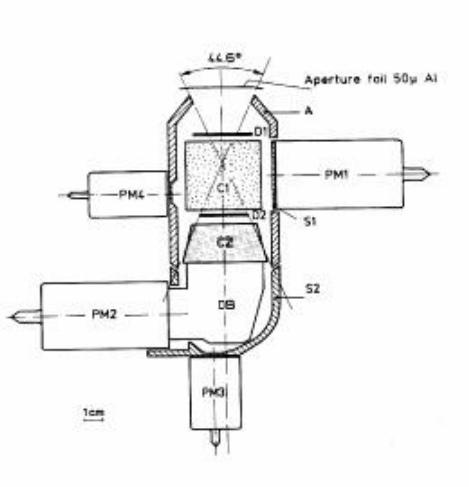

Figure 2.17: The KET sensor apparatus (Heber et al. 1999).

2.10.3 Payload for Antimatter/Matter Exploration and Light-nuclei Astrophysics (PAMELA) Spacecraft

The PAMELA detector, shown in Figure 2.18, was launched into low-Earth orbit on board the Resurs-DK1 satellite on 15 June, 2006 and started operation on 21 September 2006. The spacecraft had a launch mass of ∼6650 kg and a payload of ∼1200 kg and its height is ∼7.4 m. The PAMELA detector measures charged particles and it can distinguish electrons from positrons and protons from antiprotons (Adriani et al. 2009). During its first ∼2 years of

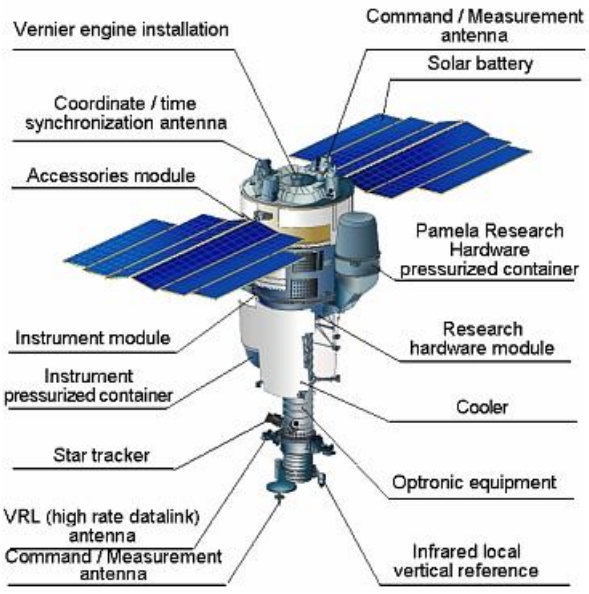

Figure 2.18: The PAMELA detector shown on board the Russian satellite. From *http://pamela.roma2.infn.it/index.php*.

data collection a total of $\sim$1000 antiprotons were identified, these included 100 in total with energy of $>\sim$20 GeV. The high energy results are tenfold improvement in statistics with respect to all previously published data of other spacecraft missions. Table 2.1 shows the PAMELA measurements of particles and the energy ranges. Some of the objectives of the PAMELA experiment are:

1. To measure in great detail, cosmic rays at Earth. Its orbit along the polar regions makes it particularly suited to study particles of galactic and heliospheric origin.

2. To search for the dark matter annihilation effects e.g. the primary black holes evaporation and also study the variations of the terrestrial radiation belts; the energetic secondary particles trapped by the magnetosphere in correspondence to the different solar events especially in the South Atlantic Anomaly region.

3. To study the existence of the nearby electron and positron sources.

4. Moreover, PAMELA is extending the observational limit in the search of antihelium to the $\sim 10^{-8}$ level in the antihelium-to-helium fraction and it is searching for exotic matter in the Universe.

5. Finally, the satellite orbit spans a significantly large region of the Earth's magnetosphere, making possible a study of its effect on the incoming radiation.

Table 2.1: Energy ranges of PAMELA measurements

Particle	Energy Range
Antiprotons	$\sim$ 80 MeV-190 GeV
Positrons	$\sim$ 50 MeV-300 GeV
Electrons	$\sim$ 50 MeV-$\sim$ 500 GeV
Protons	$\sim$ 80 MeV-$\sim$ 1 TeV

2.10.4 Summary

In this chapter background regarding cosmic ray modulation in the heliosphere was given. Cosmic rays include GCRs, which are believed to originate from sources outside our solar system, the anomalous cosmic rays (ACRs) originating in the heliosheath, solar energetic particles, which are believed to originate from solar flares and the Jovian electrons, which originate from the Jovian magnetosphere. In this work focus will be on modeling galactic cosmic rays.

Important concepts regarding cosmic ray modulation were given. These include a description of our nearest star the Sun and the supersonic solar wind, which when expanding into outer space creates a bubble around the Sun called the heliosphere. The transition of the solar wind to subsonic speeds occurs at a shock called the termination shock (TS). This shock was measured by Voyager 1 to be at $\sim$94 AU and by Voyager 2 to be at $\sim$83 AU. The difference in position between these two crossings shows that there is a time-dependence in the position of the heliosphere. Furthermore Opher et al. (2009) suggested the symmetry of the heliosphere to be caused by the pressure from the interstellar magnetic field.

A short description of the magnetic field of the Sun, which when carried into the heliosphere embedded in the solar wind forms the HMF, was also given. This field determines the passage of cosmic rays on their way into the heliosphere. During this process their intensities are changed as a function of time, energy and position, a process called cosmic ray modulation. A short description of the HCS which divides the HMF into hemispheres of opposite polarity was given. This sheet changes its waviness with solar activity. It serves as an important proxy for solar activity to understand the modulation of cosmic rays. Lastly a short description of the spacecraft missions, i.e the Ulysses mission and the PAMELA mission, were given.

Chapter 3

Cosmic ray transport and modulation models

3.1 Introduction

Galactic cosmic rays enter the heliosphere and diffuse inward toward the Sun by gyrating around the heliospheric magnetic field (HMF) and scatter at irregularities in the field. They also experience gradient and curvature drifts (Jokipii 1974; Isenberg and Jokipii 1979; Potgieter and Moraal 1985) and are convected back toward the boundary by the solar wind. During this process the particles also lose energy through adiabatic cooling (deceleration) and may also be accelerated at solar wind termination shock (TS) via diffusive shock acceleration.

Additional acceleration like adiabatic heating (see e.g. Fahr and Lay 2000; Florinski et al. 2004; Langner et al. 2006 a,b; Ferreira et al. 2007) and stochastic acceleration (Fisk and Gloeckler 2006; Ferreira et al. 2007; Moraal et al. 2008; Strauss et al. 2010) may also occur. The combined effect of all these processes is known as the modulation of cosmic rays in the heliosphere where particle intensities are changed as a function of position and energy compared to the unmodulated local interstellar spectrum. All these processes were combined by Parker (1965) into a transport equation (TPE) which is the basis of modulation models used to compute cosmic ray transport and acceleration inside the heliosphere.

3.2 The transport equation and the diffusion tensor

Cosmic rays entering the heliosphere experience different modulation processes in which their intensities are changed as a function of time, position and energy. These modulation processes were combined into one equation introduced by Parker (1965) called the Parker transport equation and is given as

$$\frac{\partial f}{\partial t} = -\left(\vec{V} + \langle \vec{V}_D \rangle\right) \cdot \nabla\, f + \nabla \cdot (\mathbf{K}_s \cdot \nabla\, f) + \frac{1}{3}\left(\nabla \cdot\, \vec{V}\right) \frac{\partial f}{\partial \ln P} + J_{source} \tag{3.1}$$

In Equation (3.1), $f(\vec{r}, P, t)$ is the omnidirectional cosmic ray distribution function, $\vec{r}$ is the position, t is the time and P is the rigidity. The rigidity is defined as the momentum per charge of the particles, given by $P = pc/q$ in GV, with p the particle's momentum, q the charge and c the speed of light in space. $\vec{V}$ is the solar wind velocity and J_{source} is the source function. $\mathbf{K}_s$ is the diffusion tensor describing the diffusion processes and $\vec{V}_D$ is the drift velocity. The TPE includes the following processes:

1. The first term on the right describes the outward particle convection due to the radially outward blowing solar wind, as well as the particle drifts in the background magnetic field.
2. The second term on the right describes the spatial diffusion parallel and perpendicular to the average magnetic field.
3. The third term on the right describes the energy changes. Because the study is limited to high energy cosmic rays it is assumed that these are only adiabatic in nature.
4. The last term J_{source} is any source function which is assumed to be zero in this study.

Equation (3.1) contains all relevant physics to describe CR transport and acceleration in the heliosphere (see Potgieter 1995, 1998; Fichtner 2005 and Heber and Potgieter 2006 for a detailed discussion) and is generally solved numerically in so called modulation models, which are discussed next.

3.3 Modulation models

A numerical approach to describe cosmic ray modulation was developed first by Fisk (1971) in a steady-state e.g $\partial f/\partial t = 0$ in Equation (3.1) and for spherically symmetric heliosphere (1-D) without drift effects. A 2-D model without drifts was developed by Moraal and Gleeson (1975) and Cecchini and Quenby (1975). A spherically symmetric time-dependent model was developed by Perko and Fisk (1983). The model was later on improved by le Roux (1990) to two dimensions including drifts to study the longterm cosmic ray modulation (see e.g. Potgieter and le Roux 1994; le Roux and Potgieter 1995).

A numerical model, which includes curvature and gradient drifts was developed by Jokipii and Kopriva (1979) and Moraal et al. (1979). A model for including the waviness of the current sheet was first developed by Potgieter and Moraal (1985) and Burger (1987) (see also Burger and Potgieter 1989). Later on Hattingh (1993) proposed an improvement to the simulation of the HCS (see also Hattingh and Burger 1995), with further refinements by Langner (2004).

Fichtner et al. (1996), Haasbroek (1997), and Haasbroek and Potgieter (1998) proposed a model for the study of the elongation and non-spherical structure of the heliosphere. A 2-D shock acceleration for the discontinuous transition of the solar wind velocity $\vec{V}$ at the

termination shock was developed by Jokipii (1986) and Steenkamp (1995). Later refinements followed from Steenberg (1998). le Roux et al. (1996) also developed a shock acceleration model which was expanded by Haasbroek (1997).

Three dimensional (3-D) models were also developed, e.g. the 3-D steady state model with drifts and a wavy HCS by Kota and Jokipii (1983) and by Hattingh (1998). A 3-D time dependent modulation model for the study of the impact of corotating interaction regions was developed by Kota and Jokipii (1991). 3-D time-dependent solutions were presented by Kota and Jokipii (1997) and Kissmann et al. (2003). A 3-D steady state model including the Jovian magnetosphere as a source for the Jovian electrons, was developed by Fichtner et al. (2000) and Ferreira et al. (2001a). Hybrid models were also developed e.g. Pauls and Zank (1996, 1997), le Roux and Fichtner (1997) and the newer models of Florinski and Jokipii (1999); see also Florinski and Jokipii (2003), and Scherer and Fahr (2003). Later on Scherer and Ferreira (2005) developed a hybrid model including dynamical effects. Hydrodynamic models refer to hydrodynamic or magnetohydrodynamic calculations of the heliosphere and the HMF which are coupled to a transport model to calculate cosmic ray modulation within.

3.4 The diffusion tensor

The symmetric diffusion tensor $\mathbf{K}_s$ in Equation (3.1) consists of a parallel diffusion coefficient $(K_\parallel)$ and two perpendicular diffusion coefficients, one in the radial direction $(K_{\perp r})$ and one in the polar direction $(K_{\perp\theta})$. This diffusion tensor can be written in spherical coordinates as

$$\begin{bmatrix} K_{rr} & K_{r\theta} & K_{r\phi} \\ K_{\theta r} & K_{\theta\theta} & K_{\theta\phi} \\ K_{\phi r} & K_{\phi\theta} & K_{\phi\phi} \end{bmatrix} = \begin{bmatrix} K_\parallel \cos^2\psi + K_{\perp r}\sin^2\psi & -K_A \sin\psi & \left(K_{\perp r} - K_\parallel\right)\cos\psi\sin\psi \\ K_A \sin\psi & K_{\perp\theta} & K_A\cos\psi \\ \left(K_{\perp r} - K_\parallel\right)\sin\psi\cos\psi & -K_A\cos\psi & K_{\perp r}\cos^2\psi + K_\parallel \sin^2\psi \end{bmatrix}. \quad (3.2)$$

In this study focus is on the diffusion coefficients in the radial and polar direction respectively. They can be written as

$$K_{rr} = K_\parallel \cos^2\psi + K_{\perp r}\sin^2\psi \quad (3.3)$$

and

$$K_{\theta\theta} = K_{\perp\theta}. \quad (3.4)$$

Also of importance in Equation (3.2) is the drift coefficient (K_A) and ψ the spiral angle which is the angle between the radial direction and the average HMF at a given position. Next these coefficients will be discussed in more detail.

3.5 Parallel diffusion

Cosmic ray diffusion occurs through interplanetary magnetic field turbulences which moves outward from the Sun with the solar wind. The diffusion coefficient according to quasi linear

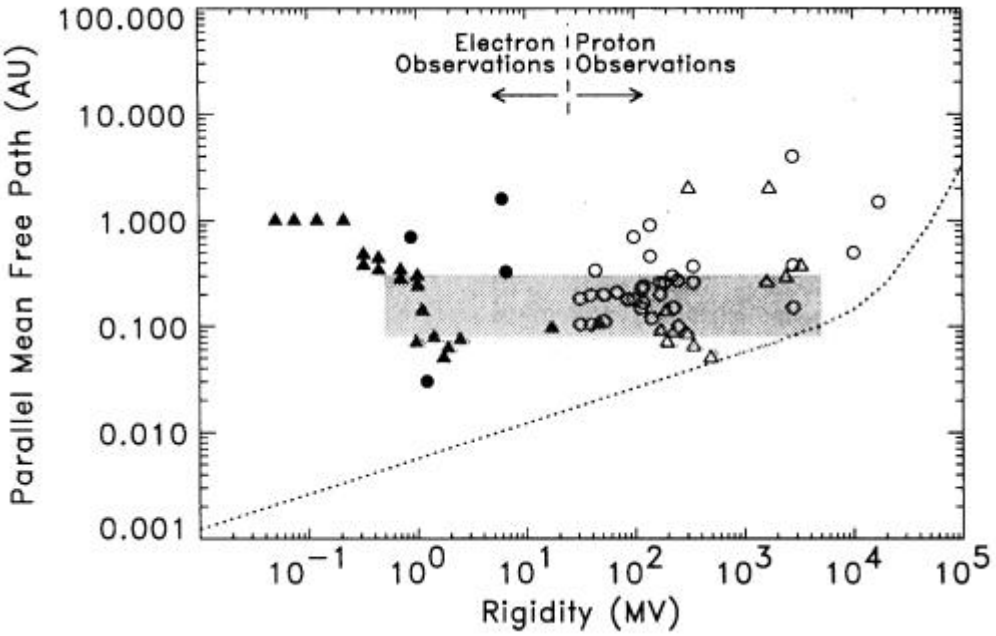

Figure 3.1: Cosmic ray parallel mean free path as a function of rigidity. Filled and open symbols denote results derived from electron and proton observations respectively. The shaded band is the observational consensus by Palmer (1982). The dotted line represents the prediction of standard quasi linear theory QLT (from Bieber et al. 1994).

theory (QLT) (Jokipii 1971) depends on the particle's rigidity and is defined by the structure of the HMF turbulence. Shown in Figure 3.1 is the parallel mean free path $\lambda_{\parallel}$ predicted by standard QLT, and it is shown as a function of rigidity (Bieber et al. 1994). Filled and open symbols denote results derived from electron and proton observations respectively. The shaded band is the observational consensus by Palmer (1982). Shown in Figure 3.1 is that predictions from QLT are not compatible with the observational consensus from Palmer (1982) and also the derived results from electron and proton observations. The observations indicate a rigidity independent $\lambda_{\parallel}$ from 0.5 to 500 MV, higher compared to QLT.

The $\lambda_{\parallel}$ as predicted by the standard QLT is given by

$$\lambda_{\parallel} = \frac{3v}{2} \int_0^1 \frac{1-\mu^2}{\Phi\mu} d\mu \tag{3.5}$$

with v the particle speed and μ the cosine of the particle pitch angle and $\Phi\mu$ the Fokker-Planck coefficient for pitch-angle scattering (Hasselmann and Wibberenz 1970; Jokipii 1971; Earl 1974). To find $\Phi\mu$ in Equation (3.5) a power spectrum of the magnetic field fluctuations is needed. Figure 3.2 shows an example of a power spectrum versus the wave number. The spectrum can be separated into three regions (e.g. Bieber et al. 1994) which are: (1) The energy range (where the energy is pumped to the system). Here the power spectrum variation is independent of the wave number k. (2) The inertial range, where the power spectrum variation is proportional to $k^{5/3}$. (3) The dissipation range where the power spectrum is proportional to k^{-3}. The dissipation range plays an important role in the resonant scattering of low energy particles where the

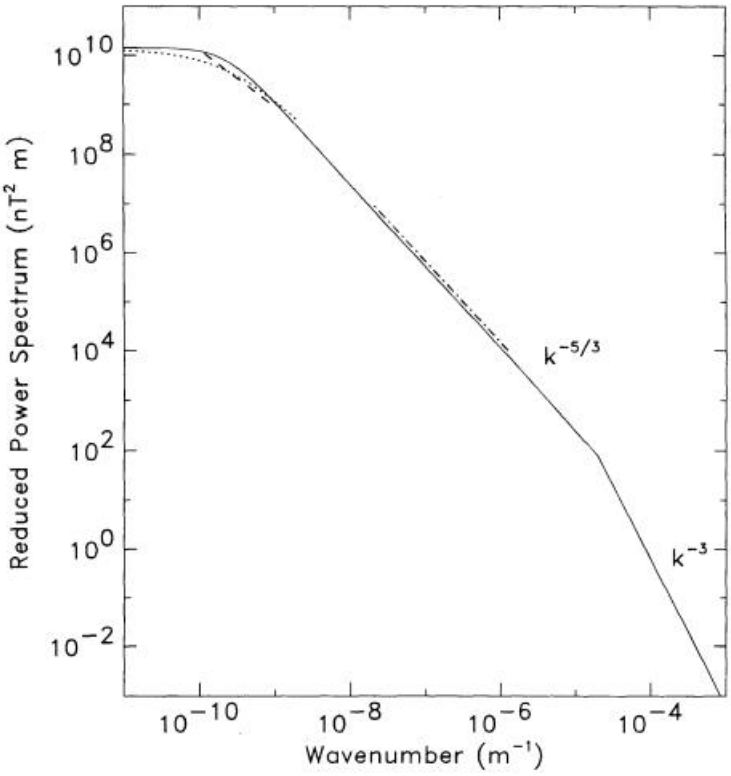

Figure 3.2: The power spectrum of the slab model (solid line) compared to the observations by Hedgecock (1975), (dotted line), Bieber et al. (1993), (dashed line), and Wanner and Wibberenz (1991, dot-dash line) (from Bieber et al. 1994).

pitch angles of these particles approach 90°.

In the original derivation of the mean free path $\lambda_{\parallel}$ (e.g. Jokipii 1966; Fisk et al. 1974) the dissipation range was neglected. However, it was proved using magnetometer and plasma wave observations in the solar wind, that the magnetic fluctuations spectra exhibit a dissipation range (e.g. Coroniti et al. 1982). Bieber et al. (1994) showed that if the dissipation range is neglected, the mean free path $\lambda_{\parallel}$ from Equation 3.5 becomes too small at low rigidities, and has the wrong rigidity dependence. In this work a simple expression for the parallel mean path (damping model) from Teufel and Schlickeiser (2002) is used

$$\lambda_{\parallel} = (\lambda_{\parallel})_0 \left(\frac{P}{P_0}\right)^{1/3} \left(\frac{r}{r_0}\right) \tag{3.6}$$

with P_0 = 1 GV, r_0 = 1 AU and $(\lambda_{\parallel})_0$ = 0.3 AU.

3.6 Perpendicular diffusion

As mentioned above, $K_{\perp}$ can be divided into two possibly independent coefficients, which are $K_{\perp r}$ and $K_{\perp \theta}$, the perpendicular diffusion in the radial and polar direction respectively.

Perpendicular diffusion in the radial direction $K_{\perp r}$ in Equation (3.3) is dominating in the outer heliosphere. Figure 3.3 shows $cos^2\psi$ and $sin^2\psi$ as a function of radial distance for $\theta = 10°$, and $\theta = 90°$ respectively. It is shown that $sin^2\psi$ in the equatorial region $(\theta = 90°)$ remains constant, except for the inner heliospheric regions, e.g. distances less than ~10 AU. In the polar regions θ = 10°, $sin^2\psi$ becomes constant only at ~40 AU outward and is significantly smaller in the inner heliosphere. Furthermore $cos^2\psi$ in the polar regions θ = 10° and equatorial regions θ = 90° is significantly smaller except for the inner heliospheric regions. Figure 3.3 shows that $K_{\perp r}$ dominates K_{rr} in the outer heliosphere, while $K_{\parallel}$ dominates in the inner heliosphere due to their dependence on ψ. This indicates that particles undergo perpendicular diffusion to cross the field lines moving inward, while only in the inner heliosphere does the parallel component contribute to radial diffusion.

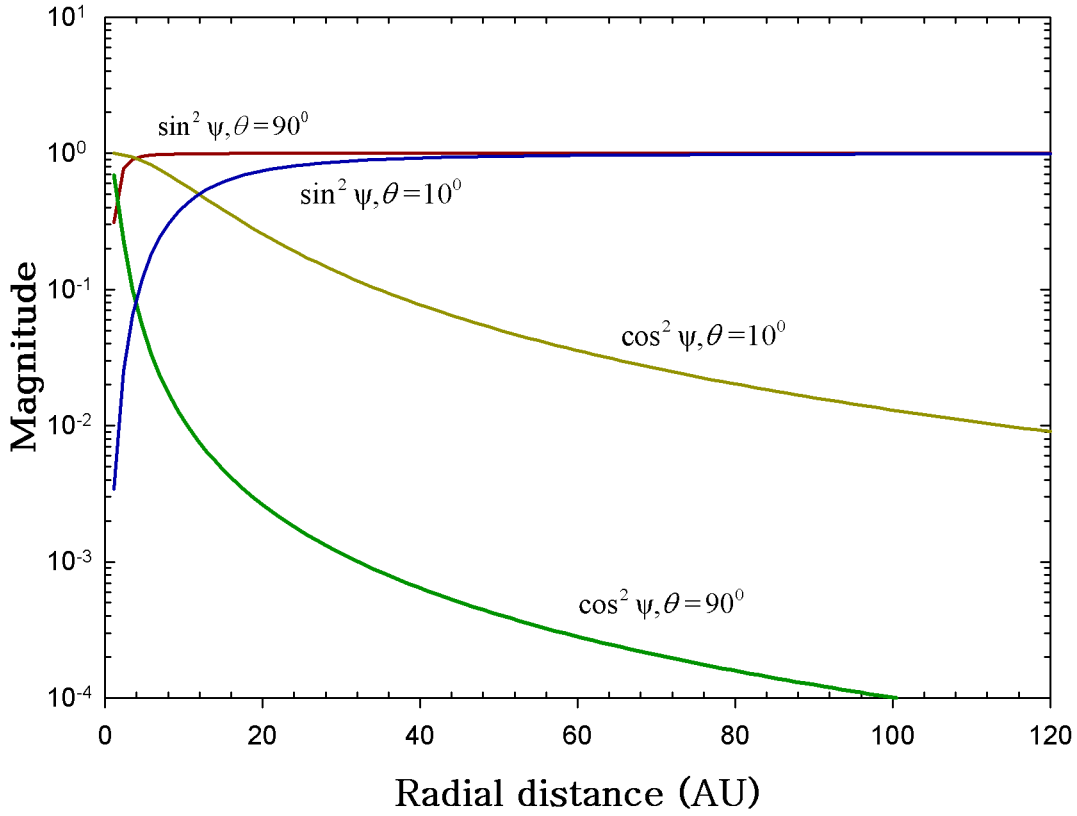

Figure 3.3: The $cos^2\psi$ and $sin^2\psi$ functions as a function radial distance for the equatorial plane $\theta = 90°$ and for the polar regions θ=10°.

It has become standard practice for most authors using modulation models to scale $K_{\perp}$ as $K_{\parallel}$ (e.g. Jokipii and Kota 1995; Potgieter 1996; Ferreira et al. 2000; Burger et al. 2000; Ferreira et al. 2001a,b) in modulation studies. This follows from simulations done by e.g. Giacalone and Jokipii (1999) and Qin et al. (2002).

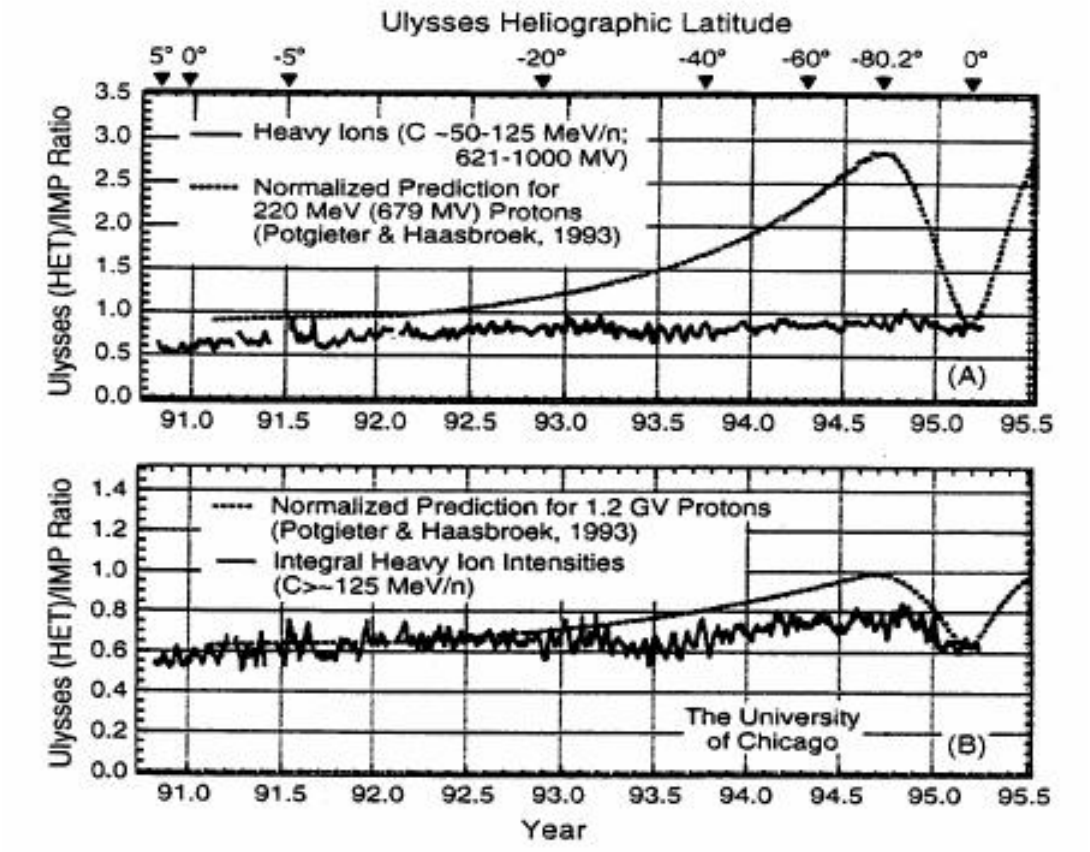

Figure 3.4: Ulysses cosmic ray measurements (e.g. Simpson et al. 1995) as a function of time and latitude (at the top) compared with classical drift-model predicted by Potgieter and Haasbroek (1993). The two panels represent measurements and model predictions at different energies (from Smith 2000b).

Therefore it is assumed that

$$K_{\perp r} = aK_{\parallel} \tag{3.7}$$

and

$$K_{\perp \theta} = bK_{\parallel} \tag{3.8}$$

where a = 0.02 and b = 0.01 are constants, or functions of rigidity (e.g. Burger et al. 2000). In this study we assume these to be constant because results are mostly computed only at 2.5 GV in order to be compared to Ulysses observations.

Before the Ulysses mission it was believed that positively charged cosmic rays preferentially enter the heliosphere easily from above the Sun's poles in an A $>$ 0 HMF polarity cycle (e.g. Potgieter and Haasbroek 1993). In Figure 3.4 (from Smith 2000b) the latitudinal dependence of cosmic ray protons, which is significantly less than what was predicted by classical drift dominated models (e.g. Potgieter and Hassbroek 1993; Heber et al. 1996), is shown. This surprising result has led Kota and Jokipii (1995, 1997) to revisit the concept that $K_{\parallel}$ must be

anisotropic and $K_{\perp\theta} > K_{\perp r}$ in off equatorial regions. Kota and Jokipii (1995); Potgieter (1996); Burger et al. (2000); and Ferreira et al.(2001a,b) assumed this in cosmic ray modulation models and it resulted in a more realistic computed latitudinal dependences of cosmic rays when compared to observations (see also Potgieter 2000).

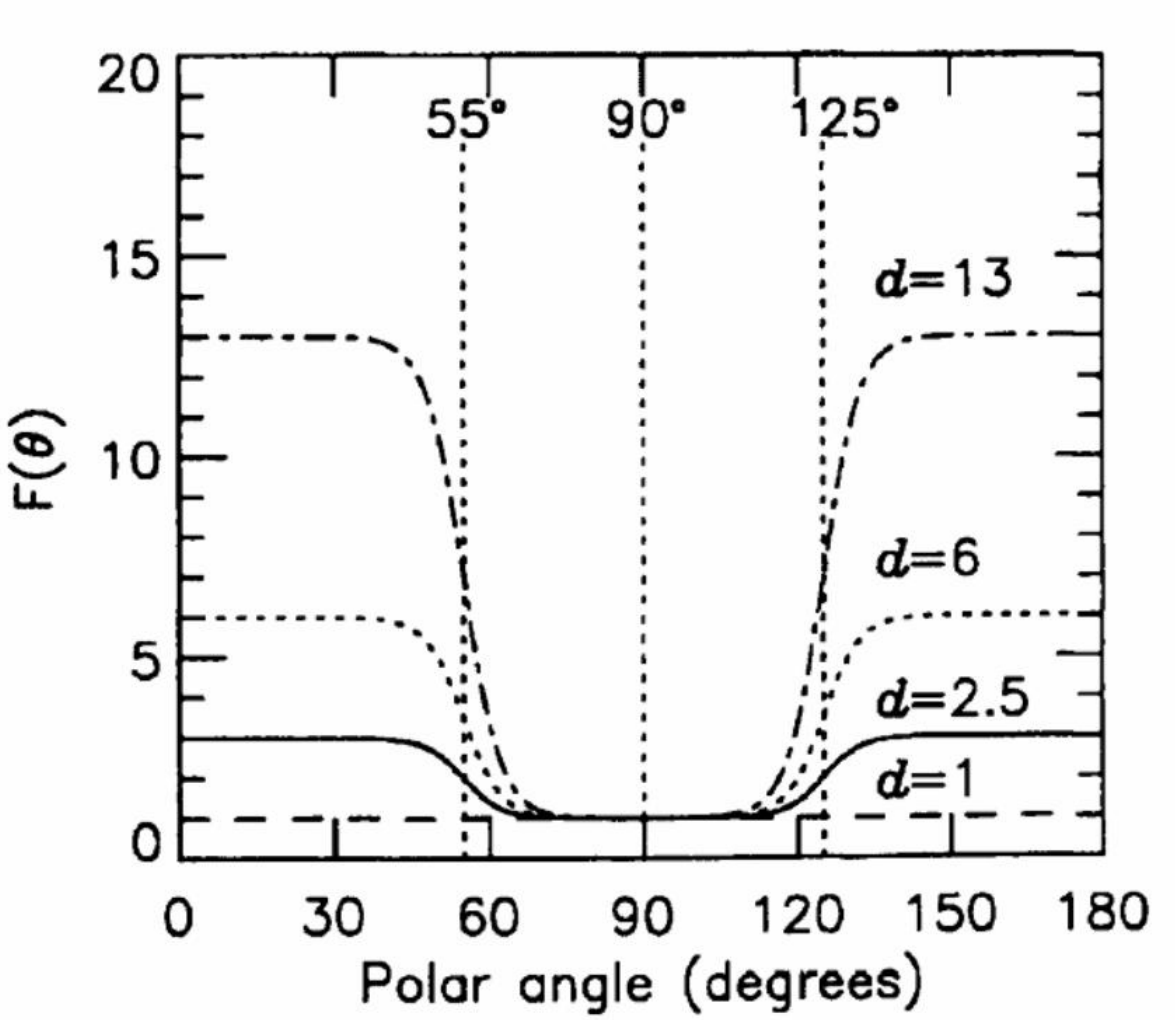

Figure 3.5: The function $F(\theta)$, given by Equation (3.8), as a function of polar angle (degrees) for four different assumptions of d, giving the magnitude of the increase in $F(\theta)$ toward the poles. The increase in $F(\theta)$ is from the equatorial plane toward the poles. The vertical dotted lines correspond to the polar angles where $F(\theta) = d/2$ (from Ferreira et al. 2001a).

It is shown by e.g. Potgieter (2000) that by assuming $K_{\perp\theta} > K_{\perp r}$ when solving the transport equation, and then by increasing $K_{\perp\theta}$ independently of $K_{\perp r}$ leads to a considerably reduction in drifts as well as to changes in the radial dependence experienced by cosmic ray protons. Furthermore, Potgieter (1997), Burger et al. (2000) and Ferreira et al. (2001a,b) illustrate that in order to produce the correct magnitude and rigidity dependence of the observed latitudinal cosmic ray proton intensity by Ulysses, enhanced latitudinal transport is required.

This is done by assuming $K_{\perp\theta}$

$$K_{\perp\theta} = bF(\theta) K_{\parallel}. \tag{3.9}$$

The function $F(\theta)$ in Equation (3.9) is given by,

$$F(\theta) = A^{+} \mp A^{-} \tanh[\frac{1}{\Delta\theta}(\theta_A - 90^{\circ} + \theta_F)], \tag{3.10}$$

where $A^{\pm} = \frac{d\pm1}{2}$, $\Delta\theta = \frac{1}{8}$, $\theta_A = \theta$ and θ_F = 35° for $\theta \leq 90^{\circ}$ while for θ >90°, θ_A = 180° $-\ \theta$ and θ_F = -35°.

From Equation (3.9), $K_{\perp\theta}$ is increased with respect to $K_{\parallel}$ from the value in the equatorial regions towards the poles by a factor d (As shown in Figure 3.5). A physical justification of this increase was given by Burger et al. (2000). Arguments were based on Ulysses observations which indicate that possible variance increases more in the transverse and normal directions of the HMF than in the radial direction. This may lead to larger diffusion in these directions. However, for a Fisk-type HMF field (Fisk 1996), or a hybrid field (Burger et al. 2008) latitudinal transport is supposedly more effective than in a Parker field, and to account for this effect $K_{\perp\theta}$ maybe enhanced toward the polar regions when a modified Parker HMF is used.

3.7 Particle drifts

Based both on general considerations and detailed numerical calculations, it has been established that gradient and curvature drifts have very significant effects on the modulation of galactic cosmic rays (see e.g. Jokipii and Kopriva 1979; Potgieter and Moraal 1985; Hattingh and Burger 1995 and Burger et al. 2000).

In Equation (3.1) the gradient, curvature and current sheet drift velocity components are given as (e.g. Hattingh 1993)

$$\begin{aligned}
\left\langle \vec{V}_D \right\rangle_r &= -\frac{sign(Bq)}{r\sin\theta}\frac{\partial}{\partial\theta}(\sin\theta k_{\theta r}) \\
\left\langle \vec{V}_D \right\rangle_\theta &= -\frac{sign(Bq)}{r}\left[\frac{1}{\sin\theta}\frac{\partial}{\partial\phi}(k_{\phi\theta}) + \frac{\partial}{\partial r}(rk_{r\theta})\right] \\
\left\langle \vec{V}_D \right\rangle_\phi &= -\frac{sign(Bq)}{r}\frac{\partial}{\partial\theta}(k_{\theta\phi})
\end{aligned} \tag{3.11}$$

or

$$\begin{aligned}
\vec{V}_D &= \nabla \times K_A \mathbf{e}_B \\
&= \nabla \times (K_A \mathbf{e}_B)\left[1 - 2H\left(\theta - \acute{\theta}\right)\right] + 2\delta_D\left(\theta - \acute{\theta}\right) K_A \mathbf{e}_B \times \nabla\left(\theta - \acute{\theta}\right)
\end{aligned} \tag{3.12}$$

with (r, θ, ϕ), the polar coordinates relative to the Sun's rotation axis, $\mathbf{e}_B = B_m/B$, B_m is the modified magnetic field given by Equation (2.8), K_A the drift coefficient which will be given below, δ_D the Dirac-function and H is the Heaviside function which causes the HMF to change polarities across the HCS given by

$$H(\theta - \theta^{'}) = \begin{bmatrix} 0, & \text{for } \theta < \theta^{'} \\ 1, & \text{for } \theta > \theta^{'} \end{bmatrix}. \tag{3.13}$$

In Equation (3.12) the first term describes the gradient and curvature drift of cosmic rays caused by the magnetic field, with the second term describing the drift caused by the HCS. A schematic explanation of the drift process for protons (positively charged particles) is shown in Figure 3.6. During the A>0 HMF polarity cycle, e.g. ∼1970 to ∼1980 and also ∼1990 to ∼2000s, positively charged particles drift from the heliospheric poles down onto the equatorial regions. They then follow the HCS and drift outward towards the boundary. In this cycle the particles are relatively insensitive to the changes in the HCS.

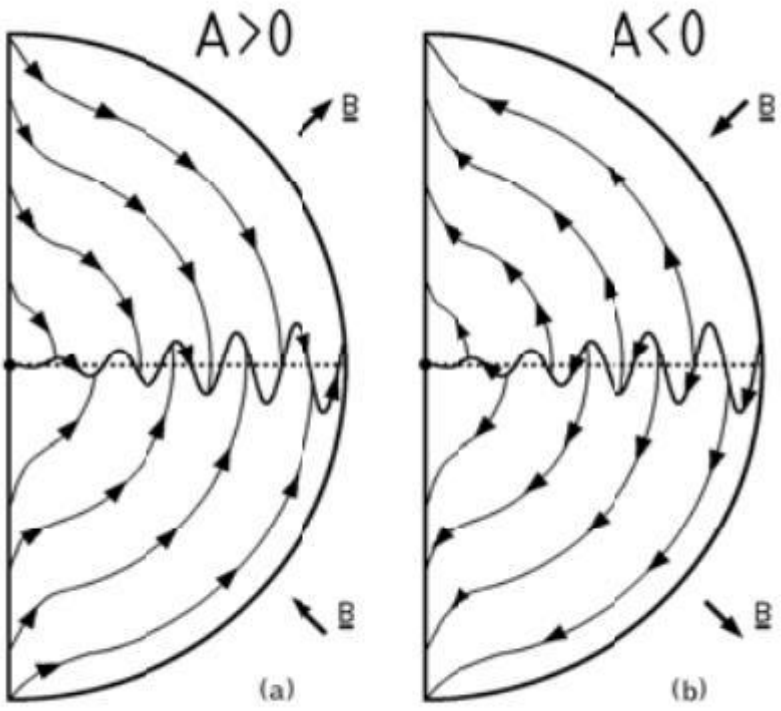

Figure 3.6: Drift directions of positively charged particles and the corresponding direction of the HMF in the heliosphere for (a) the $A > 0$ HMF polarity cycle, and (b) the $A < 0$ cycle (From Jokipii and Thomas 1981).

For the A<0 HMF polarity cycle, e.g. ∼2000 to ∼2010, positive particles then drift from

the equatorial plane following the HCS towards the Sun and then outward along the polar regions of the heliosphere. In this cycle the particles are sensitive to the changes in the HCS.

In this work a 2-D model with a simulation of the HCS as given by Hattingh (1993) (see also Potgieter and Moraal 1985 and Langner et al. 2003) is used. This is referred to as the wavy current sheet model. In this model the HCS is simulated by replacing the three-dimensional drift velocity with a 2-D drift field. Averaging Equation (3.12) over one solar rotation, a 2-D drift field can be obtained (see e.g. Hattingh 1993; Hattingh and Burger 1995; Burger and Hattingh 1995; Hattingh 1998). It was also shown by Ferreira et al. (1999) that there are no qualitative and insignificant quantitative differences between this approach and a 3-D approach incorporating an actual wavy current sheet. The drift coefficient used in this study is the same as the one used by Burger et al. (2000) and is given by:

$$K_A = (K_A)_0 \frac{vP}{3cB} \left(\frac{10P^2}{1 + 10P^2} \right) \tag{3.14}$$

with $(K_A)_0$ a dimensionless quantity, which can have values from 0 to 1.0 with no drift $(K_A) = 0$ and full drift $(K_A)_0 = 1.0$ respectively, P denotes the cosmic ray rigidity and B is the modified HMF magnitude given by Equation (2.7). Also v is the particle speed and c is the speed of light. Time dependence of the drift parameter will be discussed in detail in Chapter 4, where the need for the scaling down of this parameter during moderate to solar maximum conditions is discussed.

3.8 Summary

An overview was presented of the transport equation and of all the four major modulation processes experienced by the cosmic rays as they make their way from the outer heliosphere to the inner heliosphere. They include diffusion, convection energy changes and drifts. An overview of the modulation models was given.

In the model it is assumed for the different transport coefficients that:

- $K_{\parallel} = (K_{\parallel})_0 \frac{v}{3} \left(\frac{P}{P_0}\right)^{1/3} \left(\frac{r}{r_0}\right)$ with P rigidity, r radial distance and r_0 = 1 AU, P_0 = 1 GV and $(K_{\parallel})_0$ = 0.3 and v the particle's speed.
- $K_{\perp r} = aK_{\parallel}$ with a = 0.02.
- $K_{\perp \theta} = bK_{\parallel}F(\theta)$ with b = 0.01 and $F(\theta)$ enhancing $K_{\perp \theta}$ toward the poles by a factor of 6.
- $K_A = (K_A)_0 \frac{vP}{3cB} \left(\frac{10P^2}{1+10P^2}\right)$, where c the speed of light and B the magnetic field magnitude.

In the next chapter it will be shown how these coefficients change as a function of time and magnetic polarity in order to compute cosmic ray modulation compatible to observations.

Chapter 4

Time-dependent cosmic ray modulation

4.1 Introduction

As cosmic rays enter the heliosphere they sample the different heliospheric conditions which change over a solar cycle. This results in their intensities being modulated over 11 and 22 years due to a difference in solar activity and magnetic polarity. In this chapter a brief overview of time-dependent cosmic ray modulation is given. The compound approach of Ferreira (2002), Ferreira and Potgieter (2004) and Ndiitwani et al. (2005) is discussed and also used to calculate cosmic ray intensities along the Ulysses trajectory, comparing results to spacecraft observations. A refinement on this approach is also presented to establish a better compatibility of model results with Ulysses observations.

4.2 Propagating diffusion barriers: The effect on cosmic ray intensities

The fast solar wind streams can overtake the slower background solar wind to cause interaction regions. In the innermost regions of the heliosphere changes in the intensities of cosmic rays can be associated with these corotating interaction regions (CIRs) (e.g. Potgieter 1995). We can classify these in three general types:

Global merged interaction regions (GMIRs), which may extend 360° around the Sun in the ecliptic and reach from the heliographic equator to 30° heliographic latitude. Corotating merged interaction regions (CMIRs) are quasi-periodic structures generated by the interaction of corotating streams lasting several solar rotations; and local MIRs (LMIRs), which are non-periodic and have limited latitudinal and longitudinal extent and whose effects last less than one solar rotation (e.g. Burlaga et al. 1993). Decreases in cosmic ray intensities, as observed by Voyager 1 and Voyager 2 from 1986 to 1990, were generally related to these different propagating diffusion regions as shown in Figure 4.1.

Shown in Figure 4.1 are the $E > 70$ MeV/nucleon observed cosmic ray proton intensities in the bottom panels with the magnetic field strength, B, which is normalized by the Parker

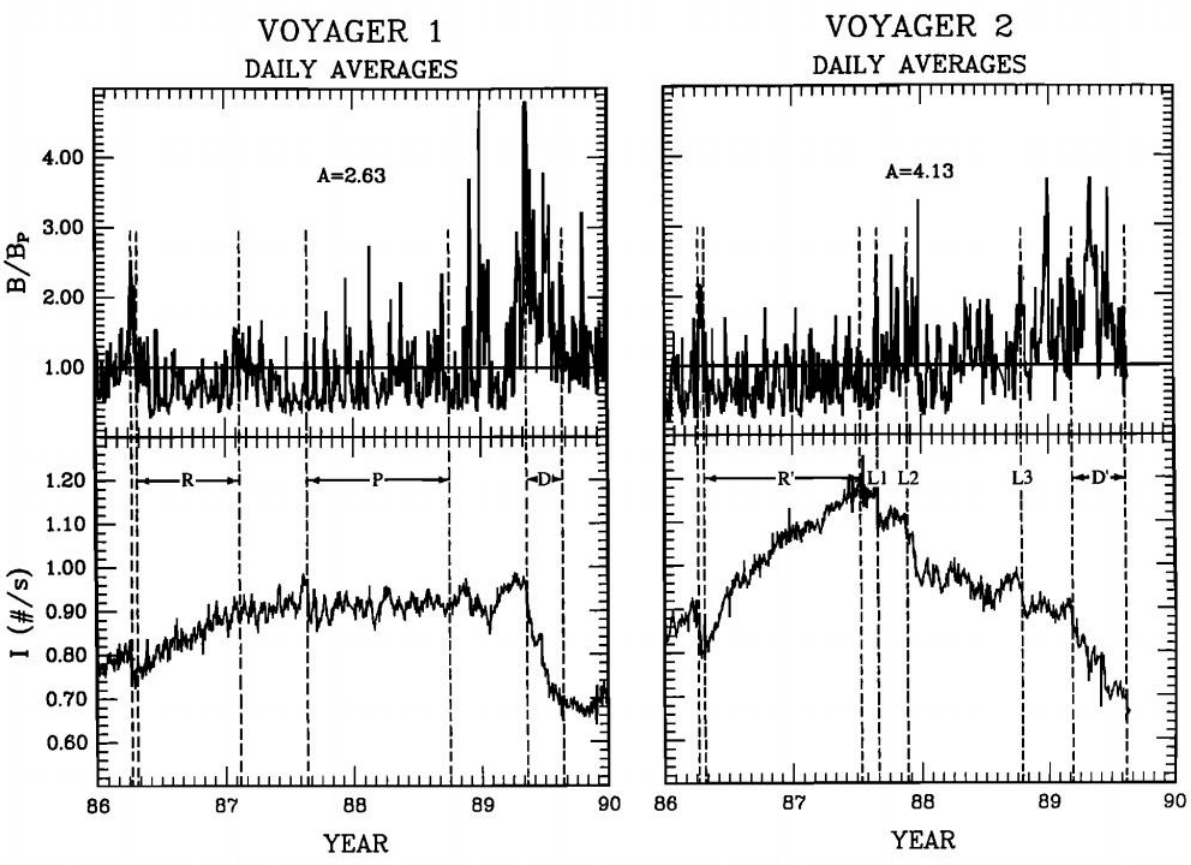

Figure 4.1: The $E > 70$ MeV/nucleon measured cosmic ray proton intensity in the bottom panels with the daily averages of the magnetic field strength normalized by the Parker magnetic field ,B_p, in the top panels. Measured results are from Voyager 1 (left panel) and Voyager 2 (right panel). Data are shown from 1986 to 1989 and plotted against time (from Burlaga et al. 1993).

magnetic field B_p at the top. Daily averages of both the magnetic field and cosmic ray intensities from 1986 to 1989 were taken. In Figure 4.1, D and D' are used in the lower panel to indicate the position of a GMIR measured by the Voyager 1 and Voyager 2 spacecraft respectively. For both D and D' the observed magnetic field increased considerably showing the presence of a GMIR, which in return caused a considerable decrease in the cosmic ray measurements. The letter P indicates the position of a CMIR. Also L1 and L2 on the Voyager 2 panel indicate the position of the LMIR, while R and R' indicate the regions where the magnetic field becomes smaller, marking the recovery in cosmic ray intensities.

Figure 4.1 shows that the observed cosmic ray intensities show a net increase with time when MIRs are weak and the magnetic field strength is relatively low, for example, from day $\sim$45 to day $\sim$120 of 1987 at Voyager 1 and from day $\sim$120 in 1986 to day $\sim$195 in 1987 at Voyager 2. The cosmic ray intensity fluctuates about a background level when CMIRs and rarefaction regions are dominant (e.g. Burlaga et al. 1993). This is the case from day $\sim$230 of 1987 to day $\sim$275 of 1988 at Voyager 1 and during the interval from day $\sim$245 of 1987 to day $\sim$60 of 1989 at Voyager 2. The cosmic ray intensity decreases locally during the passage of a LMIR. Such a local decrease was observed at both Voyager 1 and Voyager 2 near day $\sim$100 of 1986. Local

decreases in cosmic ray intensities were observed at Voyager 2 but not Voyager 1 beginning near days ∼240 and ∼320 of 1987, and near day ∼275 of 1988.

4.3 The GMIR-drift approach

Theoretical and numerical work in explaining time-dependent cosmic ray modulation was started by le Roux and Potgieter (1990) who used a modulation model with the tilt angle of the HCS as the only time varying parameter. This approach was able to compute cosmic ray modulation compatible to observations over moderate to solar minimum periods. However, le Roux and Potgieter (1995) subsequently showed that this type of model could not reproduce cosmic-ray observations during increasing solar activity with the tilt of the current sheet as the only time-dependent parameter.

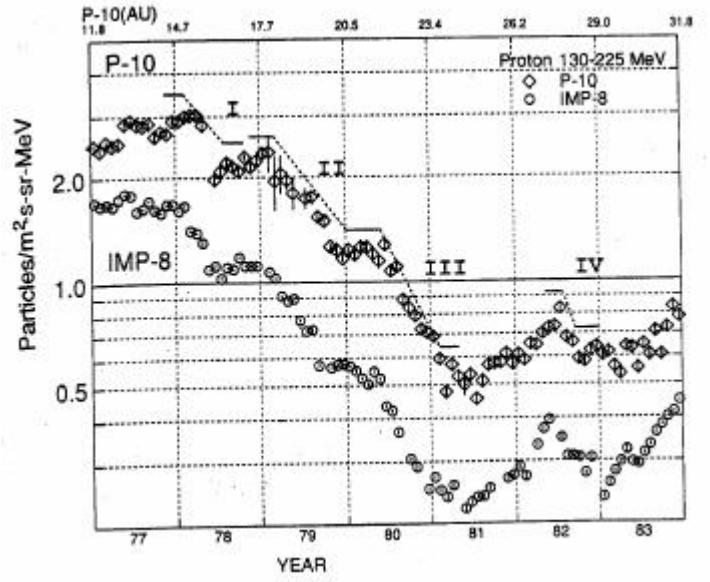

Figure 4.2: The 26 day averaged cosmic ray intensities of 130-225 MeV hydrogen from IMP 8 and Pioneer 10 starting from 1977 till 1983. The heliocentric distances are indicated at the top of the plot. The roman symbols in the graph indicate the step decrease in the observed intensities (from Fujii and McDonald 1995).

This was proved to be true especially when large step decreases in the observed cosmic-ray intensities occurred (e.g. Lockwood 1960; McDonald et al. 1981). These series of steps in cosmic ray intensities are shown in Figure 4.2 as observed by IMP 8 and Pioneer 10 from 1977 to 1983. The step decreases are shown as I to IV and are prominent during the increasing phase of solar activity, when the changes in the current sheet are no longer primarily responsible for the modulation of cosmic rays (Ferreira and Potgieter 2004).

To successfully model the cosmic-ray intensities during moderate to higher solar activity le Roux and Potgieter (1995) suggested incorporating propagating diffusion barriers (PDBs) in their model, as first introduced by Perko and Fisk (1983). These diffusion barriers are mainly GMIRs. le Roux and Potgieter (1995) showed that it was possible to simulate a complete 11

year proton modulation cycle by including the GMIRs and drifts in a time-dependent model. Their simulations were done for radial distances larger than 20 AU, allowing for merging of corotating structures to take place. These structures are believed to form beyond ∼10 AU (Burlaga et al. 1993).

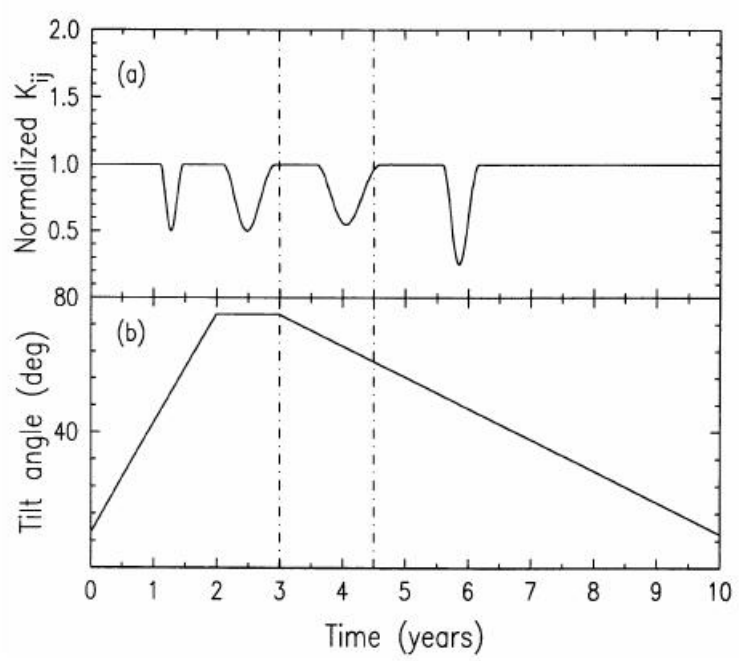

Figure 4.3: (a) The simulated time variation of the normalized diffusion tensor at 10 AU in the equatorial plane. The dashed vertical lines shows the period where there is a polarity change from $A > 0$ to $A < 0$ (b) The assumed tilt angle in the model (from le Roux and Potgieter 1995).

To illustrate the effects of GMIRs on cosmic ray intensities more clearly, we follow arguments by le Roux and Potgieter (1995). They assumed that the passage of GMIRs causes a temporal variation of the diffusion tensor from the background values. This is shown in Figure 4.3a and 4.3b where the simulated time variations of the normalized diffusion tensor at 10 AU in the equatorial plane are shown at the top and the assumed tilt angles are shown in the bottom.

Figure 4.4 shows the model results corresponding to Figure 4.3 indicating how the effects of GMIRs in the drift model are able to produce the step appearance in the long-term modulation profile in accordance with observations (e.g. McDonald et al. 1993). The dotted line in Figure 4.4 shows the effects of the changing HCS as the only time varying parameter whereas the solid line indicates the additional effects of the four mentioned GMIRs on the cosmic ray modulation. The vertical lines show the period of the polarity reversal of the magnetic field of the Sun. For the $A > 0$ cycle cosmic ray intensities are insensitive to the changes in the HCS compared to the $A < 0$ cycle. During the $A > 0$ polarity cycle the positive particles drift in from the heliospheric polar regions down to the equatorial plane and are not sensitive to changes in the tilt angle, especially if they are relatively small. For the $A < 0$ polarity cycle positive particles drifts in from the equatorial plane towards the Sun along the HCS and are highly affected

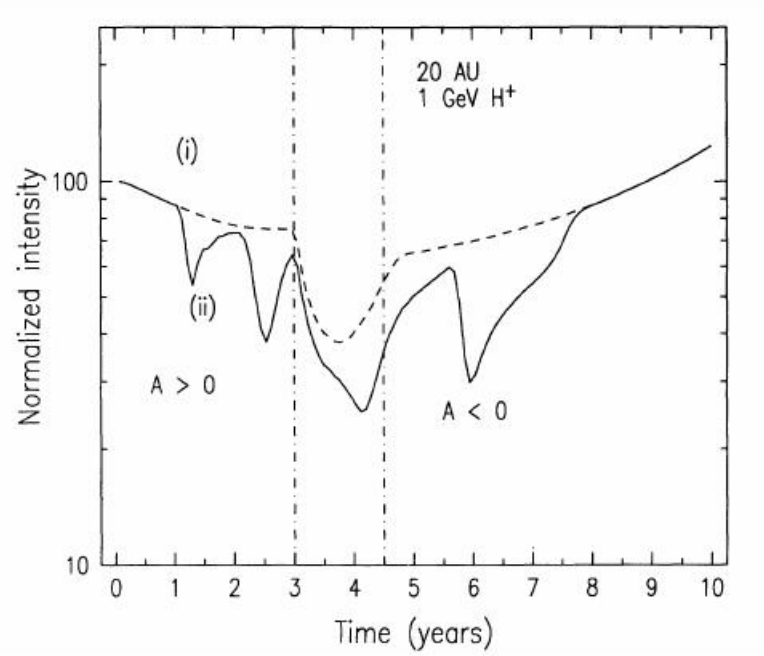

Figure 4.4: The 1 GeV normalized cosmic ray intensity as a function of time. The dashed line (i) indicates the effects of changing the wavy HCS as the only time-dependent parameter. Solid line (ii) shows the effects of the four GMIRs on cosmic ray modulation (from le Roux and Potgieter 1995).

by the changes in the tilt angle (Potgieter et al. 1995).

As shown in Figure 4.4, GMIRs strongly influence modulation where cosmic ray intensities decrease in steps toward solar maximum. le Roux and Potgieter (1995) applied their approach for a complete 22-year cycle, and results are shown in Figure 4.5. Normalized cosmic ray intensities for 1.0 GV protons for both polarity cycles at ∼20 AU are shown. This distance is chosen so that GMIRs can form. This figure shows the ability of combined efforts of drifts, HCS and GMIRs to simulate the complete 11 and 22 year modulation cycles of cosmic rays.

4.4 The compound approach

Cane et al. (1999), Wibberenz and Cane (2000) and Wibberenz et al. (2002) suggested that the decreases as observed in cosmic ray intensities at 1 AU cannot be directly caused by GMIRs (as suggested in the previous section) since they happen before any GMIRs can be formed. They proposed that the global changes in the HMF, which vary roughly by factor of ∼2 from minimum to maximum solar activity, are enough to account for solar cosmic ray modulation (see Figure 2.13). The concept was tested by Ferreira (2002) and Ferreira and Potgieter (2004) by changing all the diffusion coefficients in a fully time-dependent model reflecting time-dependent changes in the measured HMF magnitude at Earth and also including solar cycle related changes in the tilt angle.

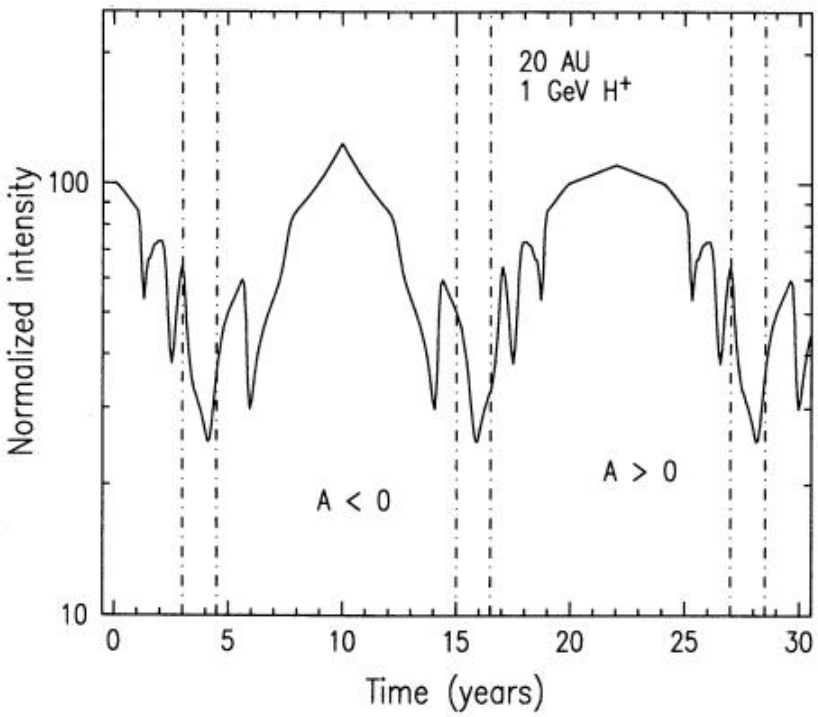

Figure 4.5: Effects of combined drifts and GMIRs on the normalized cosmic ray intensity at 20 AU calculated over a period of 30 years, for both the $A > 0$ and the A < 0 polarity cycles of the heliospheric magnetic field (from le Roux and Potgieter 1995).

Their results are shown in Figure 4.6 where model results are compared to ∼10 GeV neutron monitor observations. This figure shows that it is possible to simulate an 11 year modulation cycle successfully using only the time-dependent changes in the magnetic field and tilt angle variations without any barriers. However, for lower rigidities, e.g. 2.5 GV and less, the computed modulation amplitudes between solar minimum and maximum are too small when this approach is followed and a different approach, called the compound approach, is suggested.

For the compound approach Ferreira and Potgieter (2004) assume that for the time dependence in the diffusion $(K_{\parallel}, K_{\perp r}, K_{\perp\theta})$ and drift (K_A) coefficients that

$$K \propto f_2\,(t)\,\sigma. \tag{4.1}$$

In Equation (4.1), σ = 1.3 for A < 0 polarity cycle, when positive particle drift in along the HCS and σ = 1.0 for A > 0 epoch, when positive particles drift in from the polar regions and outward along the HCS. This is only assumed for the diffusion coefficients, for K_A, σ = 1. This results in different diffusion coefficients for two alternative epochs in agreement with what e.g. Reinecke et al. (1996), Potgieter (2000) and Langner and Potgieter (2008) found. They showed that these coefficients were not similar for consecutive solar minimum periods. This may also indicate that an additional charge-sign dependent mechanism could be contributing to modulation.

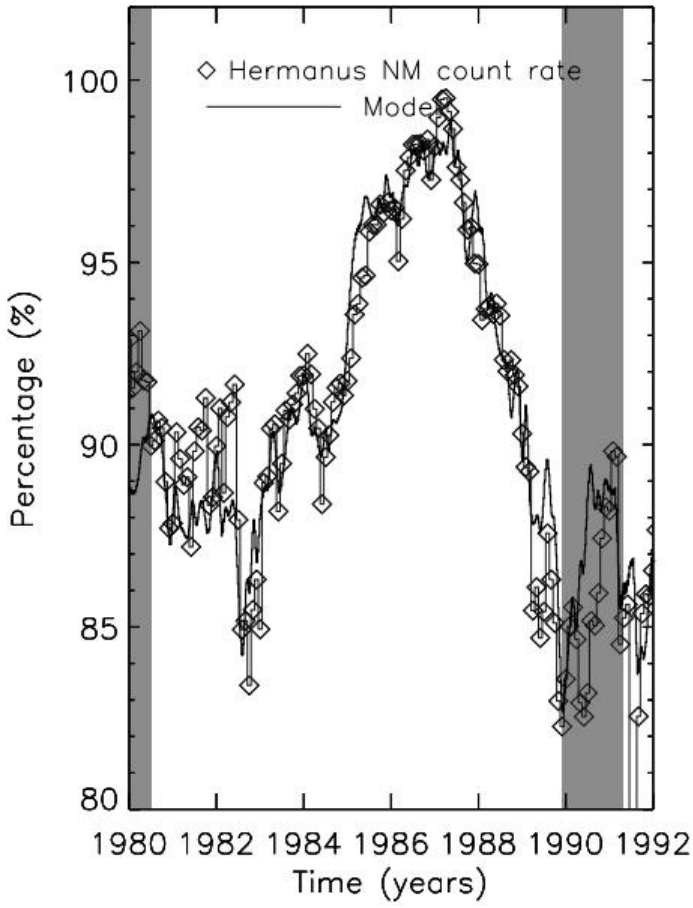

Figure 4.6: Model computations together with Hermanus NM count rates expressed as percentage values for the period of 1980-1992. Shaded areas indicate the time periods when the HMF polarity was not well defined (from Ferreira and Potgieter 2004).

Burger et al. (1997) argued that magnetic helicity may be important where the magnetic field wraps itself to an extent which will influence the particle path and also intensity, resulting into particles being modulated. However, this could not be confirmed. The function $f_2\,(t)$ in Equation (4.1) determines the dependence of diffusion and drift coefficients on time. From Ferreira and Potgieter (2004) and Ndiitwani et al. (2005) follow

$$f_2\,(t) = \left(\frac{B_0}{B(t)}\right)^n \tag{4.2}$$

where B_0 = 5 nT and $B(t)$ the HMF magnitude as measured at Earth. If $n = 1$ and changes by a factor of ~ 2 over a solar cycle, then Equation (4.2) resulted in a corresponding variation of the diffusion coefficients by a factor of ~ 2, as was used by Ferreira and Potgieter (2004) to produce Figure 4.6.

When assuming n = 1 in Equation (4.2) the model was unable to compute compatible results for rigidities $<$ 5 GV which suggested that an improvement was needed as shown by

Ferreira and Potgieter (2004). They then concluded that n could not be a constant but it should be a function of α and assumed $n = \alpha/\alpha_0$, where α is the tilt angle which varies with time and α_0 = 11 a value which may also vary with rigidity. Equation (4.2) now forms the basis of the compound approach proposed by Ferreira and Potgieter (2004). This equation includes observed time-dependent changes in the HCS angle and HMF to calculate a time dependence in the diffusion and drift coefficients over a solar cycle.

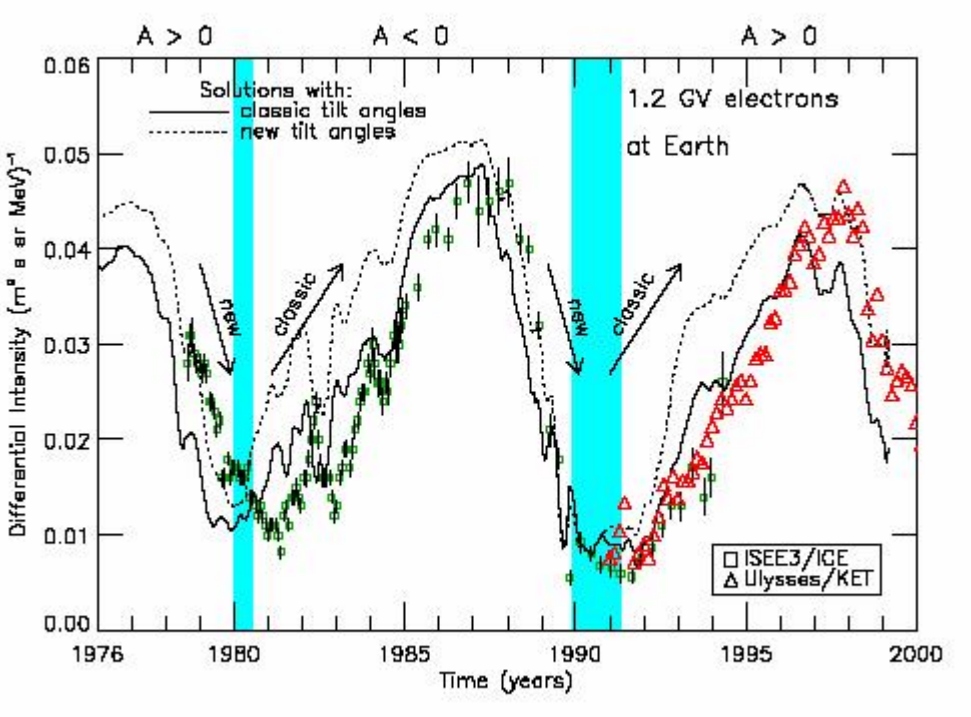

Figure 4.7: The differential intensity of 1.2 GV electrons computed at Earth implementing the compound approach for two types of α, the classical model (solid line) and the new model (dotted line). Results are compared with the data from ISSE/ICE and the Ulysses/KET. Also shown are the shaded areas indicating the periods where there are no well defined HMF polarity (Wilcox Solar Observatory: *http://quake.stanford.edu/*) (from Ferreira 2002). See also Ferreira and Potgieter (2003).

Figure 4.7 (from Ferreira 2002) shows that the model successfully computes modulation of 1.2 GV electrons over 11-year and 22-year cycles. Shown here are results for two different models of α, namely the new and classic models with calculations for both the A $>$ 0 and the A $<$ 0 polarity cycle. The new model tends to produce compatibility with the ICE/ISEE3 observations for $\sim$ 1978 - 1980 and $\sim$ 1987 - 1990 and with the Ulysses observations for $\sim$ 1997 - 2000. The classic model produced compatible results with the ICE/ISEE3 data from $\sim$ 1980 - 1987 and from 1991 - 1997, and resulted in compatibility with the Ulysses observations for the 1990's solar minimum periods. This led Ferreira and Potgieter (2003, 2004) to conclude that to compute optimal results when compared to observations, the tilt angle with the smallest rate of change over decreasing or increasing activity must be used. In this work this will also be the case.

4.5 Application of the compound approach

In this section the compound approach is applied to model the long-term modulation of 2.5 GV protons and electrons along the Ulysses trajectory. Shown in Figure 4.8 are the computed 2.5 GV proton intensities along the Ulysses trajectory in comparison with the Ulysses observations.

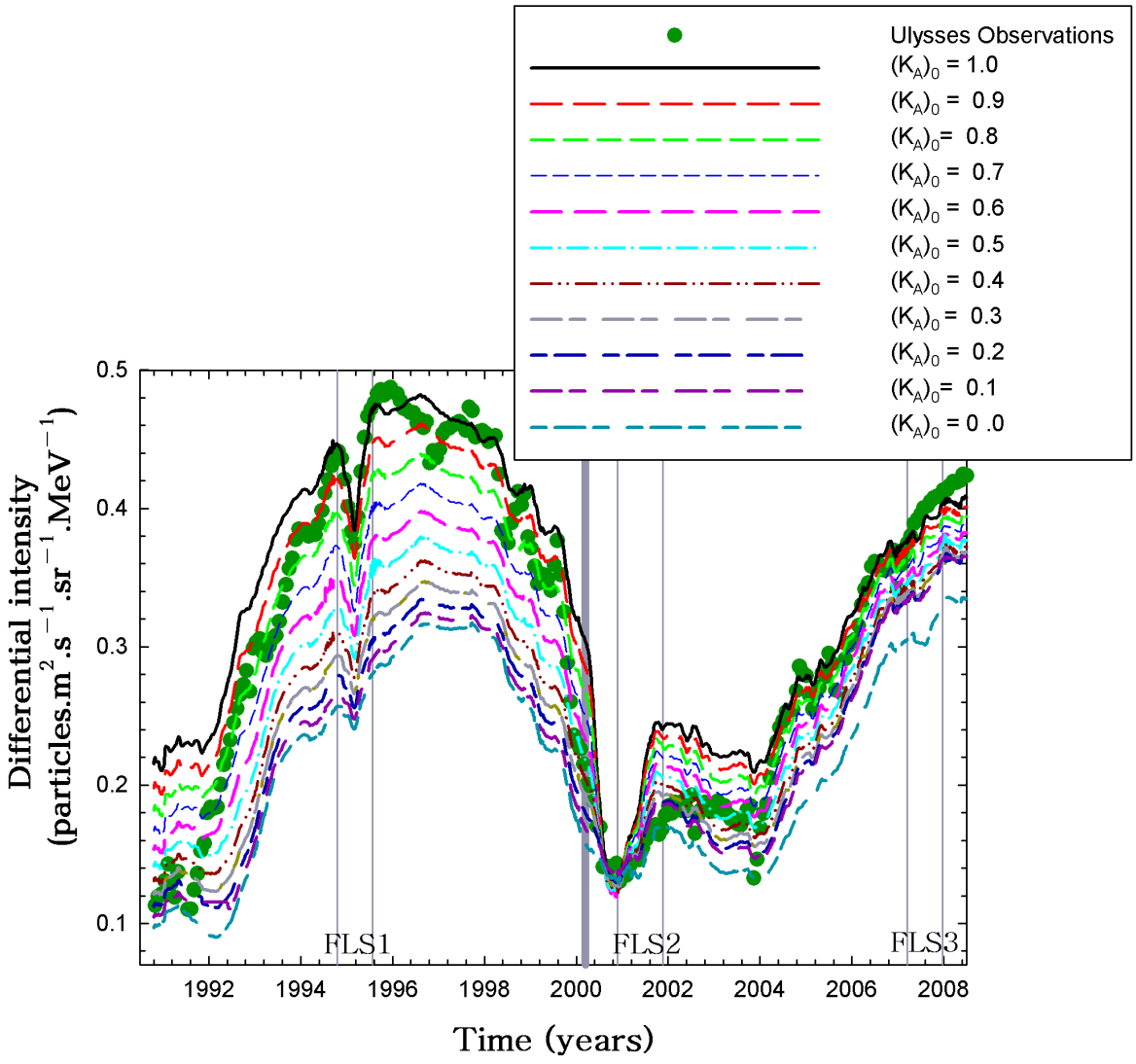

Figure 4.8: Ulysses observations of 2.5 GV protons together with model calculations corresponding to different magnitudes of the drift parameter from $(K_A)_0$=1.0 (top) to no drift $(K_A)_0$ = 0 (bottom) in intervals of 0.1. The vertical thin lines indicate the time periods in which the fast latitude scan (FLS) periods occurs. These were in ∼1995, ∼2001 and ∼2007 respectively and are called the FLS1, FLS2 and FLS3. The thick vertical line indicates the time period where the magnetic field switches polarity in the model.

Different scenarios are shown corresponding to different $(K_A)_0$ for the drift parameter given in Equation (3.14). Large scale drifts play a major role in the modulation of cosmic rays (Jokipii et al. 1977; Potgieter and Moraal 1985). However, in recent years with more realistic models

(e.g. Langner 2003; Ferreira and Potgieter 2004; Ndiitwani etal. 2005; Langner and Potgieter 2008 and Strauss et al. 2010), it was shown that drifts must be scaled down to account for cosmic ray observations (e.g. Potgieter 1989). The aim of this figure is to construct a time-dependence in $(K_A)_0$ resulting in additional scaling down of drifts toward solar maximum. A similar procedure was followed by Ndiitwani et al. (2005). Here it is repeated because of the availability of recent Ulysses observations.

Figure 4.8 shows 10 computed scenarios corresponding to different values of $(K_A)_0$, from full drift $(K_A)_0$ =1.0 to no drift $(K_A)_0$= 0, in intervals of 0.1. This exercise is done for both polarity cycles of the HMF, for both the solar minimum and the solar maximum periods. Note that the drift parameter still changes time-dependently via the compound approach. Results in Figure 4.8 thus suggest that this additional reduction in drift is required.

By comparing the different computed scenarios to the observations, it follows that for the period ∼1991 to ∼1992 the scenarios $(K_A)_0$ = 0.0 - 0.3 are required to produce compatible results with the Ulysses/KET observations. For ∼1992 to ∼1993.5, the value of $(K_A)_0$ must be increased from ∼0.3, to ∼0.7 to compute modulation compatible with observations. This is a clear indication that drifts increased gradually in this period. For the period ∼1993.5 to ∼1994.5 the scenarios $(K_A)_0$ = 0.85 → 0.90 result in compatibility, an indication of further increase in drift over this period. For the period of ∼1994.5 to ∼1994.7 the parameter needed to be increased to $(K_A)_0$= 0.95. For the period ∼1994.7 to ∼1996.5, when the Ulysses spacecraft made its FLS1, $(K_A)_0$= 1.0 results in compatibility with the observations during this solar minimum period. For the period ∼1996.5 to ∼1997.0, it drops slightly to $(K_A)_0$= 0.9. From ∼1997 to ∼1998 there is a turn back to $(K_A)_0$= 1.0, but this does not last long since for the period of ∼1998.0 to ∼1999.8, there is a decrease to $(K_A)_0$= 0.8. For the period ∼1998.5 to ∼1999.5 the scenarios $(K_A)_0$= 0.6 → 0.75 give compatible results, while for the period ∼1999.9 to ∼2000.3, the scenarios $(K_A)_0$= 0.35 → 0.65 are needed, showing a decline in drifts over this period.

For ∼2000.3 to ∼2000.9, $(K_A)_0$= 0.3 → 0.0 is needed, showing that drifts over this period of the HMF polarity reversal vanished. For this solar maximum period Figure 4.8 shows that drifts are needed to be scaled down even to zero in the model (as argued by Ferreira and Potgieter 2004 and Ndiitwani et al. 2005). Meanwhile, for the period ∼2000.9 to ∼2002.6 during the FLS2 of the Ulysses spacecraft, the scenarios $(K_A)_0$ = 0.2 → 0.4 result in compatible calculations. This is a clear indication of a quick recovery in drifts after the polarity reversal. For the period ∼2002.2 to ∼2003.9, drifts are continually recovering to $(K_A)_0$ = 0.3 → 0.7. From ∼2003.9 to ∼2008 the scenarios $(K_A)_0$= 0.8 → 1.0 represent the data well over this period, when the Ulysses spacecraft underwent its FLS3. The peak in differential intensities shows the beginning of the solar minimum period which is different from the one in 1995 due to the polarity reversal.

4.6 Constructing a time dependence in $(K_A)_0$

By inspecting the reduction in $(K_A)_0$ needed to compute realistic intensities along the Ulysses trajectory over time, one can construct a time-dependent function to scale drifts additionally toward solar maximum in the model.

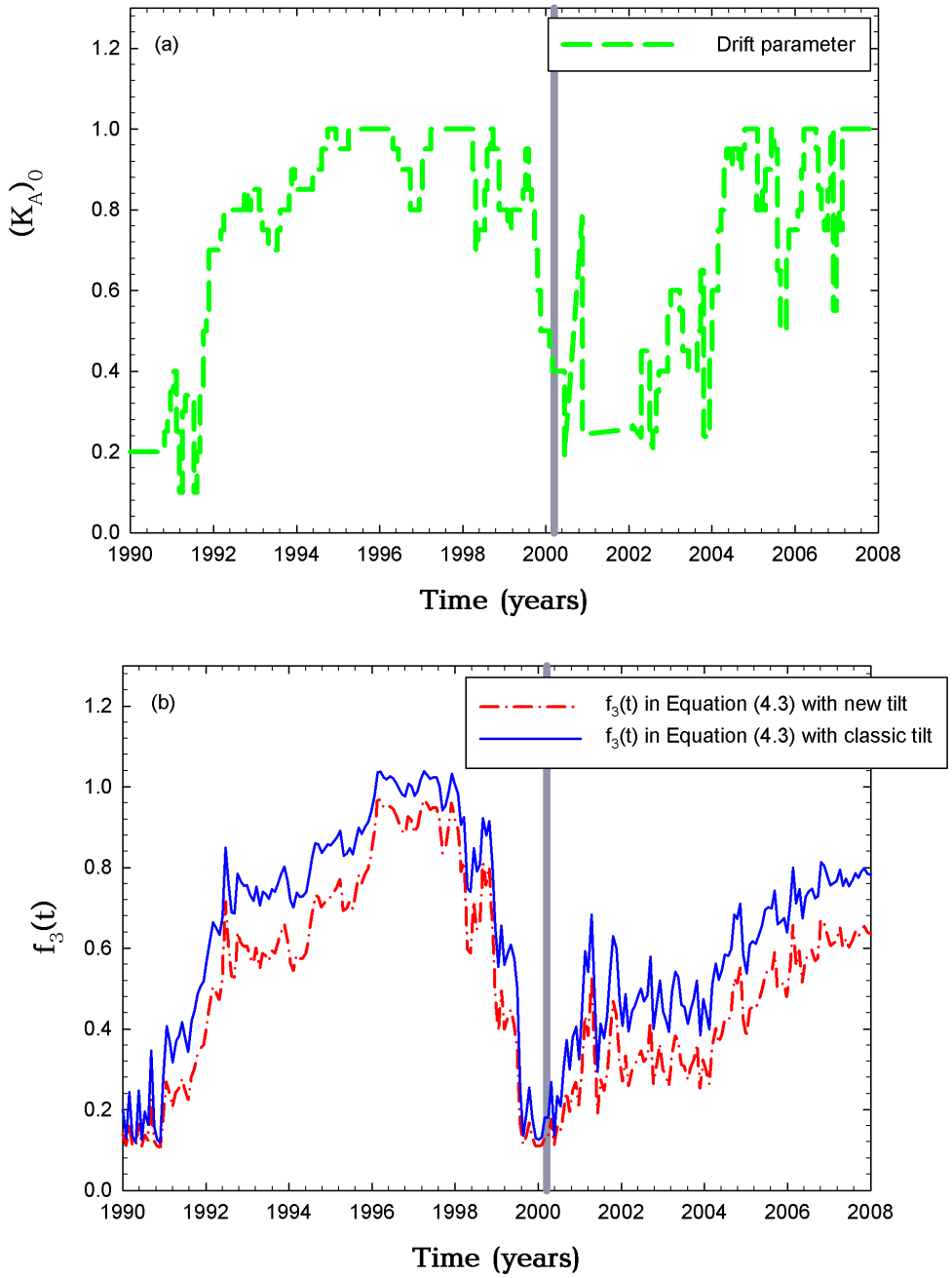

Figure 4.9: (a) The drift parameter $(K_A)_0$ plotted against time, needed to compute modulation compatible to Ulysses observations. (b) The function $f_3(t)$ with the classic tilt (solid line) and the new (long dash) tilt as input. The vertical line indicates the time in which the magnetic field changes polarity.

In Figure 4.8 the 2.5 GV Ulysses observations are compared with several model computations for different $(K_A)_0$. From this figure it was possible to pick those periods from which the model produces compatible computations. From these results a plot of $(K_A)_0$ needed to compute realistic modulation against time is shown in Figure 4.9 (a). A continuous time-dependent function is constructed to vary $(K_A)_0$ as a function of time in the model using α as input and is given by

$$f_3(t) = 1.0\left[1.1 - \frac{\alpha(t)}{75^\circ}\right]^{0.8}. \tag{4.3}$$

The solid blue line in Figure 4.9 (a) corresponds to $f_3(t)$ with the "'classic" tilt model as input while the dashed-dotted red line corresponds to $f_3(t)$ with the "new" model used as input. This expression is used to scale drift additionally over the solar maximum periods to compute compatible intensities when compared to observations and to compute realistic charge-sign dependent modulation. Equation (4.3) is now used to provide a time-dependence in $(K_A)_0$. Similar conclusions, as follow in Figure 4.9, were given by Minnie et al. (2007) showing that K_A reaches its maximum value as the magnetic variance δB reaches its peak. Figure 4.10, (from Minnie et al. 2007) shows K_A and the magnetic variations δB. This shows that the particle drifts become small as the turbulence on the magnetic field increases toward solar maximum.

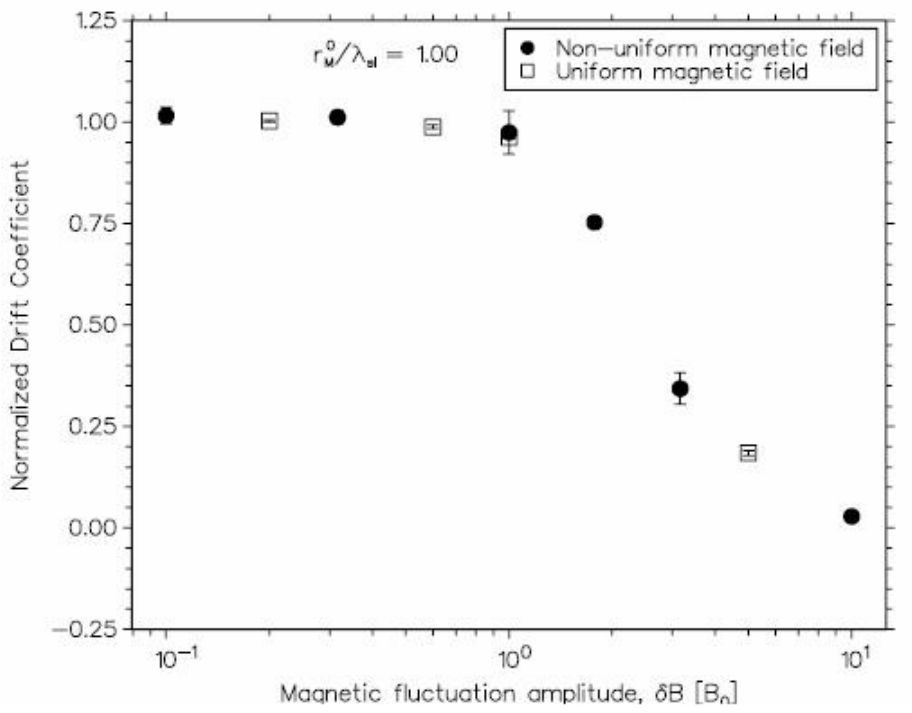

Figure 4.10: Drift coefficient K_A as a function of magnetic field fluctuation amplitude as in terms of δB normalized to B. (from Minnie et al. 2007).

4.7 Summary and conclusions

In this chapter a brief overview into time-dependent cosmic ray modulation was given. First numerical work was started by le Roux and Potgieter (1990) employing a time-dependent modulation model with drift effects. They showed that, by using the tilt angle as the only time-varying parameter, results compatible to spacecraft observations could be computed for solar minimum conditions. However, for increasing solar activity, where step-like decreases become more pronounced (Figure 4.2), propagating diffusion barriers were needed. le Roux and Potgieter (1995) showed that using a modulation model and incorporating GMIRs (Burlaga et al. 1993) with changes in tilt angle, it was possible to simulate a complete 22-year modulation cycle. Their results are shown in Figure 4.5.

However, Cane et al. (1999) and Wibberenz et al. (2002) suggested an alternative where only time-dependent changes in the HMF magnitude are responsible for changes in the magnitude at the diffusion and drift parameters. Shown by Ferreira and Potgieter (2004), using a modulation model, this resulted in computed modulation compatible to neutron monitor observations (Figure 4.6). For lower rigidities this was no longer the case. They suggested a combined approached, called the compound approach, where all the diffusion and drift coefficients are scaled time-dependently, Equation (4.2), including measured HMF magnitude and tilt angles. This resulted in computed modulation compatible with observations of different spacecraft (Figure 4.7).

However, as shown by Ndiitwani et al. (2005), drifts needed to be scaled down additionally toward solar maximum to compute realistic charge-sign dependent modulation. Ndiitwani et al. (2005) constructed a time-dependent function to scale drifts down additionally toward solar maximum. In this chapter this function was refined by also including recent observations of the Ulysses spacecraft. The function is given by Equation (4.3) and was constructed by inspecting results from different $(K_A)_0$ needed to compute realistic modulation to observations as shown in Figures 4.8 and 4.9. This phenomenological approach is supported by the theoretical work of Minnie et al. (2007) as shown in Figure 4.10.

Chapter 5

Modeling of cosmic ray proton and electron intensities along the Ulysses trajectory

5.1 Introduction

A 2D time-dependent modulation model, as discussed in Chapter 3, incorporating the compound approach and additional scaling of drifts as discussed in Chapter 4, is used to compute cosmic ray intensities along the Ulysses trajectory. Recent data from the Ulysses spacecraft (Heber et al. 2009) are used to establish compatibility of the model with observations. Also in this chapter, a more detailed investigation of the Ulysses fast latitude scan periods is presented. One of the main outcomes of this work is to show that the model, with the compound approach, can indeed produce compatible intensities when compared to observations for these periods.

5.2 Comparison between model results and the Ulysses spacecraft observations

As mentioned above, a 2D time-dependent modulation model with the compound approach is used to calculate 2.5 GV proton and electron intensities along the Ulysses trajectory. It was shown by Ferreira and Potgieter (2004) and Ndiitwani et al. (2005) that this approach, when compared to Ulysses observations (e.g. Heber et al. 2009), resulted in compatible computed intensities. This work continues on these efforts, with emphasis on the fast latitude scan periods, in particular the most recent one.

Shown in Figure 5.1 are computed 2.5 GV proton differential intensities along the Ulysses trajectory. These calculations started in 1991 and include both $A > 0$ and $A < 0$ polarity cycles. Indicated by vertical lines are the three fast latitude scan periods occurring in $\sim$1995, $\sim$2001 and $\sim$2007 respectively. The blue line shows the computed 2.5 GV proton intensities at Earth,

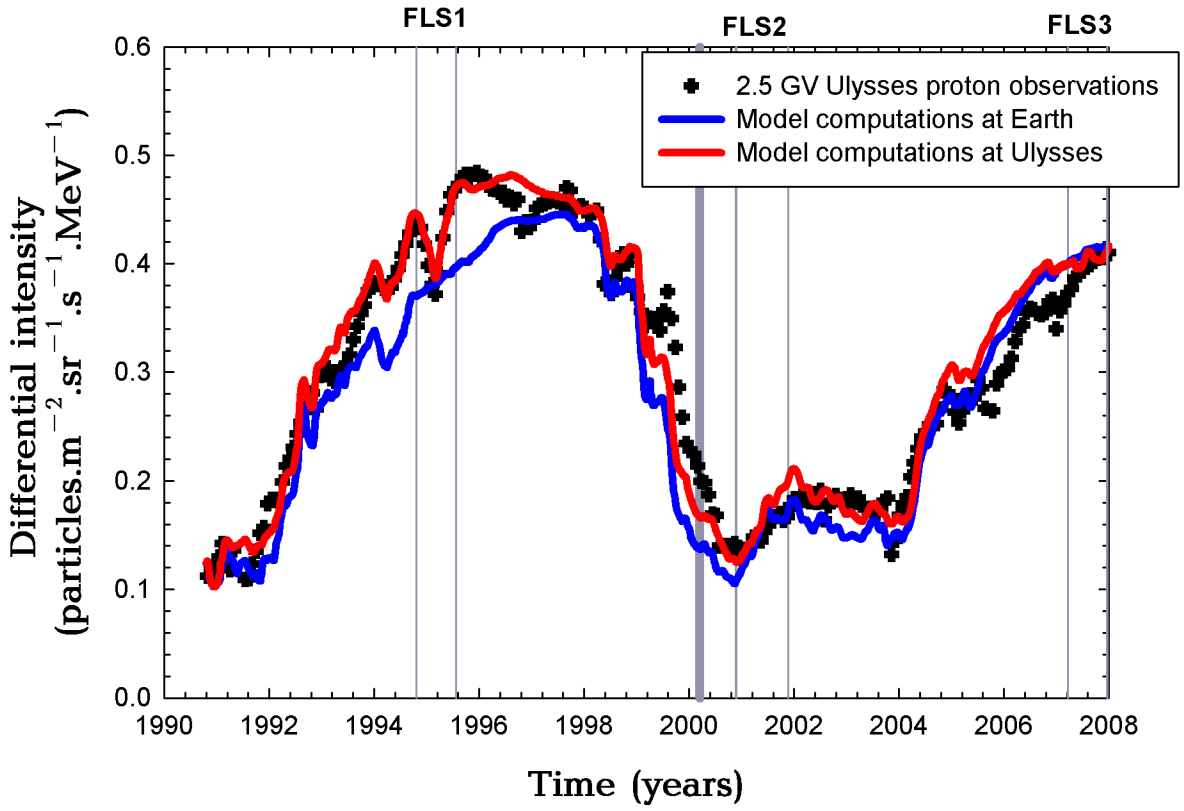

Figure 5.1: Model computations of 2.5 GV proton differential intensities against time compared to the ∼2.5 GV Ulysses observations (Heber et al. 2009). Indicated by the vertical lines are the three fast latitude scan periods of the Ulysses spacecraft, occurring in ∼1995, ∼2001 and ∼2007 respectively. It is assumed that the HMF switches polarity (from A $>$ 0 to A $<$ 0) at 2000.2 as indicated by the dark vertical line.

while the red solid line show the computations along the Ulysses trajectory. In comparison the ∼2.5 GV Ulysses observations are shown (Heber et al. 2009). New in this work, compared to the studies done by Ndiitwani (2005), is that intensities are computed up to the end of 2008 also including the third fast latitude scan.

Ulysses observations started during solar maximum in the early 1990s. Shown in Figure 5.1 is that both model and observations increase when solar activity decreased towards the mid 1990s. The FLS1 period occurred during solar minimum conditions and during the A $>$ 0 polarity cycle of the Sun. During this period positively charged particles drift into the inner heliosphere mainly over the poles and outward along the heliospheric current sheet. One therefore expects higher intensities at the polar regions. As shown, the model produces compatible results when compared to the Ulysses observations for the FLS1 in period $\sim$ 1995, with both model and observations showing a significant latitudinal gradient.

After ∼1998 the observed intensities start to decrease again, with the model also computing a decrease toward solar maximum. Note that, as reported by Ferreira (2002), the model results in a faster decrease in intensities toward solar maximum than observed for this period. As discussed by Ferreira (2002) the decrease is more rapid than what is observed for an increasing

α in this period. This was also found by le Roux and Potgieter (1992,1995). They illustrated that for periods of moderate to maximum solar activity the model computations show a stronger α dependence than what is observed. To overcome this problem, they proposed that the HCS becomes increasingly deformed further away from the Sun, especially with fast increasing solar activity (tilt angle). This deformation results in cosmic rays experiencing reduced tilt angles and therefore an effective reduction in the HCS modulation effect. To simulate this, a different set of modified α has to be used as input for the compound approach. However, this is beyond the scope of this study.

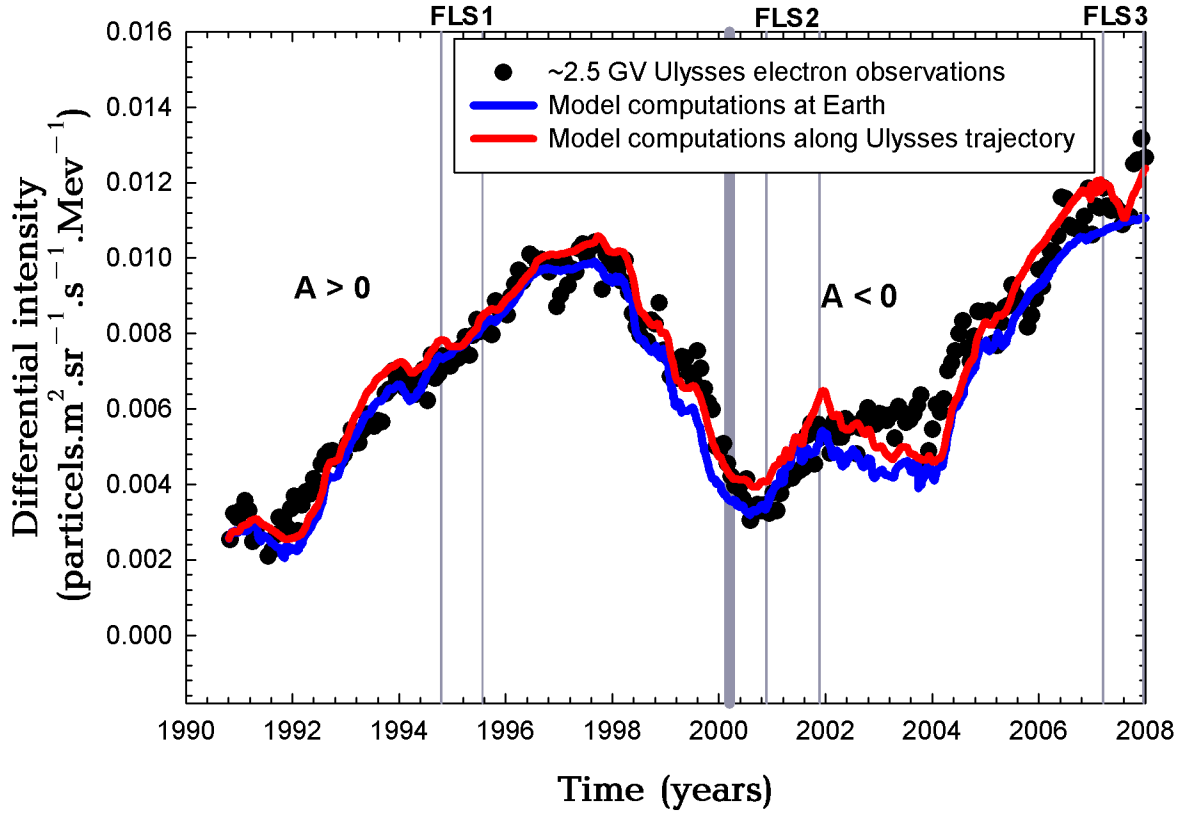

Figure 5.2: Similar to Figure 5.1 but for cosmic ray electrons.

It is assumed in this study that the Sun changes polarity at ~2000.2 represented by the thick vertical line in Figure 5.1. The intensity is lowest at ~2001 indicating extreme solar maximum. During this period the Ulysses spacecraft completed its FLS2. Because this occurred during a solar maximum period, no preferred drift direction exists. As shown in Figure 5.1 both the computed model intensities along Ulysses and at Earth are relatively close to each other and therefore, for the FLS2 period, the model shows no significant latitudinal gradient.

Cosmic ray intensities start to increase from ~2004 onward marking the beginning of the onset toward solar minimum. This time Ulysses observed cosmic ray modulation in a different polarity cycle. The model computations again follow the observations closely during this period. During this solar minimum Ulysses reached its highest heliographic southern latitude

and also northern latitude within a year marking its FLS3 in ∼2007. No similar responses in cosmic ray intensities during FLS3 were observed as in FLS1 (Heber et al. 2008). From a cosmic ray perspective the recent fast latitude scan occurred in the $A < 0$ polarity cycle where particles drifted mainly in along the current sheet and out along the poles. For this period no well defined latitudinal gradients are expected in the inner heliosphere. The solar wind observed by the Ulysses spacecraft in the current solar minimum has the lowest densities ever measured (e.g. McComas et al. 2008; Isautier et al. 2008). Furthermore, the magnetic field measured was also said to be lower compared to the last solar minimum (Smith and Balogh 2008). In contrast to what is expected Heber et al. (2009) reported that the cosmic ray proton flux, as measured by Ulysses in 2008 did not exceed the intensities as observed in the mid 1990s solar minimum. However, the 2.5 GV cosmic ray electron intensities do exceed the intensities during the mid 1990s by ∼(30 - 40)%. In the next figure the focus shifts to galactic cosmic ray electrons.

Figure 5.2 is similar to Figure 5.1 except that observations and model results for 2.5 GV electrons are shown. Again the model produces compatible intensities on a global scale when compared to observations. Compared to protons, which show a latitudinal dependence for the FLS1, and no latitudinal dependence for the FLS2 and FLS3, the opposite happens here. The FLS1 period of electrons occurs during the $A > 0$ polarity cycle where the negative particles drift in from the equatorial regions to the inner heliosphere and outwards over the poles and no significant latitude dependence is expected.

As for protons, the FLS2 period shows no latitudinal dependence due to solar maximum activity present. The electrons, however, show a latitudinal dependence during the FLS3 period (Heber et al. 2008) similar to the FLS1 for protons. Here electrons drift in along the poles and outward along the equatorial region. During the third latitude scan of Ulysses an average latitudinal gradient of ∼0.19%/degree was found (Heber et al. 2008) indicating an observable latitudinal dependence of cosmic ray electrons during this period.

5.3 The fast latitude scan periods

The fast latitude scan periods are now highlighted in Figure 5.3 (for 2.5 GV protons) and Figure 5.4 (for 2.5 GV electrons) respectively. Again the model results are shown together with the Ulysses observations. The latitude of the Ulysses spacecraft (in degrees) are also shown by dashed red lines for comparison.

Figure 5.3 shows that the model produces compatible results when compared to Ulysses observations for both the three fast latitudes scan periods for protons on this scale. During these periods the Ulysses spacecraft moved from pole to pole and if drifts were important a latitude dependence would be clearly evident.

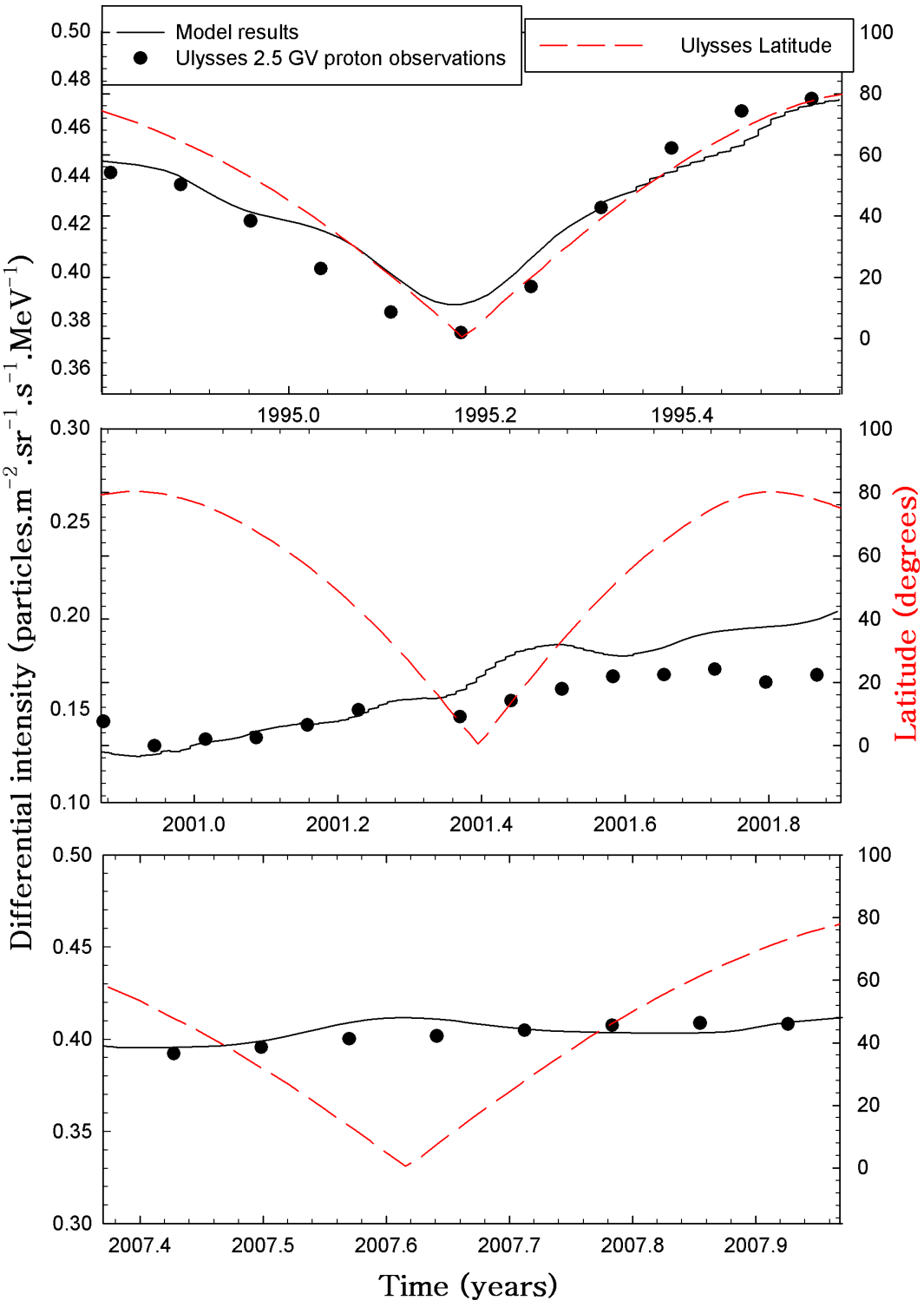

Figure 5.3: Model computations (solid line) of 2.5 GV cosmic ray proton intensities during the three fast latitude scan periods of the Ulysses spacecraft, namely FLS1, FLS2 and FLS3, which occurred in ∼1995, ∼2001 and ∼2007 respectively. Shown in comparison are the Ulysses observations (black dots) for these periods. The dashed red line indicates the latitude of the Ulysses spacecraft in degrees for comparison.

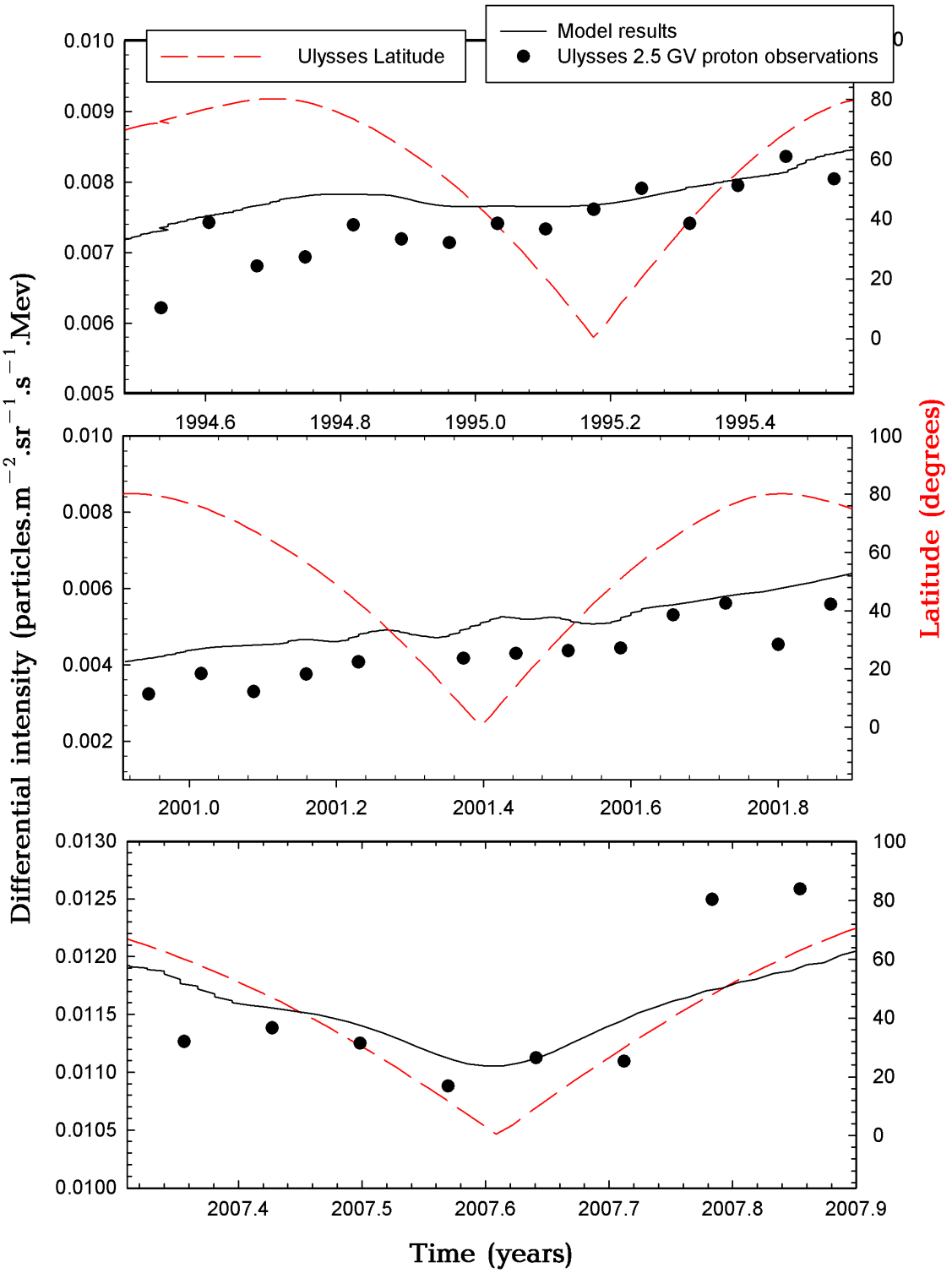

Figure 5.4: Same as Figure 5.3 but for electrons.

For the FLS1 period this happened during solar minimum and for the A $>$ 0 polarity cycle of the HMF. For this period, Ulysses observed high intensities over the poles and lower intensities in the equatorial regions as shown in the top panel of Figure 5.3. Evidently there

is a correlation between the Ulysses latitude (shown by the dashed line), the model results and observations, indicating a clear latitude dependence. The FLS2 occurred in ∼2001 during solar maximum. Shown in the second panel is that the observed and modeled intensities are almost constant. A gradual increase from about ∼0.15 to ∼ 0.20 particles.m^{-2}.s^{-1}.sr^{-1}.GV^{-1} are observed and computed, which is caused solar cycle related effects rather than a latitudinal dependence.

Recently, the Ulysses spacecraft undertook its third fast latitude scan (FLS3). This occurred in moderate to minimum solar activity conditions and for the A < 0 cycle. The result is that the observations and model seem insensitive to the latitudinal position of Ulysses as shown in the bottom panel in Figure 5.3.

Figure 5.4 shows the same, but for electrons. Here the opposite happens for FLS1 and FLS3. For the FLS1 period, the negatively charged cosmic rays drift toward the Sun from the equatorial regions. As for the FLS3 period for the protons, there is no clear latitudinal dependence with intensities fluctuating, which can be attributed to solar activity.

The FLS2 period occurred in ∼2001 at solar maximum. As for the protons, no clear latitudinal dependence is observed or calculated due to the suppression of drift effects. The FLS3 occurred during moderate to minimum solar activity. For this period, the electrons drift in from the poles and outward along the equatorial regions of the Sun. Similar to the FLS1 for protons, Ulysses observed the highest intensity of electrons over the polar regions with a clear correlation of the observed and modeled intensities with the latitudinal position of the Ulysses spacecraft.

5.4 Global distributions

This section again concentrates on the three fast latitude scan periods of the Ulysses spacecraft. Based on the success of the model in computing realistic intensities for these periods along the Ulysses trajectory, global distributions for these periods are now shown. This is done by drawing contour plots for both 2.5 GV electrons and protons for the three fast latitude scans which occurred in ∼1995, ∼2001 and ∼2007 respectively. These computations are shown in the meridional plane, with the horizontal axis the equatorial plane, and the vertical axis the polar regions.

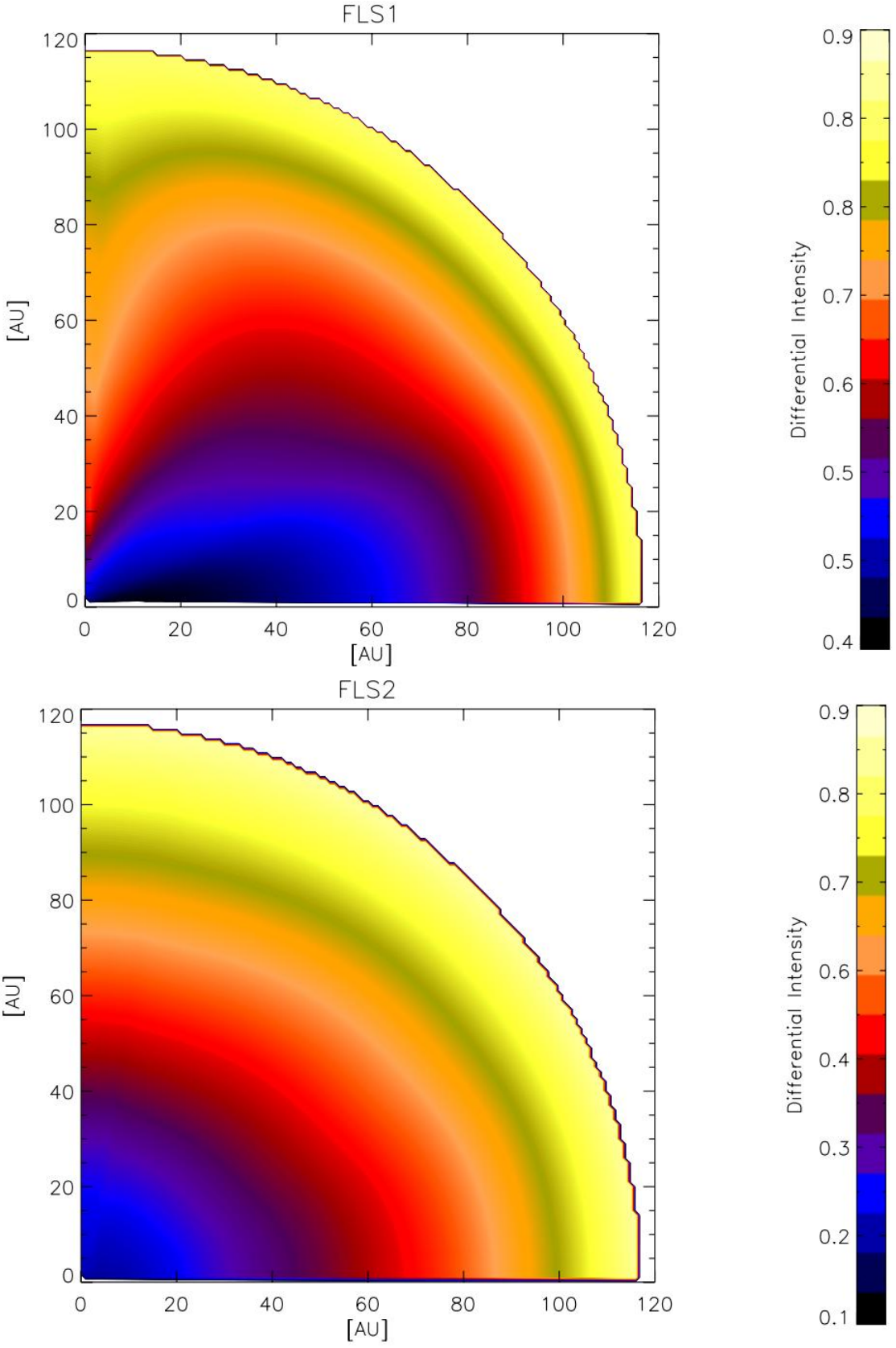

Figure 5.5: Two contour plots showing the distribution of 2.5 GV protons during FLS1 (top panel) and FLS2 (bottom panel) of the Ulysses spacecraft. The top panel illustrates solar minimum conditions while the bottom panel shows solar maximum conditions.

Shown in Figure 5.5 is a contour plot representation of the 2.5 GV proton differential intensity for FLS1 and FLS2. The modulation boundary is assumed to be at ∼120 AU in the model. As

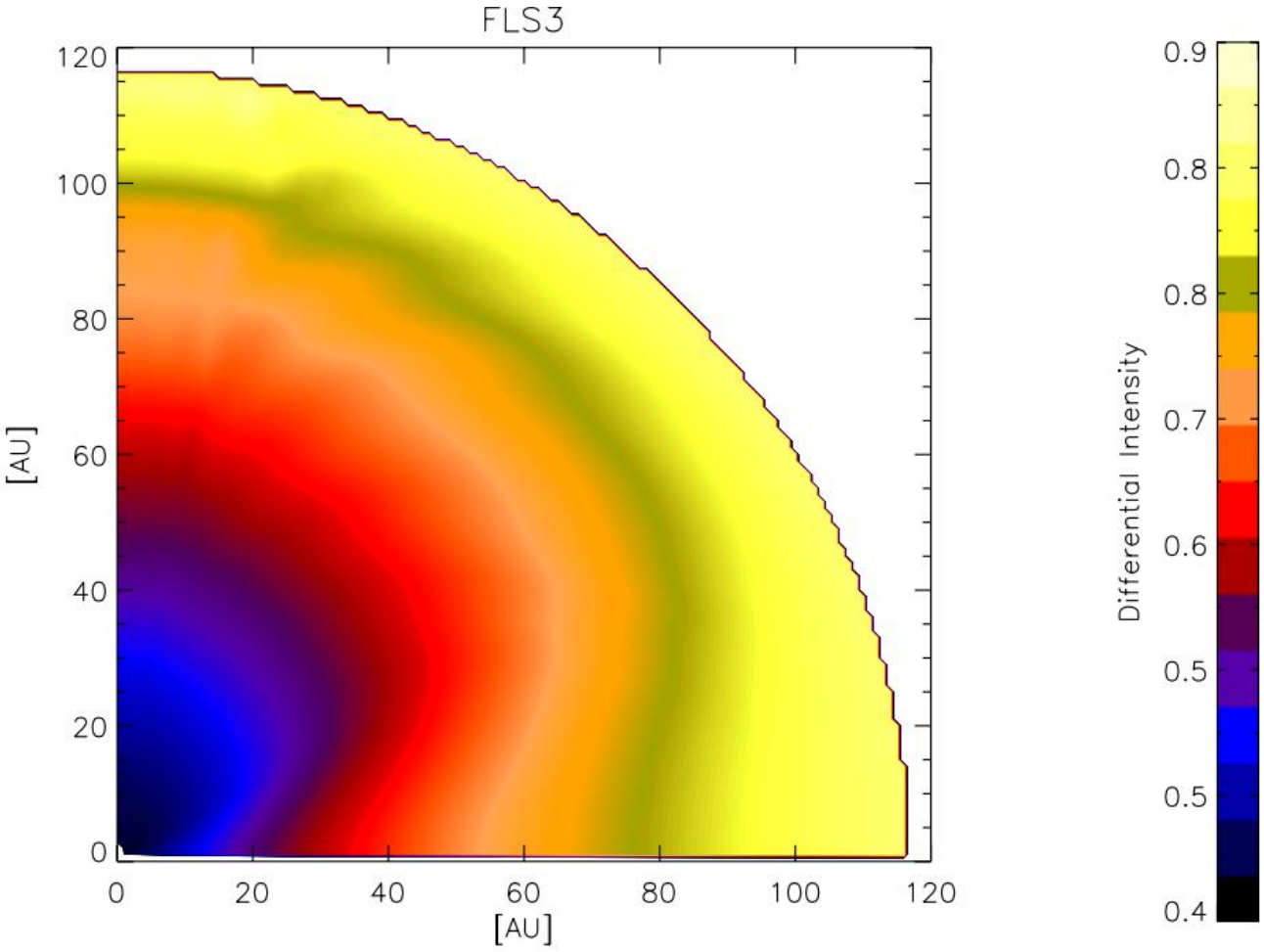

Figure 5.6: As Figure 5.5 but for the FLS3 period.

mentioned earlier, the FLS1 occurred during solar minimum in the A $>$ 0 magnetic epoch. In Figure 5.5 the different colors (shades) show intensity changes, where the gold to red (light) colors show high intensities, whereas the blue to black (dark) colors show low intensities.

Note that results are only shown for polar angles between $\theta = 0°$ to $\theta = 90°$ (heliolatitude of 0° and 90° respectively). For the FLS1 shown at the top there is also a polar inflow of cosmic rays, as shown by the gold to red colors indicating that the particles are transported into the inner heliosphere over the polar regions of the heliosphere due to drift. Evident here is a latitudinal dependence for protons for this polarity cycle.

The second fast latitude scan period occurred in ∼2001, but for solar maximum. For this period FLS2 in Figure 5.5 (bottom panel) shows no well defined and preferred inflow direction of protons. This shows that when drifts are suppressed, the modulation picture is primarily diffusive.

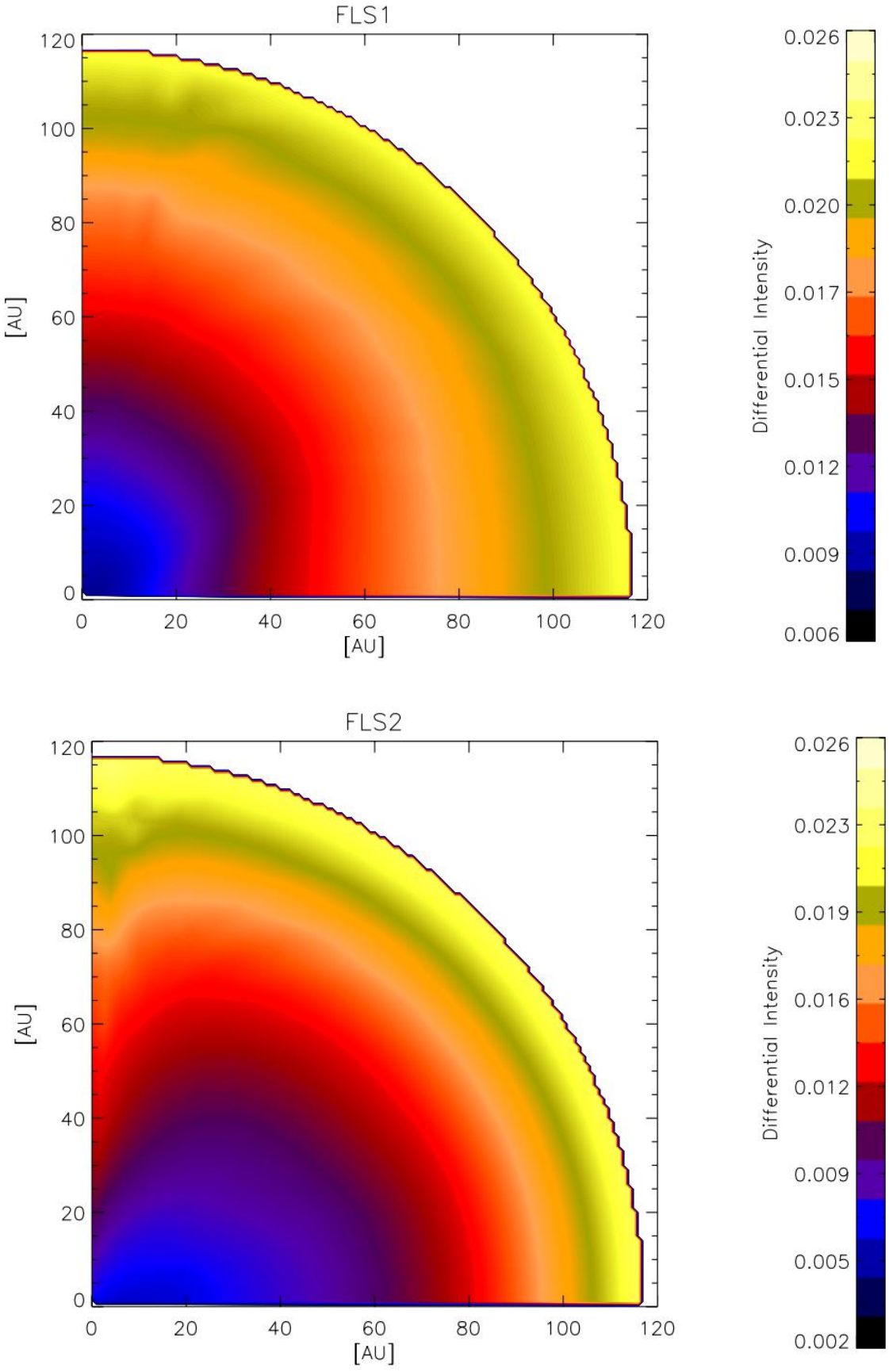

Figure 5.7: As Figure 5.5 but for 2.5 GV electrons.

Shown in Figure 5.6 is a contour plot for the FLS3 period that occurred during moderate to minimum solar activity. As expected there is an influx of particles in the equatorial regions as shown by the colors changing from gold (high intensity) to blue (low intensity). Shown here is that the opposite to FLS1 is occurring. For this cycle, the positively charged particles drift in from the equatorial regions along the HCS to the inner heliosphere. As shown there is no noticeable latitudinal dependence in the inner heliosphere (blue region), although for the set of modulation parameters assumed in the model a latitudinal dependence is expected in the outer heliosphere (look e.g. at 80 AU).

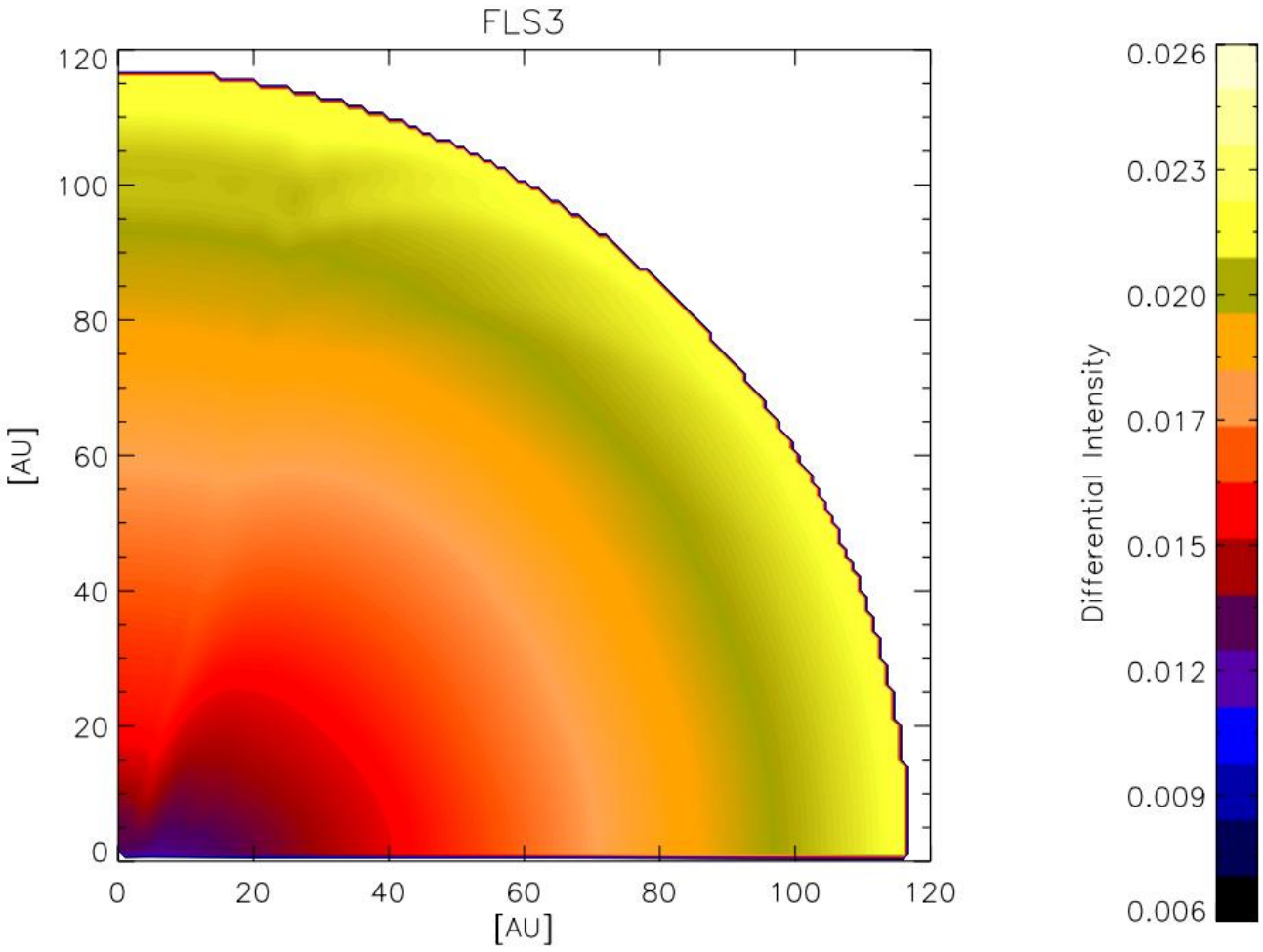

Figure 5.8: As Figure 5.7 but for the FLS3 period.

Shown in Figure 5.7 is the 2.5 GV electron distribution for FLS1 (top panel) and FLS2 (bottom panel) respectively. Electrons show a different distribution compared to that of protons. The electrons exhibit no variation in intensities in the inner heliosphere during FLS1 as shown in Figure 5.7 (top panel). During FLS1 electrons drift in from the equatorial region along the HCS to the inner heliosphere. During this period high intensities are expected in the equatorial regions of the Sun. FLS2 for electrons took place at ∼2001 during solar maximum as shown in the bottom panel of Figure 5.7. Similar to protons there is no direct region of influx of parti-

cles indicating that drift effects are suppressed by the diffusive process. During this period the electrons drift in from the poles to the inner heliosphere. Similar to FLS1, high intensities occur over the poles, indicating the inflow of electrons in this region. The FLS3 occurred during the $A < 0$ magnetic epoch and is shown in Figure 5.8.

5.5 Summary and conclusions

In this chapter a 2-D time-dependent model, incorporating the compound approach as discussed in Chapter 4, was used to calculate 2.5 GV cosmic ray proton and electron intensities at Earth and along the Ulysses trajectory. Results were compared to Ulysses observations (Heber et al.2009) as shown in Figure 5.1 and 5.2 for ∼2.5 GV protons and electrons respectively.

In particular, focus was on the three fast latitude scan periods of the Ulysses spacecraft namely FLS1, FLS2 and FLS3 which occurred in ∼1995, ∼2001 and ∼2007 respectively. It was shown that the model could compute intensities compatible to Ulysses observations for these periods. Both model and observations showed that for protons an observable latitudinal gradient is evident for the FLS1 period, and none for the FLS2 and FLS3 periods as shown in Figure 5.3. For the electrons no significant latitudinal dependence was computed for both FLS1 and FLS2 periods, but it was computed for FLS3 period as shown in Figure 5.4. Intensity contour plots for these periods were also presented in Figures 5.5 to 5.8 showing the global distribution, from the inner to the outer heliosphere, in the meridional plane.

Chapter 6

Charge-sign dependent modulation and refinement of the compound approach

6.1 Introduction

In this chapter the time-dependent model and the compound approach, as described in previous chapters, are used again to compute both cosmic ray proton and electron intensities in the inner heliosphere. However, this time higher rigidities (e.g. > 2.5 GV) are also considered. This is to get a better understanding of the dependence of the modulation amplitude as a function of rigidity. This was not considered in previous work done by Ferreira and Potgieter (2004) and Ndiitwani et al. (2005). Results are presented not just at 2.5 GV, as in previous chapters, but also at higher rigidities. These calculations are of importance, not just to Ulysses observations, but also to measurements e.g. from the PAMELA spacecraft. Also computed and presented are electron to proton ratios at different rigidities to show charge-sign dependent modulation.

6.2 Model results at higher rigidities and charge-sign dependent modulation.

Figure 6.1 shows computed proton differential intensities, at different rigidities, ranging from $\sim$2.5 GV up to $\sim$7.3 GV. Also shown are the 2.5 GV Ulysses observations as symbols (Heber et al. 2009) for comparison to the 2.5 GV model computations. The blue and green solid lines indicate both the computed 2.5 GV proton intensities at Earth and along the Ulysses trajectory respectively. Note the calculations at Earth are mostly below that for Ulysses. The other lines indicate the computed intensities only at Earth for rigidities ranging from $\sim$3.0 to $\sim$7.3 GV (from top to bottom).

The vertical lines indicate the three fast latitude scan periods of the Ulysses spacecraft. It is assumed that the Sun's magnetic field changes polarity from A > 0 to A < 0, at 2000.2. The selection of 2000.2 as the time for the Sun's magnetic field polarity reversal is optimal from a modeling part (e.g. Ndiitwani et al. 2005). If the reversal occurs earlier, the computed electron

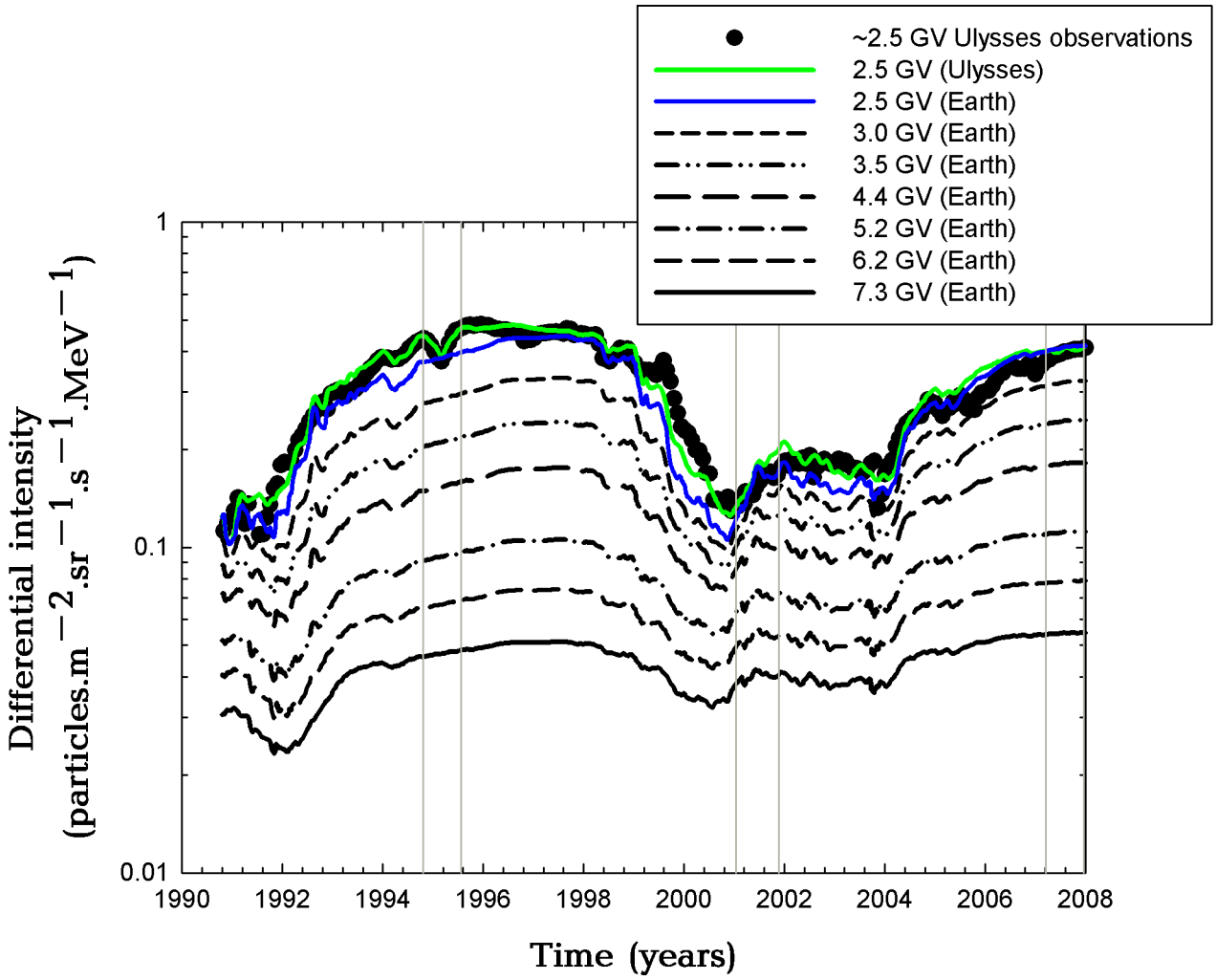

Figure 6.1: Proton differential intensities at Earth varying as a function of time at rigidities varying from 2.5 GV (top lines) to 7.3 GV (bottom line). The 2.5 GV calculations are compared to the Ulysses observations. The vertical lines indicate the three fast latitude scan periods of the Ulysses spacecraft.

to proton ratio increases too fast when compared to observations, while a later reversal lets the ratio decrease faster than the observations for the time around solar maximum.

Shown in Figure 6.1 is that for increasing rigidities, the modulation amplitude decreases, meaning a smaller percentage change in intensities between solar minimum and maximum. A flatter intensity profile is computed for e.g. 7.3 GV, represented by the bottom solid line, when compared to the 2.5 GV results. The modulation amplitude clearly decreases as a function of increasing rigidity. See also le Roux and Potgieter (1990).

Similar to Figure 6.1, Figure 6.2 shows electron differential intensities, at different rigidities. Again the 2.5 GV model calculations are also shown along the Ulysses trajectory to be compared with observations. Similar to the proton results, for increasing rigidity the modulation amplitude decreases, meaning a smaller percentage change in intensities between solar minimum and maximum.

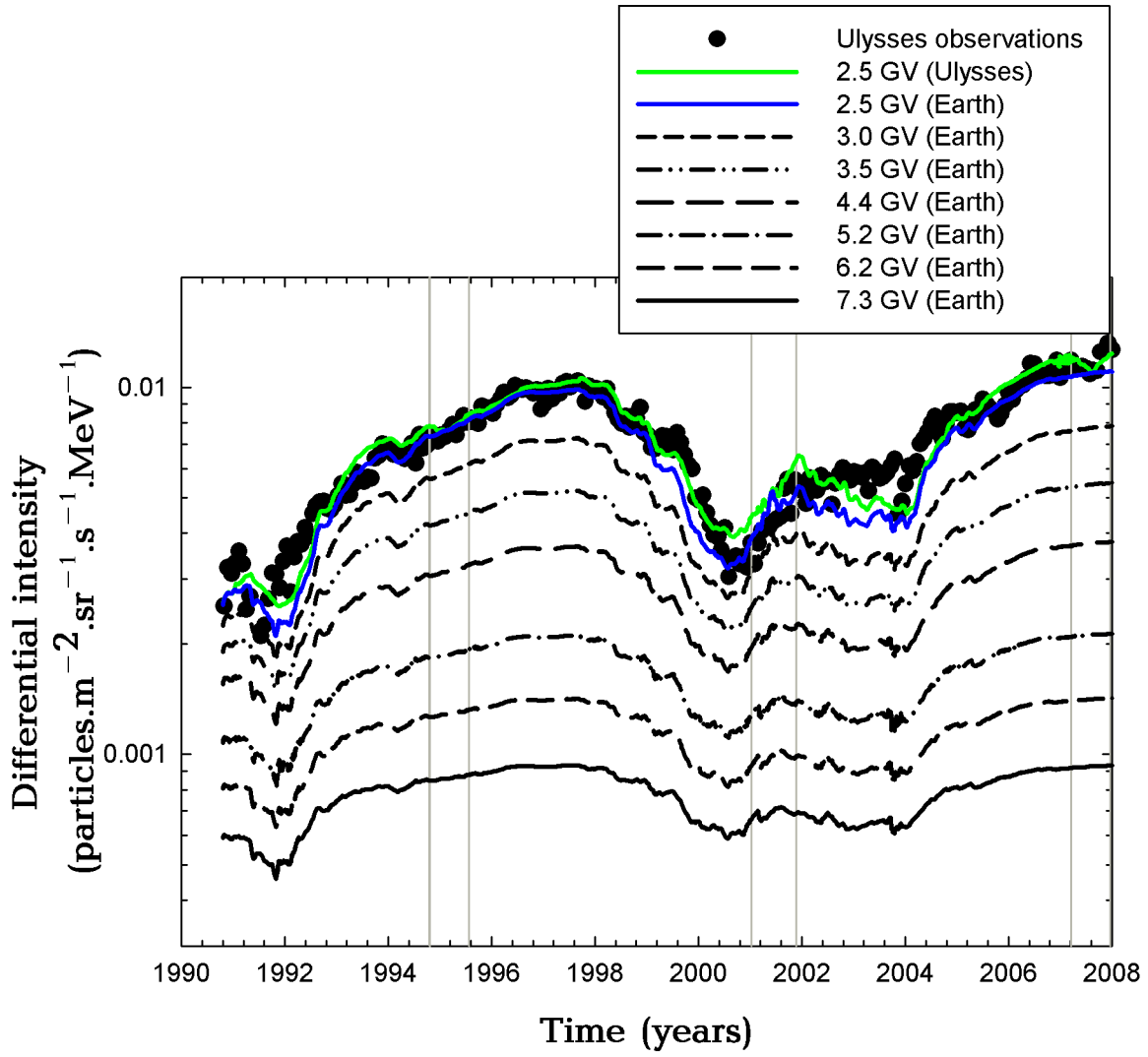

Figure 6.2: As Figure 6.1, but for electrons.

Figure 6.3 shows the electron to proton ratio calculated for rigidities varying from 2.5 GV to 7.3 GV and shown along the Ulysses trajectory. Shown in comparison are the Ulysses observations (green dots)(Heber et al. 2009). The solid line shows the ratio at 2.5 GV while the rest show the ratio from ∼3.0 GV to ∼7.3 GV as indicated in Figure 6.3.

The grey vertical lines in Figure 6.3 indicate the periods of occurrences of the fast latitude scan periods of the Ulysses spacecraft. As discussed in Chapter 5, the first two vertical lines from the left indicates the beginning and the end of the first fast latitude scan which occurred in ∼1995, while the second pair represent the second fast latitude scan which occurred in ∼2001 and lastly the third pair shows the third and most recent scan which occurred in ∼2007. As shown, from the beginning of ∼1990 the 2.5 GV model computations (solid line) follow the data closely until the beginning of ∼2000. The model computes intensities during FLS1 in ∼1995 realistically when compared to the observations. From ∼2000 till early ∼2002 there is a bump in the model computations where the computed ratios are higher than observed. This

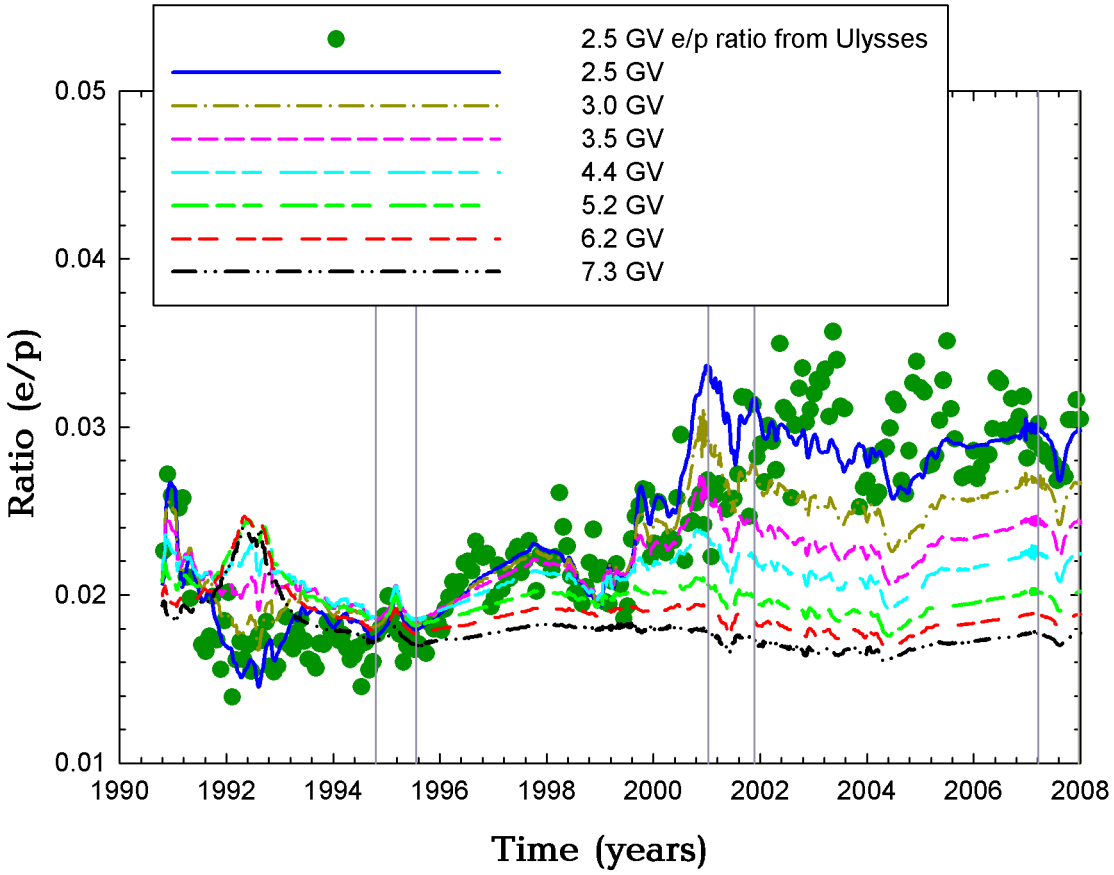

Figure 6.3: Computed 2.5 GV electron (e) to proton (p) intensity ratios at different rigidities computed along the Ulysses trajectory and compared to Ulysses observations. Different colours represent different rigidity levels as shown in the legend.

corresponds to the period where the Sun's magnetic polarity changes from A $>$ 0 to A $<$ 0, which occurred during the solar maximum period at 2000.2 in this study. Although drifts are scaled down additionally to very small values at solar maximum, the magnitude of the diffusion coefficients (as discussed in Chapter 4) is changed for different polarity cycles which results in the computed bump. As a correction to this feature in the model a gradual changing time-dependent function can be introduced. After $\sim$ 2003 the solid line is below the observations, but only for a year where the model and observations again agree after $\sim$2004 and the computed ratio for the FLS3 period is computed realistically.

Shown in Figure 6.4 is the 2.5 GV electron to proton ratios at Earth, again for rigidities ranging from $\sim$2.5 GV to $\sim$7.3 GV. The lines in Figure 6.4 indicate the various rigidity computations. The solid line indicates the 2.5 GV electron to proton ratio at Earth, the dotted line indicates the ratio at 3.0 GV and so forth up to $\sim$7.3 GV, as shown by the medium dashed line. From $\sim$1990's solar maximum, there is an increase in the $\sim$2.5 GV computed ratio. Between $\sim$1992 and $\sim$ 1993 there is a significant drop in the 2.5 GV computed ratio. From $\sim$1993 to $\sim$1996 the computed ratio fluctuates around a steady value with a slight increase after $\sim$1996. Similar to Figure 6.3 there is a significant increase in the computed ratio for the $\sim$2000 solar

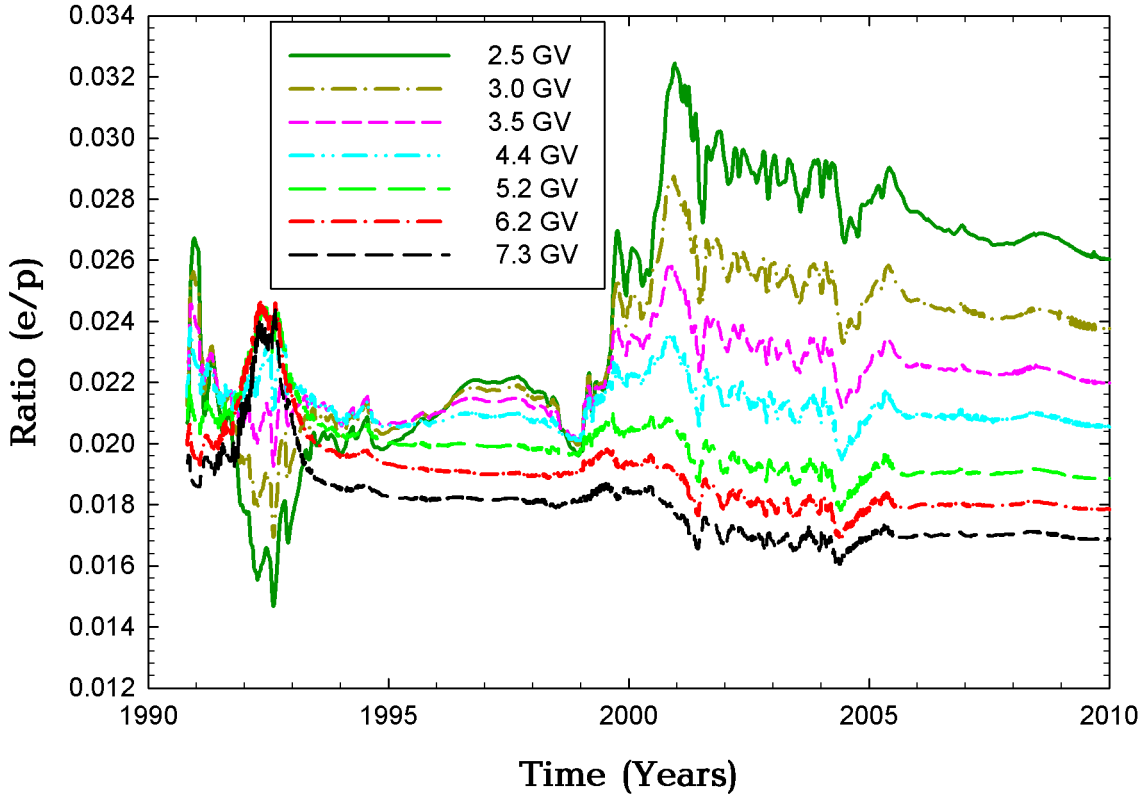

Figure 6.4: As in Figure 6.3, but for computed results at Earth, without any spacecraft observations.

maximum with a decrease after ∼2001.

6.3 Refinement of the compound approach

Shown in Figure 6.5 is the computed ratio of 2.5 to 7.3 GV proton intensities along the Ulysses trajectory as a function of time. The ratio is shown in time from the 1990s solar maximum till recently and normalised to 1.0 (minimum value). The figure shows the ratio to be ∼1 for solar maximum periods, while for solar minimum the ratio increases to ∼3. This illustrates that the modulation amplitude, with the assumption of the compound approach as in Equation (6.1), is rigidity and also solar cycle dependent. Next the focus shifts to whether the ratio, as shown in Figure 6.5, is compatible to observations. To establish this one needs an indication as to the modulation amplitude between solar minimum and solar maximum. With limited spacecraft observations for high energy cosmic rays, apart from PAMELA, neutron monitor observations may be utilized to give a clue about the modulation amplitude at high rigidities.

Figure 6.6 shows computed proton spectra for two scenarios corresponding to different n values from Equation (4.2). This equation is described in Chapter 4, and determines the time dependence of diffusion coefficients as a function of the measured HMF at Earth, and is given

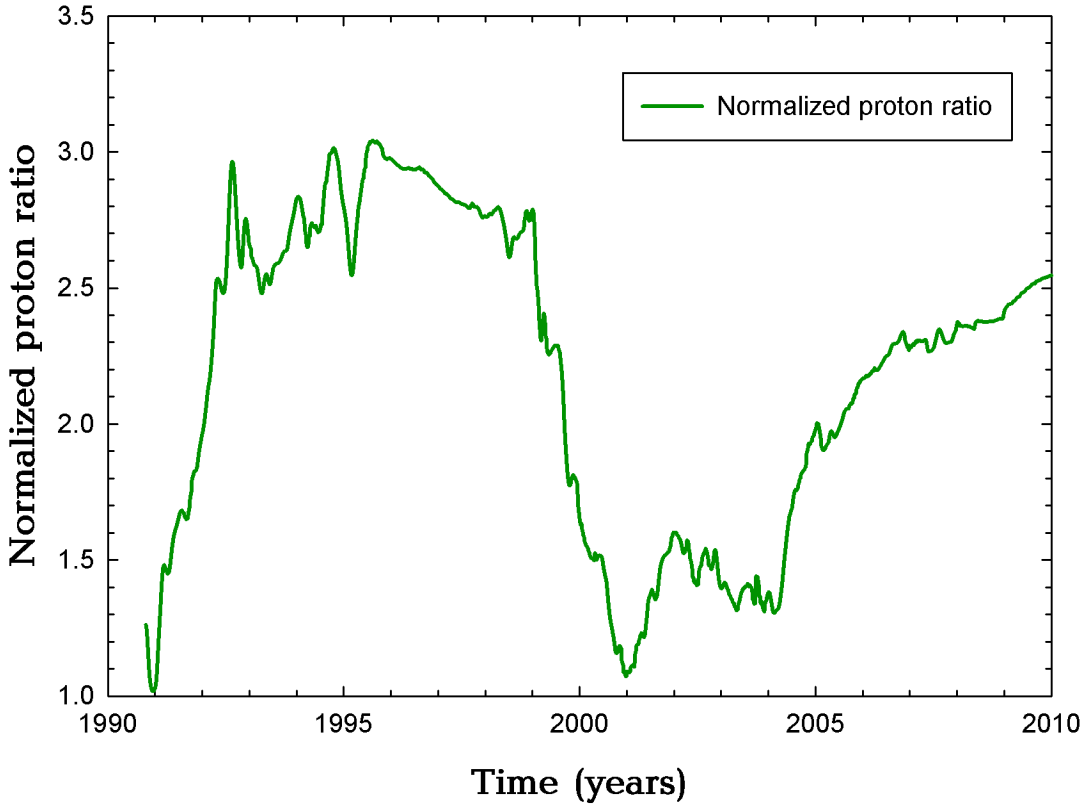

Figure 6.5: The normalised ratio of the 2.5 to 7.3 GV proton intensities at Ulysses.

here again as,

$$f_2(t) = \left(\frac{B_0}{B(t)}\right)^n \tag{6.1}$$

with B_0 = 5 nT and $B(t)$ the magnetic field magnitude measured at Earth, with n previously assumed as $n = \alpha/\alpha_0$ which is the ratio of the observed time varying tilt angle given by α and the constant tilt for a given rigidity given as α_0 = 11 in Figure 6.6 (e.g. Ferreira 2002, Ferreira and Potgieter 2004). This scenario is shown by black lines. As an indication for the modulation amplitude ∼2.5 GV Ulysses protons are used (green dots). If we assume 100% for the highest observations (solar minimum) then the lowest (solar maximum) is 27%. The top lines correspond to typical solar minima spectra and the bottom lines to solar maxima spectra. When the solid lines are then compared with the observations it is clear that the model computes compatible intensities for Ulysses at 2.5 GV.

For the scenario corresponding to the dotted lines we assumed n in Equation (6.1) as n=1. Evidently, n = 1 is in agreement with Wibberenz et al. (2002) who used mostly neutron monitor observations to study time-dependent modulation.

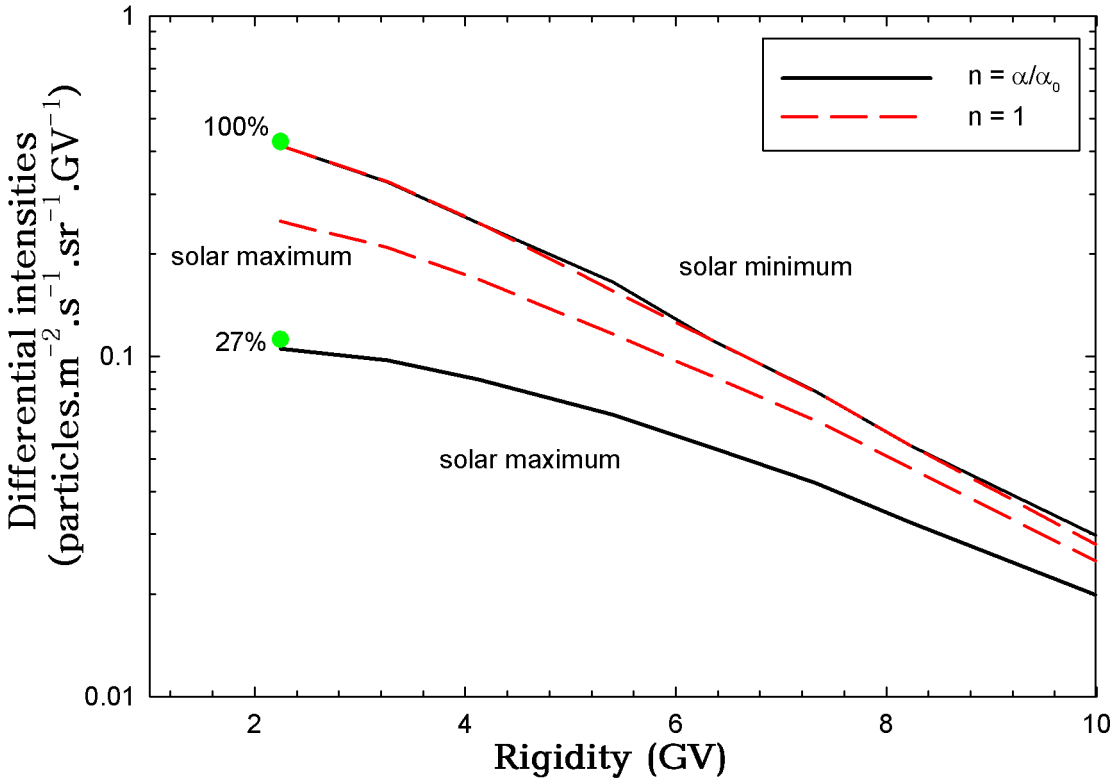

Figure 6.6: Proton spectra at Earth plotted against rigidity, for solar minimum and maximum. The Ulysses observations are indicated by green dots. Two computed scenarios corresponding to different n in Equation (6.1) are shown.

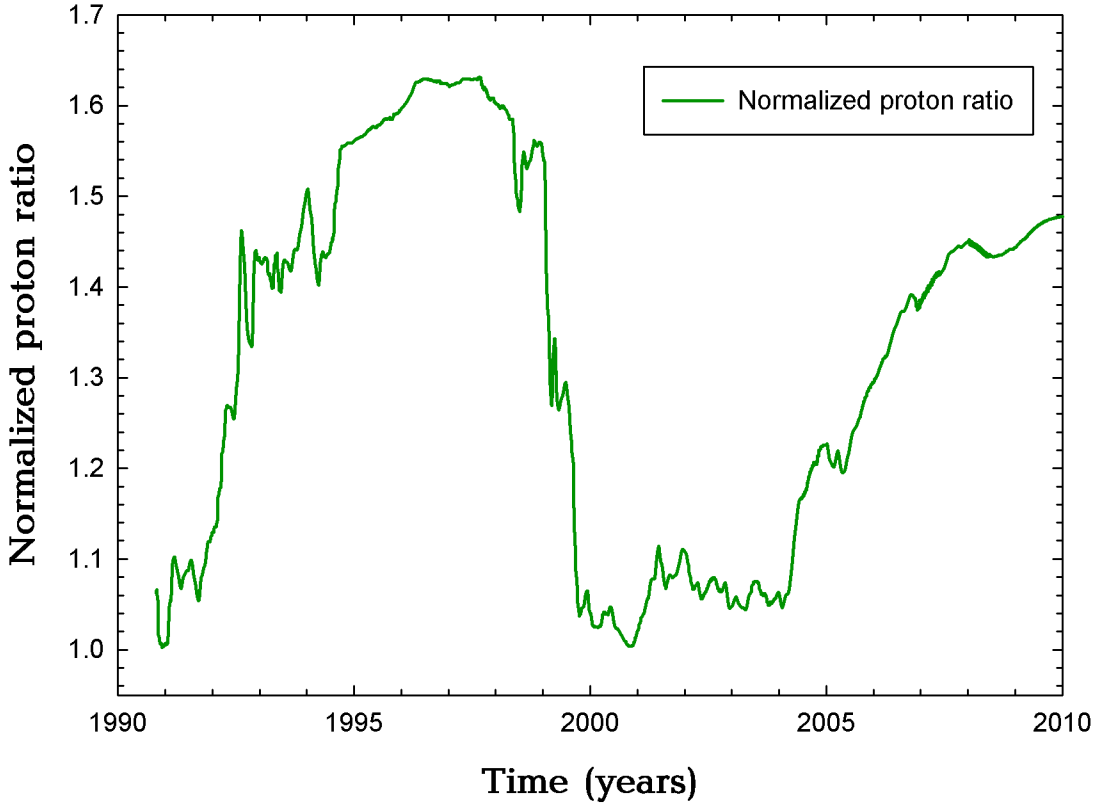

Figure 6.7: As in Figure 6.5, but at Earth and for $n = 1$ in Equation (6.1).

From Figure 6.6 it is evident that decreasing n from $n = \alpha/11$ to $n = 1$, the computed amplitude between solar maximum and minimum is decreasing. From e.g. the Hermanus neutron monitor observations follows if the highest count rate rate is 100% for solar minimum then solar maximum is around $\sim$85$\%$ so that the dashed line is more compatible than what one would expect for higher rigidities.

Shown in Figure 6.7 is the computed ratio of 2.5 to 7.3 GV protons at Earth as a function of time. In this case the ratio is shown for n = 1 in Equation (6.1) which corresponds to the dashed-line in Figure 6.6. This ratio is shown from the 1990 solar maximum till $\sim$2010 and normalized. The figure indicates that the ratio changes from $\sim$1 at the solar maximum to $\sim$1.6 for solar minimum. This is some $\sim$50$\%$ smaller than that shown in Figure 6.5. This result is important to model PAMELA spacecraft observations over a wide range of energies. Although this spacecraft has a limited operational time, time-dependent studies can be done to establish how transport parameters should change over time and as a function of rigidity.

6.4 Summary and conclusions

In this chapter model computations at Earth and along the Ulysses trajectory were presented, not only at 2.5 GV as in the previous chapters but also for higher rigidities. Also presented was the electron to proton ratio for different rigidities. It was shown that the modulation amplitude between solar minimum and maximum is rigidity and solar cycle dependent.

Furthermore, for extreme solar maximum, the model is still too sensitive when a polarity reversal is assumed. Although drifts are scaled down considerably toward solar maximum, the diffusion parameters also change for different HMF polarities. In the model this transition occurs suddenly with the polarity reversal. As a future refinement this maybe replaced by a more gradual transition.

Using Ulysses observations as a proxy for the modulation amplitude between solar minimum and solar maximum and neutron monitor observations as a guide for higher rigidities it was shown that n in Equation (6.1) must be rigidity dependent e.g. $n = \alpha/11^\circ$ for 2.5 GV and decreasing to $n = 1$ for higher rigidities at $\sim$10 GV. By using PAMELA observations this refinement is a topic for future study.

Chapter 7

Summary and conclusions

In this work numerical simulations were presented using a 2D time-dependent modulation model. The aim was to compare results with Ulysses observations to study galactic cosmic ray modulation over different solar and polarity cycles. Previous attempts started with le Roux and Potgieter (1990) who studied time-dependent modulation of cosmic rays using the tilt angle of the heliospheric current sheet (HCS) as the only time-dependent parameter. This proved to compute realistic modulation over solar minimum periods. However, le Roux and Potgieter (1995) subsequently showed that this type of model could not reproduce cosmic ray observations during increasing solar activity with the tilt angle as the only time-dependent parameter. This was confirmed when large step decreases in the observed cosmic ray intensities occurred. This series of step decreases are prominent during increasing solar activity.

le Roux and Potgieter (1995) proposed the inclusion of the propagating diffusion barriers (PDBs) to model cosmic ray intensities for both moderate to higher solar activity. They showed that it was possible to successfully simulate the 11 year proton modulation cycle by incorporating global merged interaction regions GMIRs and drifts in their model. They also assumed that the passage of GMIRs causes a temporal variation of diffusion tensor from the background values.

Later on, a different approach was suggested by Cane et al. (1999) and Wibberenz et al. (2002). They argued that the decrease in cosmic ray intensities at Earth cannot be caused by GMIRs since these decreases occured before any GMIRs could be formed. They proposed that the modulation in the inner heliosphere is rather caused by time-dependent changes in the HMF, which changes roughly by a factor of $\sim$2 between minimum to maximum solar activity. The idea was tested by Ferreira (2002) and Ferreira and Potgieter (2004) by changing all the diffusion coefficients in a fully time-dependent model reflecting time-dependent changes in the measured heliospheric magnetic field (HMF) magnitude at Earth, and also included solar cycle related changes in the tilt angle. They showed that their model could simulate the 11 year modulation successfully. However, for lower rigidities e.g. $<\sim$5 GV the computed modulation amplitude between solar minimum and maximum was too small and a different approach, called the compound approach was introduced. The compound approach was developed by

Ferreira and Potgieter (2004) and it incorporated PDBs, global changes in the HMF, and time-dependent gradient, curvature and current sheet drift. Refinements were made by Ndiitwani et al. (2005). In this study the compound approach was used and modified to model the cosmic ray intensities along the Ulysses trajectory with the aims stated in Chapter 1.

A summary of all the chapters is given below:

Chapter 1 gave an introductory background to this study, with the aim to inform the reader about the outcomes and the context of the study .

Chapter 2 gave the necessary background regarding cosmic ray modulation. Important concepts like, the Sun, the HMF, the heliosphere, HCS and the solar wind were discussed. This chapter also aimed to give the reader an understanding of the concept of solar activity and solar cycle related changes in the HMF. A brief overview was given of the spacecraft missions of which observations were used.

A full discussion of the modulation model and parameters used in this study was given in **Chapter 3**. A brief overview of the modulation processes experienced by cosmic rays as contained in the transport equation was given. Cosmic rays entering the heliosphere diffuse inward toward the Sun, gyrating around the HMF lines and scatter at irregularities in the field. They also experience gradient and curvature drifts. During this process they lose energy through adiabatic cooling and may also be accelerated at the TS. These processes are all included in Parker's transport equation (Parker 1965). This equation was numerically solved to calculate cosmic ray intensities in the inner heliosphere.

The compound approach of Ferreira (2002), Ferreira and Potgieter (2004) and Ndiitwani et al. (2005) was discussed and applied to calculate cosmic ray intensities along the Ulysses trajectory in **Chapter 4**. A refinement in this approach was presented to establish a better compatibility of the model results with Ulysses observations. For this refinement the time-dependent function, which additionally scales drifts toward solar maximum, was revisited and improved on taking into account more recent observations. A description of PDBs and their effects on cosmic ray modulation was also given. Also discussed was how the cosmic rays changes in the inner heliosphere can be caused by global changes in the HMF.

In **Chapter 5** model computations were compared to Ulysses observations at 2.5 GV to show that the compound approach can indeed produce intensities for both cosmic ray protons and electrons compatible to Ulysses observations. A more detailed investigation of the Ulysses fast latitude scan periods was given. This was the first modeling attempt for the third latitude scan period. Due to the success of the model in reproducing the observed intensities for the different fast latitude scan periods, the global distributions for the whole computed heliosphere were presented for these periods.

In **Chapter 6** the model and compound approach were again utilized to compute both proton and electron cosmic ray intensities, but at different rigidities e.g. $>\sim$ 2.5 GV. Presented was the dependence of the modulation amplitude on rigidity and solar activity. These calculations

are also important for interpreting measurements of the PAMELA mission. Also computed and discussed were the electron and proton ratios at different rigidities to show that charge-sign dependence modulation changes over a solar cycle. Two refinements were proposed. They include a possible gradual change during the period of polarity reversal in the diffusion parameters, instead of a sudden change as is currently assumed.

It was shown that the time-dependent function which changes the diffusion and drift parameters over a solar cycle, needs to change with rigidity. Neutron monitor observations were used as an indication of the amplitude between solar minimum and maximum at higher rigidities. From this followed that at 2.5 GV for Ulysses observations, n in Equation (6.1) is $n = \alpha/11$, but this should decrease to $n \approx 1$ for rigidities around 10 GV and higher. With the PAMELA spacecraft providing valuable detailed spectra up to several GV and possibly observing long enough in time, a more detailed future study is possible to construct a time-dependence for the diffusion and drift parameters to compute compatible modulation, and for different rigidities.

References

1. Adriani, O., G.C. Barbarino, G.A. Bazilevskaya, R. Bellotti, M. Boezio, E.A. Bogomolov, L. Bonechi, M. Bongi, V. Bonvicini, S. Bottai, A. Bruno, F. Cafagna, D. Campana, P. Carlson, M. Casolino, G. Castellini, M. de Pascale, G. Pand de Rosa, D. Fedele, A.M. Galper, L. Grishantseva, P. Hofverberg, A. Leonov, S.V. Koldashov, S.Y. Krutkov, A.N. Kvashnin, V. Malvezzi, L. Marcelli, W. Menn, V.V. Mikhailov, M. Minori, E. Mocchiutti, M. Nagni, S. Orsi, G. Osteria, P. Papini, M. Pearce, P. Picozza, M. Ricci, S.B. Ricciarini, M. Simon, R. Sparvoli, P. Spillantini, Y.I. Stozhkov, E. Taddei, A. Vacchi, E. Vannuccini, G. Vasilyev, S.A. Voronov, Y.T. Yurkin, G. Zampa, N. Zampa, and V.G. Zverev, New measurement of the antiproton-to-proton flux ratio up to 100 GeV in the cosmic radiation, *Physical Review Letters*, 102, 051101: 1-5, 2009.

2. Alanko-Huotari, K., I.G. Usoskin, K. Mursula, and G.A. Kovaltsov, Cyclic variations of the heliospheric tilt angle and cosmic ray modulation, *Advances in Space Research*, 40, 1064 -1069, 2007.

3. Axford, W.I., E. Leer, and G. Skadron, The acceleration of cosmic rays by shock waves, *Proceedings of the 15th International Cosmic Ray Conference* (Plovdiv), 11, 132-137, 1977.

4. Balogh, A., R.G. Marsden, and E.J. Smith, The heliosphere near solar minimum: The Ulysses perspective, edited by Balogh, A., R.G. Marsden and E.J. Smith, *Springer Praxis*, p. 419, 2001.

5. Baranov, V.B., Interaction of the solar wind with the external plasma, In: Physics of the outer heliosphere, edited by Oxford E., and N.Y. Elmsford, *Pergamon Press*, 287-297, 1990.

6. Baranov, V.B., and Y.G. Malama, Model of the solar wind interaction with the local interstellar medium - Numerical solution of self-consistent problem, *Journal of Geophysical Research*, 98, 157-15163, 1993.

7. Baranov, V.B., and Y.G. Malama, Effect of local interstellar medium hydrogen fractional ionization on the distant solar wind and interface region, *Journal of Geophysical Research*, 100, 14755-14762, 1995.

8. Bell, A.R., The acceleration of cosmic rays in shock fronts-1, *Monthly Notices of the Royal Astronomical Society*, 182, 147-156, 1978.

9. Benestad, E.R., Solar activity and earth climate, edited by Benestad E.R., *Springer Praxis*, p. 326, 2002.

10. Bieber, J.W., W.H. Mathaeus, and C.H. Smith, Proton and electron mean free paths: The Palmer consensus revisited, *Astrophysical Journal*, 420, 294-306, 1994.

11. Bieber, J.W., J. Chen, W.H. Matthaeus, C.W. Smith, and M.A. Pomerantz, Long-term variations of interplanetary magnetic field spectra with implications for cosmic ray modulation, *Journal of Geophysical Research*, 98, 3585-3603, 1993.

12. Biermann, L., Kometenschwiefe und solare Korpuskularstrahlung, *Zeitschrift fur Astrophysik*, 29, 274-286, 1951.

13. Biermann, L., The solar wind and the interplanetary media, edited by Liller, W., *Space Astrophysics*, McGraw-Hill, p.150, 1961.

14. Burger, R.A., On the theory and application of drift motion of charged particles in inhomogeneous magnetic fields, Ph.D. thesis, Potchefstroom University for CHE, South Africa, 1987.

15. Burger, R.A., Cosmic-ray modulation and the heliospheric magnetic field, *Advances in Space Research*, 35, 635-642, 2005.

16. Burger, R.A., and M. Hattingh, Steady-state drift-dominated modulation models for galactic cosmic rays, *Astrophysics and Space Science*, 230, 375-382, 1995.

17. Burger, R.A., and M. Hattingh, Effect of Fisk-type heliospheric magnetic fields on the latitudinal transport of cosmic rays, *Proceedings of the 27th International Cosmic Ray Conference* (Hamburg), 9, 3698, 2001.

18. Burger, R.A., and M. Hitge, The effect of a Fisk-type heliospheric magnetic field on cosmic-ray modulation, *Astrophysics Journal Letters*, 617, 73-76, 2004.

19. Burger, R.A., and M.S. Potgieter, The calculation of neutral sheet drift in two-dimensional cosmic-ray modulation models, *Astrophysical Journal*, 339, 501-511, 1989.

20. Burger, R.A., M. Hattingh, and J.W. Bieber, The effect of magnetic helicity on the propagation of galactic cosmic rays, *Advances in Space Research*, 19, 897-900, 1997.

21. Burger, R.A., M.S. Potgieter, and B. Heber, Rigidity dependence of cosmic-ray proton latitudinal gradients measured by the Ulysses spacecraft: Implications for the diffusion tensor, *Journal of Geophysical research*, 105, 27447-27456, 2000.

22. Burger, R.A., T.P.J. Kruger, M. Hitge, and N.E. Engelbrecht, A Fisk-Parker hybrid heliospheric magnetic field with a solar-cycle dependence, *Astrophysics Journal*, 674, 511-519, 2008.

23. Burlaga, L.F., and L. Klein, Magnetic clouds in the solar wind, *NASA technical report*, 80, 1980.

24. Burlaga, L.F., and A.F. Vinas, Triangle for the entropic index of q of non-extensive statistical mechanics observed by Voyager 1 in the distant heliosphere, *Physica A: Statistical mechanics and its applications*, 356, 375-384, 2005.

25. Burlaga, L.F., F.B. McDonald, and N.F Ness, Cosmic ray modulation and the distant heliospheric magnetic field Voyager 1 and 2 observations from 1986 to 1989, *Journal of Geophysical Research*, 98, 1-8, 1993.

26. Burlaga, L.F., N.F. Ness, and J.D. Richardson, Sectors in the distant heliosphere: Voyager 1 and 2 observations from 1999 through 2002 between 57 and 83 AU, *Journal of Geophysical Research* ,108, 8028: 1-15, 2003.

27. Burlaga, L.F., N.F. Ness, M.H. Acuna, R.P. Lepping, and J.E.P. Connerney, Voyager 1 observations of the heliospheric magnetic field: Crossing the termination shock into the heliosheath, *Proceedings of the solar wind Conference* (Canada), edited by Fleck,B., T.H. Zurbuchen and H. Lacoste, p. 255, 2005.

28. Burlaga, L., N. Ness, M. Acuna, J. Richardson, E. Stone, and F.B. McDonald, Obervations of the heliosheath and solar wind termination shock by Voyager 2, Fall Meeting, *American Geophysical Union*, 2008.

29. Blandford, R.D., and J.P. Ostriker, Particle acceleration by astrophyical shocks, *Astrophysical Journal*, 221, 29-32, 1978.

30. Bravo, S., B. Mendoza, R. Perez-Enriquez, and J. Valdes-Galicia, On the role of equatorial coronal holes in cosmic ray modulation, *Annales Geophysicae*, 6, 377-380, 1988.

31. Cane, H.V., Coronal mass ejections and Forbush decreases, *Space Science Reviews*, 93, 55-77, 2000.

32. Cane, H.V., G. Wibberenz, I.G. Richardson, and T.T. Von Rosenvinge, Cosmic ray modulation and the solar magnetic field, *Geophysical Research Letters*, 26, 565-568, 1999.

33. Cecchini, S., and J.J. Quenby, Three-dimensional models of galactic cosmic ray modulation, *Proceedings of the International Cosmic ray Conference* (Munich), 3, 911-914, 1975.

34. Chenette, D.L., T.F. Conlon, and J.A. Simpson, Bursts of relativistic electrons from Jupiter observed in interplanetary space with the time variation of the planetary rotation period, *Journal of Geophysical Research*, 79, 3551-3558,1974.

35. Cliver, E.W., Solar energetic particles: Acceleration and transport, *26th International Cosmic Ray Conference*, edited by Dingus, B.L., D.B. Kieda and M.H. Salamon, 516, 103-119, 2000.

36. Coroniti, F.V., C.F. Kennel, F.L. Scarf, and E.J. Smith, Whistler mode turbulence in the disturbed solar wind, *Journal of Geophysical Research*, 87, 6029-6044, 1982.

37. Czechowski, A., and I. Mann, Formation and acceleration of nano dust in the inner heliosphere, *Astrophysical Journal*, 714, 89-99, 2010.

38. Decker, R.B., S.M. Krimigis, E.C. Roelof, M.E. Hill, T.P. Armstrong, G. Gloeckler, D.C. Hamilton, and L.J. Lanzerotti, Voyager 1 in the foreshock, termination shock and heliosheath, *Science*, 309, 2020-2024, 2005.

39. Decker, R.B., S.M. Krimigis, E.C. Roelof, and M.E. Hill, Energetic particle populations in the heliosheath measured at Voyagers 1 and 2, Fall Meeting, *American Geophysical Union*, 2008.

40. Earl, J.A., The diffusive idealization of charged-particle transport in random magnetic fields, *Astrophysical Journal*, 193, 231-242, 1974.

41. Eraker, J.H., Origins of the low-energy relativistic interplanetary electrons, *Astrophysical Journal*, 257, 862-880, 1982.

42. Fahr, H.J., and H. Fichtner, Physical reasons and consequences of a three-dimensionally structured heliosphere, *Space Science Reviews*, 58, 193-258, 1991.

43. Fahr, H.J., and G. Lay, Remote diagnostic of the heliospheric termination shock using neutralised post shock pick-up ions as messengers, *Astronomy and Astrophysics*, 356, 327-334, 2000.

44. Fahr, H.J., T. Kausch, and K. Scherrer, A 5-fluid hydrodynamic approach to model the solar system-interstellar medium interaction, *Astronomy and Astrophysics*, 357, 268-282, 2000

45. Ferreira, S.E.S., A study of the modulation of cosmic ray electrons and jovian electrons, Ph.D. thesis Potchefstroom University for CHE, South Africa, 2002.

46. Ferreira, S.E.S., and M.S. Potgieter, Long-term cosmic ray modulation in the Heliosphere, *Astrophysical Journal*, 603, 744752, 2004.

47. Ferreira, S.E.S., M.S. Potgieter, and K. Scherer, Modeling of the heliospheric interface, magnetic field and cosmic ray transport, *Astrophysical Journal*, 659, 1777-1783, 2007.

48. Ferreira, S.E.S., M.S. Potgieter, and K. Scherer, Transport and acceleration of anomalous cosmic rays in the inner heliosheath, *Journal of Geophysical Research*, 112, A11101:1-11, 2007.

49. Ferreira, S.E.S., M.S. Potgieter, and K. Scherer, Stochastic acceleration and adiabatic heating of anomalous cosmic rays in the inner heliosheath, *AIP Conference Proceedings*, 1039, 355-360, 2008.

50. Ferreira, S.E.S., M.S. Potgieter, R.A. Burger, B. Heber, and H. Fichtner, Modulation of jovian and galactic electrons in the heliosphere 1. Latitudinal transport of few MeV electrons, *Journal of Geophysical Research*, 106, 24979-24988, 2001a.

51. Ferreira, S.E.S., M.S. Potgieter, R.A. Burger, B. Heber, H. Fichtner, and C. Lopate, Modulation of Jovian and galactic electrons in the heliosphere: 2. Radial transport of a few MeV electrons, *Journal of Geophysical Research*, 106, 29313-29322, 2001b.

52. Ferreira, S.E.S., M.S. Potgieter, B.Heber, and H. Fichtner, Charge sign dependent modulation over a 22-year cycle, *Annales Geophysicae*, 21, 1359-1366, 2003.

53. Fichtner, H., Production of energetic particles at the heliosphere shock-implications for the global structure of the heliosphere, *Reviews in Modern Astronomy*, 9, 191-220, 1996.

54. Fichtner, H., Cosmic rays in the heliosphere: Progress in the modeling during the past 10 years, *Advances in Space Research*, 35, 512-517, 2005.

55. Fichtner, H., and K. Scherer, The heliosphere: A brief overview, In: The outer heliosphere: Beyond the planets, edited by Scherrer, K., H. Fichtner, and E. Marsch, *Copernicus Publications*, p. 436, 2000.

56. Fichtner, H., S.R. Sreenivasan, and H.J. Fahr, Cosmic ray modulation and a non-spherical shock, *Astronomy and Astrophysics*, 308, 248-260, 1996.

57. Fichtner, H., H.J. Fahr, W. Neutsch, R. Schlickeiser, A. Crusius-Watzel, and H. Lesch, Cosmic-ray-driven galactic wind, *Nuovo Cimento*, 106, 909-925, 1991.

58. Fichtner, H., M.S. Potgieter, S.E.S. Ferreira, and R.A. Burger, On the propagation of Jovian electrons in the heliosphere: transport modelling in 4-D phase space, *Geophysical Research Letter*, 27, 1611-1614, 2000.

59. Fitchtner, H., M.S. Potgieter, S.E.S. Ferreira, and B.Heber, Time-dependent 3-D modelling of the heliospheric propagation of few-MeV electrons, *Proceedings 27th International Cosmic Ray Conference* (Hamburg), 8, 3666-3669, 2001.

60. Fisk, L.A., Solar modulation of galactic cosmic rays, 2, *Journal of Geophysical Research*, 76, 221-226, 1971.

61. Fisk, L.A., Modulation of solar cosmic rays high energy phenomenon of the Sun, Proceedings at Goddard Space Flight Center, edited by Ramaty, R., and R.G. Stone, *NASA Special Publication*, p. 418, 1973.

62. Fisk, L.A., Motion of the foot points of heliospheric magnetic field lines at the Sun: Implications for recurrent energetic particle events at high heliographic latitudes, *Journal of Geophysical Research*, 101, 15547-15554, 1996.

63. Fisk, L.A., and G. Gloeckler, The common spectrum for accelerated ions in the quite-time solar wind, *Astrophysical Journal*, 640, 79-82, 2006.

64. Fisk, L.A., and N.A. Schwadron, The behavior of the open magnetic field of the Sun, *Astrophysical Journal*, 560, 425-438, 2001.

65. Fisk, L.A., B. Koslovsky, and R. Ramaty, An interpretation of the observed oxygen and nitrogen enhancement in low energy cosmic rays, *Astrophysical Journal*, 190, 35-37, 1974.

66. Florinski, V., and J.R. Jokipii, A two dimensional, self-consistent model of galactic cosmic rays in the heliosphere, *Astrophysical Journal*, 523, 185-188, 1999.

67. Florinski, V., and J.R. Jokipii, Cosmic-ray spectra at spherical termination shocks, *Astrophysical Journal*, 591, 454 460, 2003.

68. Florinski, V., N.V. Pogorelov, and G.P. Zank, On the possibility of a strong magnetic field in the local interstellar medium, *Astrophysical Journal*, 604, 700-706, 2004.

69. Forbush, E., Three unusual cosmic ray increases probably due to the charged particles from the Sun, *Physical Review*, 70, 771-772, 1946.

70. Fujii, Z., and F.B. McDonald, Properties of step decreases observed in solar cycle 22, *Proceedings of the International Cosmic Ray Conference* (Italy), edited by Iucci, N., and E. Lamanna, 4, 776-779, 1995.

71. Garcia - Munoz, M., G.M. Mason, and J.A. Simpson, The abundances of galactic cosmic - ray carbon, nitrogen, and oxygen and their astrophysical implications, *Astrophysical Journal*, 184, 967-994, 1973.

72. Giacalone, J., Cosmic rays transport coefficients, *Space Science Reviews*, 83, 351-363, 1998.

73. Giacalone, J., and J.R. Jokipii, The transport of cosmic rays across a turbulent magnetic field, *Astrophysical Journal*, 520, 204-214, 1999.

74. Gleeson, L.J., and W.I. Axford, Cosmic rays in the interplanetary medium, *Astrophysical Journal*, 149, 115-118, 1967.

75. Gleeson, L.J., and W.I. Axford, Solar modulation of galactic cosmic rays, *Astrophysical Journal*, 154, 1011-1026, 1968.

76. Gombosi, T.I., Physics of the space environment, *Cambridge University Press*, edited by Houton J.T., M.J. Rycroft and A.J. Dessler, p. 360, 1994.

77. Haasbroek, L.J., Modulation of cosmic rays in the heliosphere: A model study of Ulysses mission (in Afrikaans), M.Sc. dissertation, Potchefstroom University for CHE, South Africa, 1993.

78. Haasbroek, L.J., The transport and acceleration of charged particles in the heliosphere, Ph.D. thesis, Potchefstroom University for CHE, South Africa, 1997.

79. Haasbroek, L.J., and M.S. Potgieter, A new model to study galactic cosmic ray modulation in an asymmetrically boundend heliosphere, *Journal of Geophysical Research*, 103, 2099-2104, 1998.

80. Hasselmann, K., and G. Wibberenz, A note on the parallel diffusion coefficient, *Astrophysical Journal*, 162, 1049-1051, 1970.

81. Hatting, M., Drift of cosmic rays at a wavy neutral sheet in the heliosphere (in Afrikaans), M.Sc. dissertaion, Potchefstroom University for CHE, South Africa, 1993.

82. Hattingh, M., The modulation of galactic cosmic rays in a three-dimensional heliosphere, Ph.D. thesis, Potchefstroom University for CHE, South Africa, 1998.

83. Hattingh, M., and R.A. Burger, A new simulated wavy neutral sheet drift model, *Advances Space Research*, 16, 213-216, 1995.

84. Heber, B., and M.S. Potgieter, Cosmic rays at high heliolatitudes, *Space Science Reviews*, 127, 117-194, 2006.

85. Heber, B., W. Droge, P. Fernando, L.J. Haasbroek, H. Kunow, R. Müller-Mellin, C. Paizis, M.S. Potgieter, A. Raviart, and G. Wibberenz, Spatial variation of $>$ 40 MeV/n nuclei fluxes observed during the Ulysses rapid latitude scan, *Astronomy and Astrophysics*, 316, 538-546, 1996.

86. Heber, B., V. Bother, W. Droge, H. Kunow, R. Müller-Mellin, A. Posner, P. Ferrando, A. Raviart, and C. Paizis, Spatial evolution of 26-day recurrent galactic cosmic ray decreases: correlated Ulysses COSPIN/KET and SOHO COSTEP Observations, 31st ESLAB Symposium, ESA Special Publication, edited by Wilson, A., 415, 331-336, 1997.

87. Heber, B., A. Raviart, G. Wibberenz, R. Müller-Mellin, H. Kunow, H. Sierks, V. Bother, A. Bothmer, A. Posner, C. Paizis, and M.S. Potgieter, Differences in temporal variations of galactic cosmic ray electrons and protons: Implications from Ulysses at solar minimum, *Geophysical Research Letters*, 26, 2133-2136, 1999.

88. Heber, B. R. Gömez-Herrero, O. Sternal, A. Klassen, R. Müller-Mellin, H. Kunow, M.S. Potgieter, and H. Fichtner, Jovian electrons in the three dimensional heliosphere, ESA Special Publication, 616, 1-4, 2006.

89. Heber, B., J. Gieseler, P. Dunzlaff, R. Gömez-Herrero, A. Klassen, R. Müller-Mellin, R. A. Mewaldt, M.S. Potgieter, and S.E.S. Ferreira, Latitudinal gradients of galactic cosmic rays during the 2007 solar minimum, *Astrophysical Journal*, 689, 1443-1447, 2008.

90. Heber, B., A. Kopp, J. Gieseler, R. Müller-Mellin, H. Fichtner, K. Scherer, M.S. Potgieter, and S.E.S Ferreira, Modulation of galactic cosmic ray protons and electrons during an unusual solar minimum, *Astrophysical Journal*, 699, 1956-1963, 2009.

91. Hedgecock, P.C., and B.T. Thomas, HEOS observations of the configuration of the magnetosphere, *Geophysical Journal International*, 41, 391 403, 1975.

92. Hess, V.F., Physikal Zeits, 12, 998, 1911.

93. Hoeksema, J.T., Large scale structure of the heliospheric magnetic field: 1976-1991, edited by Marsch, E., and R. Schwenn, Pergamon Press, p. 191, 1992.

94. Hoeksema, J.T., J.M. Wilcox, and P.H. Scherer, The structure of the heliospheric current sheet - 1978-1982, *Journal of Geophysical Research*, 88, 9910-9918, 1983.

95. Holzer, T.E., Interaction between the solar wind and the interstellar medium, IN: Annual review of astronomy and astrophysics. *Annual Reviews Astronomy and Astrophysics*, 27, 199-234, 1989.

96. Hundhausen, A.J., Plasma flow from the Sun, In: The solar output and its variation, edited by White, O.R., p. 36, 1977.

97. Hundhausen, A.J., An interplanetary view of coronal holes, In: Coronal holes and high speed wind streams, edited by Zirker, J.B., p. 225-329, 1977.

98. Huotari, K.A., I.G. Usoskin, K. Mursula, and G.A. Kovaltsov, Cyclic variations of the heliospheric tilt angle and cosmic ray modulation, *Advances in Space Research*, 40, 1064-1069, 2007.

99. Isenberg, P.A., and J.R. Jokipii, Gradient and curvature drifts in magnetic fields with arbitrary spatial variation, *Astrophysical Journal*, 234, 746-752, 1976.

100. Issautier, K., S. Hoang, G. Le Chat, N. Meyer-Vernet, and M. Moncuquet, Ulysses mission: The end of an odyssey, SF2A-2008: *Proceedings of the Annual meeting of the French Society of Astronomy and Astrophysics*, edited by Charbonnel, C., F. Combes and R. Samadi, p.551, 2008.

101. Jokipii, J.R., Cosmic-ray propagation. I. Charged particles in a random magnetic field, *Astrophysical Journal*, 146, 480-487, 1966.

102. Jokipii, J.R., Propagation of cosmic-rays in the solar wind, *Review of Geophysics and Space Physics*, 9, 27-87, 1971.

103. Jokipii, J.R., Particle acceleration at a termination shock. 1. Application to the solar wind and the anomalous component, *Journal of Geophysical Research*, 91, 2929-2932, 1986.

104. Jokipii, J.R., and D.A. Kopriva, Effects of particle drift on the transport of cosmic rays. III-Numerical models of galactic cosmic-ray modulation, *Astrophysical Journal*, 234, 384-392, 1979.

105. Jokipii, J.R., and J. Kota, On the interpretation of the high cosmic-ray electron fluxes observed in 1986, *Proceedings of the 22nd International Cosmic ray Conference* (Dublin), 3, 569-572, 1991.

106. Jokipii, J.R., and J. Kota, The polar heliospheric magnetic field, *Geophysical Research Letters*, 16, 1-4, 1989.

107. Jokipii, J.R., and J. Kota, The maximum energy of anomalous cosmic rays, *Proceedings of the 24th International Cosmic Ray Conference* (Rome), 4, 718-721, 1995.

108. Jokipii, J.R., and J. Kota, Galactic and anomalous cosmic rays in the heliosphere, *Proceedings of the 25th International Cosmic Ray Conference* (Durban), edited by Potgieter, M.S., Raubenheimer, C. and D.J. van der Walt, 8, p.151, 1997.

109. Jokipii, J.R., and A.J. Owens, Cross correlation between cosmic-ray fluctuations and interplanetary magnetic-field fluctuation, *Geophysical Research Letters*, 1, 329-332, 1974.

110. Jokipii, J.R., and E.N. Parker, On the convection, diffusion, and adiabatic deceleration of cosmic rays in the solar wind, *Astrophysical Journal*, 160, 735-744, 1970.

111. Jokipii, J.R., and B. Thomas, Effects of drift on the transport of cosmic rays, IV, Modulation by a wavy interplanetary current sheet, *Astrophysical Journal*, 243, 1115-1122, 1981.

112. Jokipii, J.R., E.H. Levy, and W.B. Hubbard, Effects of particle drift on cosmic ray transport. i. General properties application to solar modulation, *Astrophysical Journal*, 213, 861-868, 1977.

113. Kallenbach, R., K. Bamert, M. Hilchenbach and C.W. Smith, Observations of turbulence near interplanetary traveling shocks, In: The physics of collisionless shocks, *Proceedings of the AIP conference*, 781, 129-134, 2005.

114. Kissmann, R., H. Fichtner, B. Heber, S.E.S. Ferreira, and M.S. Potgieter, The influence of CIRs on the energetic electron flux at 1 AU, *Advance Space Research*, 419, 357-363, 2003.

115. Klein, L., and L.F. Burlaga, Interplanetary sector boundaries 1971-1973, *Journal of Geophysical Research*, 85, 2269-2276, 1980.

116. Kota, J., and J.R. Jokipii, Effects of drift on the transport of cosmic rays. VI - A three-dimensional model including diffusion, *Astrophysical Journal*, 265, 573-581, 1983.

117. Kota, J., and J.R. Jokipii, The role of corotating interaction regions in cosmic-ray modulation, *Geophysical Research Letters*, 18, 1797-1800, 1991.

118. Kota, J., and J.R. Jokipii, 3-D simulation of heliospheric transport: A comparison of models, *Proceedings of the 25th International Cosmic ray Conference* (Durban), 2, 25-28, 1997.

119. Kota, J., and J.R. Jokipii, Cosmic ray modulation and the structure of the heliospheric magnetic field, *Proceedings of the 26th International Cosmic ray Conference* (Salt Lake City) 7, 9-12, 1999.

120. Krieger, A.S., A.F. Timothy, and E.C. Roelof, A coronal hole and its identification as the source of a high velocity solar wind stream, *Solar Physics*, 29, 505-512, 1973.

121. Krimigis, S.M., R.B. Decker, E.C. Roelf, and D. Lario, Energetic particle intensity increases at Voyagers 1 and 2 during 2002 - 2003, *Proceedings of the 28th International Cosmic Ray conference* (Tsukuba), 7, 3769-3772, 2003.

122. Langner, U.W., Effects of termination shock acceleration on cosmic rays in the heliosphere, Ph.D. thesis Potchefstroom University for CHE, South Africa, 2004.

123. Langner U.W., and M.S. Potgieter, The role of radial perpendicular diffusion and latitude dependent acceleration along the solar wind termination shock, *Advances in Space Research*, 41, 368-372, 2008.

124. Langner, U. W., M.S. Potgieter, H. Fichtner, and T. Borrmann, Effects of solar wind speed changes in the heliosheath on the modulation of cosmic ray protons, *Astrophysical Journal*, 640, 1119-1134, 2006a.

125. Langner, U. W., M.S. Potgieter, H. Fichtner, and T. Borrmann, Modulation of anomalous protons: Effects of different solar wind speed profiles in the heliosheath, *Journal of Geophysical Research*, 111, A1106: 1-14, 2006b.

126. Lee, M.A., and H. Fichtner, Cosmic rays as messengers from outside the inner heliosphere, In: The outer heliopshere: The next frontiers, edited by Scherer, K., H. J. Fahr and E. Marsch, *COSPAR colloquia Series* (Amsterdam), p. 183, 2001.

127. le Roux, J.A., The solar modulation of galactic cosmic rays as described by a time-dependent drift model, Ph.D. thesis, Potchefstroom University for CHE, South Africa, 1990.

128. le Roux, J.A., and H. Fichtner, A self consistent determination of the heliospheric termination shock structure in the presence of pickup, anomalous, and galactic cosmic ray protons, *Journal of Geophysical Research*, 102, 17365-17380, 1997.

129. le Roux, J.A., and H. Fichtner, The simulation of step decrease in the cosmic ray intensity with a cosmic rays in the hydrodynamic model, *Advaced Space Research*, 23, 501-504, 1999.

130. le Roux, J.A., and M.S. Potgieter, A time-dependent drift model for the long-term modulation of cosmic rays with special reference to asymmetries with respect to the solar minimum of 1987, *Astrophysical Journal*, 361, 275-282, 1990.

131. le Roux, J.A., and M.S. Potgieter, The Simulated features of heliospheric cosmic ray modulation with a time-dependent drift model. II. On the energy dependence of the onset of new modulation in 1987, *Astrophysical Journal*, 390, 661-667, 1992.

132. le Roux, J.A., and M.S. Potgieter, The simulations of complete 11 and 12 year modulation cycles for cosmic rays in the heliosphere using a drift model with global merged interaction regions, *Astrophysical Journal*, 442, 847-851, 1995.

133. le Roux, J.A., M.S. Potgieter, and V.S. Ptuskin, A transport model for the diffusive acceleration and modulation of anomalous cosmic rays in the heliosphere, *Journal of Geophysical Research*, 101, 4791-4804, 1996.

134. Lockwood, J.A., On the long-term variation in the cosmic radiation, *Journal of Geophysical Research*, 65, 19-25, 1960.

135. Lockwood, J.A., and M.A. Shea, Variations of the cosmic radiation in November 1960, *Journal of Geophysical Research*, 66, 3083-3093, 1961.

136. Marsch, E., Kinetic physics of the solar wind plasma, In: Physics of the inner heliosphere II, edited by Schwenn R., and E. Marsch, *Springe-Verlag*, 21, p. 45-133, 1991.

137. Marsden, R.G., The Sun and the heliosphere in three dimensions, *Proceedings of the Nineteenth ESLAB Symposium* (Switzerland), edited by Marsden R.G., 123, p.542, 1986.

138. Marsden, R.G., Ulysses at solar maximum and beyond, *Space Science Reviews*, 87, 1-7, 2000.

139. Marsden, R.G., The 3-D heliosphere at solar maximum, *Space Science Reviews*, 97, 1-4, 2001.

140. McComas, D.J., H.A. Elliot, and R. von Steiger, Solar wind from high-latitude coronal holes at solar maximum, *Geophysical Research Letters*, 29, 1-4, 2002.

141. McComas, D.J., B.L. Barraclough, H.O. Funsten, J.T. Gosling, E. Santiago-Munoz, R.M. Skoug, B.E. Goldstein, M. Neugebauer, P. Riley, and A. Balogh, Solar wind observations over Ulysse's first full polar orbit, *Journal of Geophysical Research*, 105, 10419-10434, 2000.

142. McComas, D.J., H.A. Elliott, J.T. Gosling, and R.M. Skoug, Ulysses observations of very different heliospheric structure during the declining phase of solar activity cycle 23, *Geophysical Research Letters*, 33, 1-4, 2006.

143. McComas, D.J., R.W. Ebert, H.A. Elliott, B.E. Goldstein, J.T. Gosling, N.A. Schwadron, and R.M. Skoug, Weaker solar wind from the polar coronal holes and the whole sun, *Geophysical Research Letters*, 35, 1-5, 2008.

144. McDonald, F.B., N. Lal, and R.E. McGuire, Role of drifts and global merged interaction regions in the long-term modulation of cosmic rays, *Journal of Geophysical Research*, 98, 1243-1256, 1993.

145. McDonald, F.B., N. Lal, J.H. Trainor, M.A.I. Van Hollebekke, and W.R. Webber, The solar modulation of galactic cosmic rays in the outer heliosphere, *Astrophysical Journal*, 249, 71-75, 1981.

146. Mewaldt, R.A., Galactic cosmic ray composition and energy spectra, *Advances in Space Research*, 14, 737-747, 1994.

147. Mewaldt, R.A., E.C. Stone, and R.E. Vogt, Observations of jovian electrons at 1 AU, *Journal of Geophysical Research*, 81, 2397-2400, 1974.

148. Mewaldt, R.A., E.C. Stone, and R.E. Vogt, The isotropic composition of hydrogen and helium in low-energy cosmic rays, *Astrophysical Journal*, 206, 616-621, 1976.

149. Minnie, J., J.W. Bieber, W.H. Matthaeus and R.A. Burger, Suppression of particle drifts by turbulence, *Astrophysical Journal*, 670, 1149-1158, 2007.

150. Moeketsi, D.M., M.S. Potgieter, S.E.S. Ferreira., B. Heber, H. Fichtner, and V. K. Henize, The heliospheric modulation of 3-10 Mev electrons: modeling of changes in the solar wind speed in relation to perpendicular polar diffusion, *Advances in Space Research*, 35, 597-604, 2005.

151. Moraal, H., and L.J. Gleeson, Three dimensional models of galactic cosmic ray modulation, *Proceedings of the 14th International Cosmic Ray Conference* (Munich), 12, 4189-4192, 1975.

152. Moraal, H., and L.J. Gleeson, and G.M. Webb, Effects of charged particles drifts on the modulation of the intensity of galactic cosmic rays, *Proceedings of the 16th International Cosmic Ray Conference* (Kyoto), 3, 1-4, 1979.

153. Moraal, H., R.A. Caballero-Lopez, K.G. McCracken, F. B. McDonald, R. A. Mewaldt, V. Ptsukin, and M.E. Wiedenbeck, Cosmic ray energy changes at the termination shock and in the heliosheath, *Proceedings of the 5th Annual IGPP International Astrophysics Conference*, 858, 219-225, 2006.

154. Myasnnikov, A.V., V.V. Izmodenov, D.B. Alexashov, and S.V Chalov, Self-consistent model of the solar wind interaction with two-component circumsolar interstellar cloud: Mutual influence of thermal plasma and galactic cosmic rays, *Journal of Geophysical Research*, 105, 5179-5188, 2000.

155. Ndiitwani, D.C., S.E.S. Ferreira, M.S. Potgieter, and B. Heber, Modelling cosmic ray intensities along the Ulysses trajectory, *Annales Geophysicae*, 23, 1061-1070, 2005.

156. Ngobeni, M.D., and M.S. Potgieter, Cosmic ray anisotropies in the outer heliosphere, *Advances in Space Research*, 41, 373-380, 2008.

157. Opher, M., E.C. Stone, and T. Gombosi, The orientation of the local interstellar magnetic field, *Science*, 316, 875-878, 2007.

158. Opher, M., E.C. Stone, P.C. Liewer, and T. Gombosi, Global asymmetry of the heliosphere, *Proceedings of the 5th Annual IGPP International Astrophysics Conference*, 858, 45-50, 2006.

159. Opher, M., J.C. Richardson, G. Toth, and T.I. Gombosi, Confronting observations and modeling: The role of the interstellar magnetic field in Voyager 1 and 2 asymmetries, *Space Science Reviews*, 143, 43-55, 2009.

160. Paizis, C., B. Heber, P. Ferrando, A. Raviart, B. Fakoni, S. Marzolla, M.S. Potgieter, V. Bothmer, H. Kunow, R. Muller-Mellin and A. Posner, Amplitude evolution and rigidity dependence of the 26-day recurrent cosmic ray decreases: COSPIN/KET results, *Journal of Geophysical Research*, 104, 28241-28248, 1999.

161. Palmer, I.D., Transport coefficients of low-energy cosmic rays in interplanetary space, *Reviews of Geophysics and Space Physics*, 20, 335-351, 1982.

162. Parker, E.N., Cosmic ray modulation by the solar wind, *Physical Reviews*, 110, 1445-1449, 1958.

163. Parker, E.N., The passage of energetic charged particles through interplanetary space, *Planetary and Space Science*, 13, 9-45, 1965.

164. Parks, G.K., Physics of space plasmas: An introduction, *Addison-Wesley*, edited by Parks, G.K., p. 560, 1991.

165. Pauls, H.L., and G.P. Zank, Interaction of a nonuniform solar wind with the local interstellar medium, *Journal of Geophysical Research*, 101, 17081-17092, 1996.

166. Pauls, H.L., and G.P. Zank, Interaction of a nonuniform solar wind with the local interstellar medium 2, A two fluid model, *Journal of Geophysical Research*, 100, 19779-19788, 1997

167. Perko, J.S., and L.A. Fisk, Solar modulation of galactic cosmic rays. V. Time-dependent modulation, *Journal of Geophysical Research*, 88, 9033-9036, 1983.

168. Phillips, J.L., A. Balogh, S.J. Bame, B.E. Goldstein, J.T. Gosling, J.T. Hoeksema, D.J. McComas, M. Neugebauer, N.R. Sheeley, and Y.M. Wang, Ulysses at 50° south: constant immersion in the high speed solar wind, *Geophysical research Letters*, 21, 1105-1108, 1994.

169. Phillips, J.L., S.J. Bame, A. Barnes, B.L. Barraclough, W.C. Feldman, B.E. Goldstein, J.T. Gosling, G.W. Hoogeveen, D.J. McComas, M. Neagebauer, and S.T. Suess, Ulysses solar wind plasma observation from pole to pole, *Geophysical Research Letters*, 22, 3301-3304, 1995.

170. Pogorelov, N.V., J. Heerikhuisen, and G.P. Zank, Probing heliospheric asymmetries with an MHD-kinetic model, *Astrophysical Research*, 675, 41-44, 2008.

171. Potgieter, M.S., The modulation of galactic cosmic rays as described by a three-dimensional drift model, Ph.D. thesis, Potchefstroom University for CHE, South Africa, 1984.

172. Potgieter, M.S., Heliospheric terminal shock acceleration and modulation of the anomalous cosmic-ray component, *Advances Space Research*, 9, 21-24, 1989.

173. Potgieter, M.S., The long-term modulation of galactic cosmic rays in the heliosphere, *Advances in Space Research*, 16, 191-203, 1995.

174. Potgieter, M.S., Heliospheric modulation of galactic electrons: Consequences of new calculations for the mean free path of electrons between 1 MeV and $\sim$ 10 GeV, *Journal Geophysical Research*, 101, 24411-24422, 1996.

175. Potgieter, M.S., The heliospheric modulation of galactic cosmic rays at solar minimum, *Advances in Space Research*, 19, 883-892, 1997.

176. Potgieter, M.S., The modulation of galactic cosmic rays in the heliosphere: Theory and models, *Space Science Reviews*, 83, 147-158, 1998.

177. Potgieter, M.S., The heliospheric modulation of cosmic ray protons : The role of enhanced perpendicular diffusion during periods of minimum solar modulation, *Journal of Geophysical Research*, 105, 18295-18304, 2000.

178. Potgieter, M.S., and R.A. Burger, The modulation of cosmic-ray electrons, protons and helium nuclei, as predicted by a drift model with a simulated wavy neutral sheet, *Astronomy and Astrophysics* 23, 463-466, 1999a.

179. Potgieter, M.S., and L.J. Haasbroek, The simulation of base line cosmic ray modulation for the Ulysses trajectory, *Proceeding of the 23rd International Cosmic ray conference* (Calgary), 3, 457-460, 1993.

180. Potgieter, M.S., and H. Moraal, A drift model for the modulation of galactic cosmic rays, *Astrophysical Journal*, 294, 425-440, 1985.

181. Potgieter, M.S., and J.L. le Roux, The long-term heliospheric modulation of galactic cosmic rays according to a time-dependent drift model with merged interaction regions, *Astrophysical Journal*, 423, 817-827, 1994.

182. Qin, G., K.L. Wang, and Z.D. Wang, Exact analytical solution of a polariton model: Undetermined coefficient approach, *Physical Review*, 66, 025804: 1-4, 2002.

183. Rastoin, C., P. Ferrando, A. Raviart, R. Ducros, P.O. Petrucci, C. Paizis, H. Kunow, R. M*ü*ller-Mellin, H. Sierks, and G. Wibberenz, Time and space variations of the galactic cosmic ray electron spectrum in the 3-D heliosphere explored by Ulysses, *Astronomy and Astrophysics*, 307, 981-995, 1996.

184. Reinecke, J.P.L., H. Moraal, and F.B. McDonald, The cosmic radiation in the heliosphere at successive solar minima 3. Steady state drift solutions of the transport equation, *Journal of Geophysical Research*, 101, 21581-21588, 1996.

185. Richardson, J.D., and E.C. Stone, The solar wind in the outer heliosphere, *Space Science Review*, 143, 7-20, 2009.

186. Richardson, J.D., C. Wang, and K.I. Paularena, The solar wind from solar minimum to solar maximum, *Advances in Space Research*, 273, 471- 479, 2001.

187. Richardson, J.D., Y. Liu, and C. Wang, Solar wind structure in the outer heliosphere, *Advances in Space Research*, 41, 237244, 2008.

188. Rosenberg, R.L., and P.J. Coleman, Heliographic latitude dependence of the dominant polarity of the interplanetary magnetic field, *Journal of Geophysical Research*, 74, 5611-5622, 1969.

189. Rucinski, D., A.C. Cummings, G. Gloeckler, A.J. Lazarus, E. Mobius, and M. Witte, Ionization processes in the heliosphere-rates and methods of their determination, *Space Science Reviews*, 78, 73-84, 1996.

190. Schatten, K.H., Current sheet magnetic model for the solar corona, edited by Sonnet, C.P., P.J. Coleman and J.M. Wilcox, *NASA Special Publication*, 308, p.44, 1972.

191. Scherer, K., and H.J. Fahr, Solar cycle induced variations of the outer heliospheric structures, *Geophysical Research Letters*, 30, 17-44, 2003.

192. Scherer, K., and S.E.S. Ferreira, A heliospheric hybrid model: hydrodynamic plasma flow and kinetic cosmic ray transport, *Astrophysics and Space Sciences Transactions (ASTRA)*, 1, 17-27, 2005.

193. Scherer, K., H. Fitchner, S.E.S. Ferreira, I. Busching, and M.S. Potgieter, Are anomalous cosmic rays the main contribution to the low energy galactic cosmic ray spectrum?, *Astrophysical Journal*, 680, 105-108, 2008.

194. Schwadron, N.A., and D.J. McComas, Solar wind scaling law, *The Astrophysical Journal*, 599, 1395-1403, 2003.

195. Schwadron, N.A., and D.J. McComas, Particle acceleration at a blunt termination shock, In: Physics of the Inner Heliosheath, edited by Heerikhuisen, J., V. Florinski, G.P. Zank, and N.V. Pogorelov, *Proceedings of the 5th International Annual IGPP Astrophysics Conference*, 858, p. 165-170, 2006.

196. Schwenn, R., The average solar wind in the inner heliosphere: Structures and slow variations, *NASA Conference Publication*, 228, 489-507, 1983.

197. Schwenn, R., and E. Marsch, Physics of the inner heliosphere I. Large-scale phenomena, *Physics and Chemistry in Space*, 20, 1990.

198. Simpson, J.A., Cosmic radiation: Particle astrophysics in the heliosphere, edited by Mendell, B.R., and I.A. Mincer, *Annals of the New York Academy of Sciences*, 655, p.95, 1992.

199. Simpson, J.A., M. Zhang, and S. Bame, A solar polar North-South asymmetry for cosmic-ray propagation in the heliosphere: The Ulysses pole to pole rapid transit, *Astrophysics Journal*, 465, 69-72, 1996.

200. Simpson, J.A., D. Hamilton, G. Lentz, R.B. McKibben, A. Mogro-Campero, M.Perkins, K.R. Pyle, A.J. Tuzzolino, and J.J. O'Gallagher, Protons and electrons in Jupiter's magnetic field: Results from the University of Chicago experiment on Pioneer 10, *Science*, 183, 306-309, 1974.

201. Simpson, J.A., J.J. Connel, C. Lopate, R. B. Mckibben, and M. Zhang, The latitude gradients of galactic cosmic ray and anomalous helium fluxes measured on Ulysses from the Sun's south polar region to the equator, *Geophysical Research Letters*, 22, 3337-3340, 1995.

202. Smith, C.W., N.F. Ness, L.F. Burlaga, R.M. Skoug, D.J. McComas, T.H. Zurbuchen, G. Gloeckler, D.K. Haggerty, R.E. Gold, M.I. Desai, G.M. Mason, J.E. Mazur, J.R. Dwyer, M.A. Popecki, E. Mobius, C.M.S. Cohen, and R.A. Leske, ACE Observations of the bastille day 2000 interplanetary disturbances, *Solar Physics*, 204, 227-252, 2001.

203. Smith, E.J., and A. Balogh, Decrease in heliospheric magnetic flux in this solar minimum: Recent Ulysses mangetic field observations, *Geophysical Research Letters*, 35, 22103-22107, 2008.

204. Smith, E.J., and R.G. Marsden, Ulysses observations at solar maximum: Introduction, *Geophysical Research Letters*, 30, 1-4, 2003.

205. Smith, E.J., and K.P. Wenzel, Introduction to the Ulysses encounter with Jupiter, *Geophysical Research*, 98, 21111-21127, 1993.

206. Smith, E.J., B.T. Tsurutani, and R.L. Rosenberg, Observations of the interplanetary sector structure up to heliographic latitude of 16°: Pioneer 11, *Journal of Geophysical Research*, 83, 717-724, 1978.

207. Smith, J.A., The Sun, solar wind and magnetic field. I', edited by Coppi, B., A. Ferrari and E. Sindoni, *Proceedings of the International School of Physics "'Enrico Fermi"' Course* (Amsterdam), p.179, 2000a.

208. Smith, J.A., The heliosphere and beyond. II', edited by Coppi, B., A. Ferrari and E Sindoni, *Proceedings of the International School of Physics "Enrico Fermi" course CXLII* (Amsterdam), p.205, 2000b.

209. Steenberg, C.D., Modeling of anomalous and galactic cosmic ray modulation in the outer heliosphere, Ph.D. thesis, Potchefstroom University, South Africa, 1998.

210. Steenkamp, R., Shock acceleration as source of the anomalous component of cosmic rays in the heliosphere, Ph.D. thesis, Potchefstroom University for CHE, South Africa, 1995.

211. Sternal, O., Transport of galactic cosmic rays in different heliospheric magnetic field configurations, Ph.D. thesis, Christian-Albrechts University Kiel, Germany, 2010.

212. Stone, E.C., A.C. Cummings, F.B. McDonald, B.C. Heikkila, N. Lal, and W.R. Webber, Voyager1 explores the termination shock region and the heliosheath beyond, *Science*, 309, 2017-2020, 2005.

213. Stone, E.C., A.C. Cummings, F.B. McDonald, B.C. Heikkila, N. Lal, and W.R. Webber, An asymmetric solar wind termination shock, *Letters*, 454, 71-74, 2008.

214. Strauss, R.D., Modelling anomalous cosmic rays, M.Sc thesis, Potchefstroom University for CHE, South Africa, 2009.

215. Strauss, R.D., M.S. Potgieter, S.E.S. Ferreira and M.E. Hill, Modelling anomalous cosmic ray oxygen in the heliosheath, *Astronomy and Astrophysics*, 522, 1-8, 2010.

216. Svalgaard, L., and J.M. Wilcox, The spiral interplanetary magnetic field: a polarity and sunspot cycle variation, *Science*, 186, 51-53, 1974.

217. Svalgaard, L., and J.M. Wilcox, A view of solar magnetic fields, the solar corona, and the solar wind in three dimensions, *Annual Review of Astronomy and Astrophysics*, 16, 429-443,1978.

218. Teegarden, B.J., F.B. McDonald, J.H. Trainor, W.R. Webber, and E.C. Roelof, interplanetary MeV electrons of jovian origin, *Journal of Geophysical Reasearch*, 79, 3615-3622, 1974.

219. Teufel, A., and R. Schlickeiser, Analytic calculation of the parallel mean free path of heliospheric cosmic rays. I. Dynamical magnetic slab turbulence and random sweeping slab turbulence, *Astronomy and Astrophysics*, 393, 703-715, 2002.

220. Thomas, B.T., and E.J. Smith, The structure and dynamics of the heliospheric current sheet, *Journal of Geophysical Research*, 86, 11105-11110, 1981.

221. Thomas, J.H., and N.O. Weiss, The theory of sunspots, In: Sunspots theory and observations: *Proceedings of the NATO advance research workshop on the theory of sunspots* (Cambridge), 375, 3-59, 1992.

222. Wang, Y.M., and N. R. Sheeley, Solar implications of Ulysses interplanetary field measurements, *Astrophysical Journal*, 447, 143-146, 1995.

223. Wang, Y.M., N.R. Sheeley, R.A. Howard, J.R. Kraemer, N.B. Rich, M.D. Andrews, G.E. Brueckner, K.P. Dere, M.J. Koomen, C.M. Korendyke, D.J. Michels, J.D. Moses, S.E. Paswaters, D.G. Socker, D.Wang, P.L. Lamy, A.Llebaria, D.Vibert, R.Schwenn, and G.M. Simnett, Origin and evolution of coronal streamer structure during the 1996 minimum activity phase, *Astrophysical Journal*, 485, 875-889, 1997.

224. Wanner, W., and G. Wibberenz, Mean free paths from magnetic field power density spectra for selected helios solar proton events, *Proceedings of the 22nd International Cosmic Ray Conference* (Ireland), 3, 221-224, 1991.

225. Washimi, H., and T. Tanaka, MHD structure of the heliosphere and its response to the 11-year solar cycle variations, *Advances Space Research*, 551, 551-560, 1999.

226. Wenzel, K.P., R.G. Marsden, D.E. Page, and E.J. Smith, The Ulysses mission, *Astronomy and Astrophysics Supplement Series*, 92, 207-219, 1992.

227. Wibberenz, G., and H.V. Cane, Simple analytical solutions for propagating diffusive barriers and application to the 1974 minicycle, *Journal of Geophysical Research*, 105, 315 318, 2000.

228. Wibberenz, G., I.R. Richardson and H. V. Cane, A simple concept for modeling cosmic ray modulation in the inner heliosphere during solar cycles 2023, *Journal of Geophysical Research*, 107, 1-15, 2002.

229. Wilcox, J.M., and N.F. Ness, Quasi stationary corotating structure in the interplanetary medium, *Journal of Geophysical Research*, 70, 5793-5805, 1965.

230. Withroe, G.L., W.C. Feldman, and H.S. Ahluwalia, The solar wind and its coronal origins, In: Solar interior and atmosphere, edited by Cox A.N., W.C. Livingstone and M.S. Mathews, *University of Arizona Press*, p.1089, 1992.

231. Zank, G.P., and H.L. Pauls, Modelling the heliosphere, *Space Science Reviews*, 78, 95-106, 1996.

232. Zank, G.P., and H.L. Pauls, Shock propagation in the outer heliosphere 1. Pickup ions and gas dynamics, *Journal of Geophysical Research*, 102, 7037-7050, 1997.

233. Zhang, M., A linear relationship between the latitude gradient and 26 day recurrent variation in the fluxes of galactic cosmic rays and anomalous nuclear components I. Observations, *Astrophysics Journal*, 488, 841-853, 1997.

234. Zhang, M., A Markov stochastic process theory of cosmic ray modulation, *Astrophysical Journal*, 513, 409-420, 1999.

235. Zhang, M., Acceleration of galactic and anomalous cosmic rays in the heliosheath, *Astrophysical Journal*, 858, 226-232, 2006.

236. Zirker, J.B., Coronal holes and high speed wind streams, *Reviews of Geophysics and Space Physics*, 15, 257-269, 1977.

237. Zhou, X.Y., E.J. Smith, D. Winterhalter, D.J. McComas, R.M. Skoug, B.E. Goldstein, and C.W. Smith, Morphology and evolution of the heliospheric current and plasma sheets from 1 to 5AU, *Proceedings of the Solar Wind 11 Conference* (Canada), edited by Fleck, B., T.H. Zurbuchen and H. Lacoste, p. 659, 2005.

238. Zurbuchen, T.H., N.A. Schwadron, and L.A, Fisk, Direct observational evidence for a heliospheric magnetic field with large excursions in latitude, *Journal of Geophysical Research*, 102, 24175-24182, 1997.

Acknowledgements

I have to express my sincere gratitude to the following people and different offices, in no particular order:

- The sovereign God for his unfailing love and grace that he has shown in me since the beginning of my life and during my studies.
- My mother, for being a special mother, who has been there for me during trials and tribulations.
- My supervisor, Prof. Stefan Ferreira, for guiding me through all my writings, for having patience and trust in me and lastly for spending time with me even during busy schedules.
- Prof. Marius Potgieter for his assistance and all the discussions we had during my writing process and also his leadership.
- Prof. Bernd Heber, for his contribution to and assistance on this successful work.
- Mathew Holleran and Hennie Boshoff for their assistance on all computer related problems.
- My friends, Dima Visser and Lientjie de Villiers for being there for me when I needed them most and being the best office mates ever.
- Mrs. Sieberhagen, Lee-Ann van Wyk and Elanie van Rooyen for their administrative assistance.
- Mr. Donald Ngobeni, Mr Rex Manuel, Dr. MP Mulaudzi and Mr Enos Marubini for their friendship and advices.
- The Unit for Space Physics (USP) at the North-west University, Potchefstroom Campus and the National Research Foundation for financial support.

Special thanks to:

1. Potchefstroom Students Christians Fellowship (PSCF), for their prayers when I needed them most and also for being a family to me.
2. My brother and his wife, Mr and Mrs Mdau for taking the huge step of welcoming me in their family since my varsity life. May God richly bless you.
3. My sisters and brothers, Aifheli, Mercy, Irene, Judith, Richard and Ntanganedzeni, you are the best family ever.

The world is given to me only once, not one existing and one perceived. Subject and object are only one. The barrier between them cannot be said to have broken down as a result of recent experience in the physical sciences, for this barrier does not exist.
– Erwin Schrödinger

Edwin Magidimisha
Centre for Space Research, North-West University
December 2010